

**MODELLING THE IMPACT OF  
LAND COVER CHANGE ON  
URBAN HEAT/COOL ISLAND OF  
BENGALURU METROPOLITAN CITY**

**Thesis**

**Submitted in partial fulfillment of the requirements for the degree of**

**Doctor of Philosophy**

by

**NITHYA R GOVIND**



**DEPARTMENT OF WATER RESOURCES AND OCEAN  
ENGINEERING  
NATIONAL INSTITUTE OF TECHNOLOGY KARNATAKA  
SURATHKAL, MANGALORE – 575025  
JANUARY 2023**

**MODELLING THE IMPACT OF  
LAND COVER CHANGE ON  
URBAN HEAT/COOL ISLAND OF  
BENGALURU METROPOLITAN CITY**

**Thesis**

**Submitted in partial fulfillment of the requirements for the degree of  
Doctor of Philosophy**

by

**NITHYA R GOVIND**

Under the guidance of

**Dr. RAMESH H.**

Associate Professor,  
Dept. of Water Resources and Ocean Engineering  
NITK, Surathkal



**DEPARTMENT OF WATER RESOURCES AND OCEAN  
ENGINEERING  
NATIONAL INSTITUTE OF TECHNOLOGY KARNATAKA  
SURATHKAL, MANGALORE – 575025  
JANUARY 2023**

## DECLARATION

*By the Ph.D. Research Scholar*

I hereby *declare* that the Research Thesis entitled **Modelling the impact of Land Cover Change on Urban Heat/Cool Island of Bengaluru Metropolitan city** which is being submitted to the **National Institute of Technology Karnataka, Surathkal** in partial fulfilment of the requirements for the award of the Degree of **Doctor of Philosophy in Water Resources and Ocean Engineering Department** is a *bonafide report of the research work* carried out by me. The material contained in this Research Thesis has not been submitted to any University or Institution for the award of any degree.



165029 AM16F06, NITHYA R GOVIND

(Register Number, Name & Signature of the Research Scholar)

Department of Water Resources and Ocean Engineering


Place: NITK-Surathkal

Date: 01-02-2023

# CERTIFICATE

This is to certify that the Research Thesis entitled **Modelling the impact of Land Cover Change on Urban Heat/Cool Island of Bengaluru Metropolitan city** submitted by NITHYA R GOVIND (Register Number: 165029 AM16F06) as the record of the research work carried out by her, is *accepted as the Research Thesis submission* in partial fulfilment of the requirements for the award of degree of **Doctor of Philosophy**.

 01/02/2023

 **Dr. RAMESH H.**  
Research Guide  
Associate Professor  
Dept. of Water Resources & Ocean Engineering  
NITK-Surathkal, Mangaluru-575 029  
(Name and Signature with Date and Seal)

  
Chairman - DRPC

(Signature with Date and Seal)

Chairman (DRPC)  
Dept. of Water Resources & Ocean Engineering



## ACKNOWLEDGEMENT

---

I am deeply indebted to my doctoral advisor **Dr. Ramesh H.**, Water Resources and Ocean Engineering Department, NITK Surathkal, for supervising my research work. I express my sincere gratitude to my supervisor for his logical and tactical suggestions and encouragement during the development of this research.

I am very much grateful to former Heads of the Department **Prof. G.S. Dwarakish**, **Prof. A. Mahesha**, **Prof. Amba Shetty** and the present Head of the Department, **Prof. B. M. Dodamani** for providing necessary support and facilities for my research work. I express my sincere gratitude to the Research Progress Assessment Committee (RPAC) members, **Prof. S. M. Murigendrappa**, Department of Mechanical Engineering and **Prof. Amba Shetty**, Water Resources and Ocean Engineering Department for their valuable insights and encouragements during the entire period of my research work. I thank to all the faculty members of the Water Resources and Ocean Engineering Department for their support.

I would like to express my gratitude to the former Director of NITK, Surathkal, **Prof. Karanam Uma Maheshwar Rao** and present Director In-charge, **Prof. Udaykumar R. Yaragatti** for granting me the permission to use the infrastructure facilities of the institute.

I sincerely acknowledge the help and support rendered by the staff and research scholars of the Department of Water Resources and Ocean Engineering. I take this opportunity to thank **Mr. Seetharam**, **Mr. Balakrishna**, **Mrs. Parthima**, **Ms. Sweekritha**, **Mr. Ananda Devadiga**, **Mr. Gopalakrishna**, **Mr. Harisha** and **Mr. Anil Kumar** for all their support during my research work.

I sincerely acknowledge the help and support rendered by all the faculties, staffs and Research scholars of Department of Water Resources and Ocean Engineering. My

sincere thanks to **Dr. Sinan, Dr. Rishikesh, Dr. Diwan, Dr. Sylus, Dr. Beena, Dr. Viboosha, Dr. Spoorthi, Dr. Pooja, Ms.Chaitanya, Ms.Anjali, Ms. Dinu, Ms. Chinmayi, Ms. Arya, Ms. Ashwitha, Mr. Parthasarathy, Mr. Vijay, Mr. Tom, Mr. Athul** and **Mr. Rony** for their technical and moral support during the course of my research work.

Most importantly, I render my deep sense of gratitude to my father **Mr. M Govindapillai** and mother **Mrs. Remadevi Amma** for their constant motivation and support throughout my life. I greatly acknowledge the support rendered by my brothers **Mr. Gopu** and **Dr. Sooryajith** during my hard times. Last but not the least, I owe gratitude to my husband **Rakesh** for his support and understanding during the course of this research.

- **NITHYA R GOVIND**

## ABSTRACT

Urbanization has emerged as the most drastic and irreversible form of human-induced landscape change. Rise in temperature in urban area leads to high building energy consumption and degraded environmental qualities in the built environment. Hence, Urban Heat Island (UHI) effect has emerged as a key research top in the field of urban ecology and urban climatology. In most of the developing countries, man-made developments in the environment have led to the growing demand to contextualize the Land Use Land Cover (LULC) changes and Land Surface Temperature (LST) variations. Due to the modification in the surface properties of the cities, a difference in energy balance between the cities and its non-urban surroundings is observed. The present study was focussed on the analysis of spatial and temporal patterns of LULC and LST and its interrelationship in Bengaluru Urban district, India during the period from 1989 to 2017 using remote sensing data. Bengaluru is one of the rapidly growing cities in India and there is an urgent need for investigating the spatio-temporal patterns of LULC and LST in the region. The datasets used for the study mainly comprises of Landsat images and MODIS data from 1989 to 2020.

The land cover maps of the study area were prepared for the years 1989, 1994, 2001, 2005, 2014 and 2017 using supervised classification. Intensity analysis was performed for the interval to analyse the LULC change and identify the driving forces. The impact of land cover change on LST was assessed using hot spot analysis (Getis-Ord  $G_i^*$  statistics). The results of this study show that (a) dominant land cover change experienced is the increase in urban area (approximately 40%) and the rate of land cover change was faster in the time period 1989-2001 than 2001-2017. (b) the major transition witnessed is from barren and agricultural land to urban (c) Over the period of 28 years, LST patterns for different land cover classes exhibit an increasing trend with an overall increase of approximately 6°C and the mean LST of urban area increased by about 8°C (d) LST pattern change can be effectively analysed using hot spot analysis (e) As the urban expansion occurs, the cold spots have increased, and it is mainly clustered in the

urban area. It confirms the presence of an urban cool island effect in Bengaluru urban district.

LST and land cover interaction was modelled in a comprehensive and efficient way in the semi-arid tropical metropolitan city. Even though this interaction has been discussed widely in many literatures, the study facilitates the modelling and parameterization of LST and urban growth in an adequate way. Spatial distribution of LST and land cover types of the area were examined in the circumferential direction, and the contribution of land cover classes on LST was studied over 28 years. Urban growth and LST were modelled using Landsat and MODIS (Moderate Resolution Imaging Spectroradiometer) data for the years 1989, 2001, 2005 and 2017 based on the concentric ring approach. The study provides an efficient methodology for modelling and parameterization of LST and urban growth by fitting an inverse S-curve into Urban Density (UD) and mean LST data. In addition, Multiple Linear Regression (MLR) models which could effectively predict the LST distribution based on surface area ratios were developed for both day and night time. Further, the relationship between land cover types such as urban, vegetation, water and LST is determined for different years emphasizing the impact of land cover change on the daytime and night time surface heating. The non-linear relationship between surface area ratios and LST was established using a hybrid Particle Swarm Optimization - Support Vector Regression (PSO-SVR) model for the years 1989, 2001, 2005 and 2017.

Based on the analysis of remotely sensed data for LST, it is observed that over the years, urban core area has increased circumferentially from 5 km to 10 km, and the urban growth has spread towards outskirts beyond 15 km from the city centre. As urban expansion occurs, the area under the study experiences an expansive cooling effect during day time; at night, an expansive heating effect is experienced in accordance with the growth in UD in the suburban area and outskirts. The regression models that were developed have relatively high accuracy with  $R^2$  value of more than 0.94 and could explain the relationship between LST and land cover types. The study also revealed that there exists a negative correlation between urban, vegetation, water body and LST during day time while a positive correlation is observed during night.



The values of the statistical indices prove the feasibility and efficacy of PSO algorithm in tuning the hyperparameters of SVR. The Hybrid PSO-SVR model was built on the tuned hyperparameters for modelling LST with different surface area ratios at different time frames. For surface area ratio,  $R^2$  value in the range of 0.94 and 0.97 was obtained for MLR and Hybrid PSO-SVR model respectively.

The spatio-temporal variation of urban surface characteristics and its relationship with LST was also modelled over the period from 1989 to 2017. Remote sensing indices such as NDVI (Normalized Difference Vegetation Index), NDWI (Normalized Difference Water Index), and NDBI (Normalized Difference Built-up Index), was determined from Landsat images for the years 1989, 2001, 2005 and 2017. Linear relationship between LST and these remote sensing indices were studied by employing MLR technique. Further, the proposed Hybrid PSO-SVR model was applied to the datasets to predict the values of LST based on these remote sensing indices. Hypothetical scenarios were introduced in the prediction to assess the impact of change in vegetation and water bodies on LST. Temporal variation of urban heat anomaly of the region over the period of study was also investigated.

NDBI has drastically increased in the year 2017 which is caused by the increase in barren land and urban areas while NDVI and NDWI has decreased over the years. Higher values of NDBI are scattered in the outskirts while higher NDVI and NDWI values are distributed in the urban centre.  $R^2$  value in the range of 0.80 and 0.85 was obtained for MLR and Hybrid PSO-SVR model respectively. Hybrid PSO-SVR model proved to be effective in establishing the relationship between LST and urban surface characteristics, NDVI, NDBI and NDWI and in predicting the future LST. From the hypothetical scenario analysis, it can be concluded that introduction of vegetation and water bodies in the suburban and urban fringes will reduce the difference in LST between urban and rural areas. The magnitude of urban heat anomaly can be curtailed by developing green corridors and artificial lakes in the suburban and urban fringes of Bengaluru.

Thus, this study could assist urban planners and policymakers in understanding the scientific basis of urban heating effect and predict LST for the future implementation of green infrastructure. The findings of this work can be used as a scientific basis for the sustainable development and land use planning of the region in the future. The proposed methodology could be applied to other urban areas for quantifying the distribution of LST and different land cover types and their interrelationships.

**Keywords:** Land use land cover, Land surface temperature, Intensity analysis, Urban cool island, Urban density, Concentric ring approach, Multiple linear regression, Support vector regression, Particle swarm optimization, Bengaluru.

## CONTENTS

<b>CONTENTS</b>	<b>i</b>
<b>LIST OF FIGURES</b>	<b>vi</b>
<b>LIST OF TABLES</b>	<b>ix</b>
<b>ABBREVIATIONS</b>	<b>x</b>
<b>CHAPTER 1 INTRODUCTION</b>	<b>1</b>
1.1 GENERAL	1
1.2 IMPACT OF URBANIZATION ON TEMPERATURE	2
1.3 URBANIZATION IN INDIA	4
1.4 SCOPE OF THE RESEARCH WORK	7
1.5 RESEARCH OBJECTIVES	7
1.6 ORGANIZATION OF THESIS	8
<b>CHAPTER 2 LITERATURE REVIEW</b>	<b>11</b>
2.1 GENERAL	11
2.2 LAND SURFACE TEMPERATURE RETRIEVAL	11
2.3 IMPACT OF LAND USE LAND COVER CHANGE ON LAND SURFACE TEMPERATURE	13
2.4 STUDIES ON SURFACE URBAN HEAT ISLAND AND SURFACE URBAN COOL ISLAND	15
2.5 STUDIES ON IMPACT OF URBANIZATION ON BENGALURU	19
2.6 APPLICATION OF SUPPORT VECTOR MACHINE ALGORITHM IN REMOTE SENSING	20
2.7 SUMMARY OF LITERATURE	23
2.8 RESEARCH GAPS	24
<b>CHAPTER 3 STUDY AREA</b>	<b>25</b>

3.1	INTRODUCTION	25
3.2	PHYSIOGRAPHY AND CLIMATE	25
3.2.1	Geomorphology	26
3.2.2	Climate	27
3.2.2.1	Rainfall Pattern	27
3.2.2.2	Temperature	28
3.2.2.3	Wind Pattern	28
3.2.3	Soil	29
3.3	URBANIZATION	29
3.3.1	Demography	29
3.3.2	Impact of Urbanization on Climate	30
<b>CHAPTER 4</b>	<b>DATA AND METHODS</b>	<b>33</b>
4.1	DATA	33
4.2	COMPUTATIONAL TOOLS	33
4.2.1	ArcGIS 10.1	33
4.2.2	ERDAS IMAGINE 14	35
4.2.3	R 4.1.0	35
4.2.4	MATLAB 2015a	35
4.3	OVERALL METHODOLOGY	36
4.4	ALGORITHMS	37
4.4.1	Multiple Linear Regression	37
4.4.2	Support Vector Regression	38
4.4.3	Particle Swarm Optimization	42
<b>CHAPTER 5</b>	<b>SPATIO-TEMPORAL PATTERNS OF LAND COVER AND LST</b>	<b>45</b>
5.1	INTRODUCTION	45
5.2	METHODOLOGY	45

5.2.1	Land Use Land Cover Mapping	46
5.2.2	Accuracy assessment	47
5.2.3	Intensity Analysis	48
5.2.4	LST Retrieval	52
5.2.5	Hot Spot Analysis	54
5.2.6	Pearson's Correlation Coefficient	56
5.3	RESULTS	56
5.3.1	Land Cover Classification	56
5.3.2	Intensity Analysis of Land Cover Change	59
5.3.3	Spatio-temporal variation of LST	68
5.3.4	LST and LC relationship	71
5.3.5	Impact of LC on LST	74
5.4	DISCUSSION	75
5.5	CONCLUSION	77
<b>CHAPTER 6</b>	<b>MODELLING LST AND LAND COVER INTERACTION</b>	<b>79</b>
6.1	INTRODUCTION	79
6.2	METHODOLOGY	79
6.2.1	Land Density Estimation	79
6.2.2	Inverse S-shape Function	83
6.2.3	Model Parameter Estimation	84
6.2.4	Normalized LST	84
6.2.5	Multiple Linear Regression	85
6.2.6	Establishment of proposed Hybrid PSO-SVR Model	85
6.3	RESULTS AND DISCUSSION	88
6.3.1	Urban land density modelling	88
6.3.2	Normalized LST modelling	92

6.3.3	Relationship between urban density and normalized LST	100
6.3.4	Relationship between LST and surface area ratio	101
6.3.5	Hybrid PSO-SVR Model	104
6.3.6	Results of Hyperparameter tuning	105
6.3.6	Capability of Hybrid PSO-SVR model	107
6.4	CONCLUSION	112
<b>CHAPTER 7</b>	<b>MODELLING AND PREDICTION OF LST BASED ON URBAN SURFACE CHARACTERISTICS</b>	<b>113</b>
7.1	INTRODUCTION	113
7.2	METHODS	113
7.2.1	Urban Surface Characteristics	114
7.2.1.1	NDVI	114
7.2.1.2	NDWI	115
7.2.1.3	NDBI	115
7.2.2	Multiple linear regression analysis	115
7.2.3	Establishment of proposed Hybrid PSO-SVR model	116
7.2.4	Formulation of hypothetical scenarios	117
7.2.5	Urban Heat Anomaly	117
7.3	RESULTS AND DISCUSSION	118
7.3.1	Characteristics of LST, NDBI, NDVI & NDWI	118
7.3.2	Multiple Linear Regression Analysis	124
7.3.3	Hybrid PSO-SVR Model	125
7.3.4	Capability of Hybrid PSO-SVR Model	126
7.3.5	Comparison of MLR and Hybrid PSO-SVR results	131

7.3.6	Prediction of LST	131
7.3.7	Hypothetical Scenario Analysis	133
7.3.8	Analysis of Urban Heat Anomaly	135
7.4	CONCLUSION	137
<b>CHAPTER 8</b>	<b>SUMMARY AND CONCLUSIONS</b>	<b>139</b>
8.1	SUMMARY	139
8.2	CONCLUSIONS	140
8.3	LIMITATIONS	142
8.4	FUTURE PERSPECTIVES	143
	<b>REFERENCES</b>	<b>145</b>
	<b>APPENDIX</b>	<b>161</b>
	<b>PUBLICATIONS</b>	<b>165</b>
	<b>RESUME</b>	<b>167</b>

## LIST OF FIGURES

<b>Fig No.</b>	<b>Figure Caption</b>	<b>Page No.</b>
1.1	Urbanization trends in India (Source: Franco et al., 2017)	5
3.1	Location map of the study area	26
3.2	Distribution of annual rainfall in the region from 1901 to 2011	27
3.3	Variation of monthly mean temperature and rainfall of Bengaluru district based on 1900-2000 data.	28
3.4	Distribution of the population in the region from 1901 to 2011	30
3.5	Annual Temperature variation with number of rainy days in the Bengaluru region from 1978 to 2016	30
4.1	Overall methodology of the research work	36
4.2	Solution of SVR problem in graphical form (Smola and Scholkopf, 2004)	40
4.3	The tube of radius $\epsilon$ defined by SVR algorithm within which the forecasted value must lie (Panahi et al., 2021).	40
5.1	Flowchart of methodology	46
5.2	LC map of the study area for the years (a)1989 (b) 1994 (c) 2001 (d) 2005 (e) 2014 (f) 2017.	58
5.3	Time intensity analysis for two periods: 1989-2001 and 2001-2017.	60
5.4	Category intensity analysis for the period-1 1989-2001	61
5.5	Category intensity analysis for the period-2, 2001-2017.	62
5.6	Transition intensity analysis to urban for 1989 -2001	64
5.7	Transition intensity analysis to urban for 2001-2017	65
5.8	Transition intensity analysis from vegetation for 1989-2001	66
5.9	Transition intensity analysis from vegetation for 2001-2017.	67
5.10	LST Map of the study area for the years (a)1989 (b) 1994 (c) 2001 (d) 2005 (e) 2014 (f) 2017.	69
5.11	The variation of LST in the study area	70



5.12	Comparison of LST and Air temperature for the study area	71
5.13	Variation of mean LST for different land use classes	73
5.14	Hot spot map of the study area for the years (a) 1989 (b) 2001 (c) 2017	74
6.1	Data and methodology flowchart for LST modelling	80
6.2	Concentric ring-based partitioning of Bengaluru illustrates the urban area in 1989, 2001 and 2017.	82
6.3	Illustration of different zones of urban area from the urban centre (Source: (Jiao, 2015)).	83
6.4	Flowchart of the establishment of Hybrid PSO-SVR Model	86
6.5	Urban land density from city centre for the years 1989, 2001, 2005, 2017.	88
6.6	Fitting of urban land density function to the land density data for the years (a) 1989 (b) 2001 (c) 2005 (d) 2017.	91
6.7	Mean normalized LST with distance from the city centre (a) Daytime for the years 1989, 2001, 2005, 2017 (b) Night-time for the years 2005 and 2017	93
6.8	Fitting of the function for the mean LSTn values of day time from urban centre: (a) 22 February 1989 (b) 27 March 2001 (c) 18 February 2005 (d) 23 March 2017	97
6.9	Fitting of the function for the mean LSTn values of the night-time from urban centre: (a) 18 February 2005 (b) 23 March 2017	98
6.10	The plot of urban land density with normalized daytime LST computed for each concentric ring: 1989, 2001, 2005, 2017	100
6.11	Plot of urban land density with normalized night-time LST computed for each concentric ring: 2005 and 2017	101
6.12	Comparison of observed and predicted normalized LST for the daytime	103
6.13	Comparison of observed and predicted normalized LST for the night-time	103
6.14	Fitness curves for optimizing hyperparameters using PSO for the years 2017, 2005, 2001, 1989	106
6.15	Performance of Hybrid PSO-SVR model at training and testing stages for the four time steps	110
7.1	Flowchart of methodology	114

7.2	Spatial Distribution of NDBI, NDWI, NDVI and LST for the year 1989	119
7.3	Spatial Distribution of NDBI, NDWI, NDVI and LST for the year 2001	120
7.4	Spatial Distribution of NDBI, NDWI, NDVI and LST for the year 2005	121
7.5	Spatial Distribution of NDBI, NDWI, NDVI and LST for the year 2017	122
7.6	Performance of Hybrid PSO-SVR model at training and testing stages for the four-time steps.	130
7.7	Performance of Hybrid PSO-SVR model for LST prediction at the training stage	132
7.8	Performance of Hybrid PSO-SVR model for LST prediction at the testing stage	133
7.9	Spatial variation of difference in LST for scenario1 and 3 compared to the estimated LST of the year 2020	134
7.10	Change in area experiencing a different range of predicted LST for the four scenarios.	135

## LIST OF TABLES

<b>Table No.</b>	<b>Table Caption</b>	<b>Page No.</b>
4.1	Specifications of the remote sensing data used in the study	34
5.1	Equations for intensity analysis (Aldwaik and Pontius, 2012)	50
5.2	Land transition matrix of the study area for period-1(1989-2001) in sq. km	51
5.3	Land transition matrix of the study area for period-2 (2001-2017) in sq.km	52
5.4	Mean LST and land cover area of the study region	72
6.1	PSO and SVR parameter values	87
6.2	Model evaluation metrics for urban land density	91
6.3	Slope of the modified sigmoid function for urban land density	92
6.4	Model evaluation metrics for normalized LST	95
6.5	Slope of the modified sigmoid function for normalized LST	99
6.6	Optimal SVR hyperparameters and evaluation indices for train and test dataset	111
7.1	PSO and SVR parameter values	116
7.2	Descriptive statistics of LST, NDVI, NDBI and NDWI	123
7.3	MLR results for different window size	124
7.4	Optimal SVR hyper-parameters and evaluation indices for train and test dataset	126
7.5	Temporal variation of UHI intensity in the study area	136

## ABBREVIATIONS

UHI	-Urban Heat Island
UCI	-Urban Cool Island
SUHI	-Surface Urban Heat Island
SUHII	-Surface Urban Heat Island Intensity
SUCI	-Surface Urban Cool Island
UHII	-Urban Heat Island Intensity
UHIII	-Urban Heat Island Intensity Index
GIS	-Geographic Information System
LST	-Land Surface Temperature
LULC	-Land Use Land Cover
LC	-Land Cover
IT	-Information Technology
TM	-Thematic Mapper
ETM	-Enhanced Thematic Mapper
OLI	-Operational Land Imager
MODIS	-Moderate Resolution Imaging Spectroradiometer
ESRI	-Environmental Systems Research Institute
GPS	-Global Positioning System
NIR	-Near Infra-Red
NDVI	-Normalized Difference Vegetation Index
NDWI	-Normalized Difference Water Index
MNDWI	-Modified Normalized Difference Water Index
NDBI	-Normalized Difference Built-up Index
CC	-Correlation Coefficient
RMSE	-Root Mean Square Error
MSE	-Mean Squared Error
MAE	-Mean Absolute Error
UD	-Urban Density
VD	-Vegetation density

WD	-Water Density
BD	-Barren Density
SVM	-Support Vector Machine
SVR	-Support Vector Regression
PSO	-Particle Swarm Optimization
RBF	-Radial Bias Function
AOD	-Aerosol Optical Depth
LCZ	-Local Climate Zone
LAI	-Leaf Area Index
ANFIS	-Adaptive Neuro Fuzzy Inference System
RTE	-Radiate Transfer Equation
FVC	-Fractional Vegetation Cover

# CHAPTER 1

## INTRODUCTION

---

---

### 1.1 GENERAL

Urbanization is regarded as one of the main apprehensions of a rapidly developing world. Due to urbanization, the magnitude of human activities is increased which in turn lead to the rapid change in the surface cover and climate of the region. The 20<sup>th</sup> century is witnessing "the rapid urbanization of the world's population", as the global proportion of urban population rose dramatically from 13% (220 million) in 1900 to 29% (732 million) in 1950, to 49% (3.2 billion) in 2005 and is projected to rise to 60% (4.9 billion) by 2030 (Ramachandra and Uttam 2009). India will also face a high rate of urbanization. It is estimated that the country's population will reach 1.47 billion in 2030, with around 40 percent urbanization; close to 590 million will be living in cities (UN-DESA, 2012). This will lead to tremendous pressure on providing civic amenities such as water supply, sewerage, drainage and housing.

Urban ecosystems are the consequence of the fundamental nature of humans as social beings to live together. The growth of villages into towns, towns into cities and cities into metros can be attributed to infrastructure initiatives, population growth and migration which are the outcome of the process of urbanization. Urbanization and urban sprawl have posed severe challenges to the decision-makers in the city planning and management process. It involves a series of issues like infrastructure development, traffic congestion, and basic amenities such as electricity, water and sanitation.

Urban sprawl is perceived as one of the potential threats to development as the biggest confront is to ensure adequate housing with basic infrastructure and amenities including health, sanitation, etc. The dynamics and pattern of urbanization can be studied using differential urbanization models. This model will identify the cities which grow in each

stage of development by describing the clustering and de-clustering based on the city size (Jain and Korzhenevych 2020). Remote sensing coupled with geospatial analysis aid significantly in monitoring and management of the urbanization process. The spectral pattern present within the remote sensing data for each pixel is used to perform the classification and is used as the numerical basis for categorizing various spatial features. The proposed research aims to develop a relationship between land surface temperature and significant land use classes to predict the impacts of urbanization such as Urban Heat Island (UHI) and Urban Cool Island (UCI).

The effect of urbanization can be evaluated in several ways. With the rapid development of earth observation systems, satellite-based imaging technology has been widely applied to study urban climate change. The main advantage of this approach is that it can offer an efficient way to monitor the effect of urbanization across different spatio-temporal scales. From the perspective of remote sensing technique, it has been proved that the most suitable spatial resolution for urban thermal anomaly studies is approximately less than 100 m since coarser resolution may result in the loss of details for urban structures (Liu et al., 2016).

## **1.2 IMPACT OF URBANIZATION ON TEMPERATURE**

One of the critical factors causing an abnormal change in climate patterns across the globe is urbanization. The population of the cities tends to increase in comparison to the population of rural areas. The 21<sup>st</sup> century is witnessing rapid urbanization with 55% of the population dwelling in urban areas (2018) and is projected to increase to 68% in 2050 (Bocquier, 2005). The most significant urban expansion is expected to occur in Asia, especially in India and China in the future (Jiao, 2015; Seto et al., 2012). The land conversion from one type to another can cause positive and negative impacts on the region and its communities (Aryal et al., 2019; Bhatti et al., 2019). Urbanization has led to the conversion of natural land surfaces comprising of pervious surfaces and vegetation into built-up and impervious surfaces, one of the main reasons for global climate change (Mathew et al., 2016; Streutker, 2002; Touchaei & Wang, 2015).

Unplanned and uncontrolled urban growth has led to several severe social and environmental problems and influences various climate variables like rainfall, temperature, etc. (Bhat et al., 2017). Hence, there is a need to explore the environmental physics of an urban conglomeration as it directly affects labour productivity, well-being and health of the urban inhabitants through air quality and thermal comfort (Theeuwes et al., 2015). Urban land use strongly influences the energy and water balance of the city and impacts the weather and climate of a region (Shastri et al., 2017). Developments in remote sensing technologies have enabled the acquisition of satellite images at large spectral ranges with suitable spatial resolution. The satellite images are available at reasonable time intervals for monitoring the land surface features while in-situ reading can be obtained from specific ground based stations and at particular time spans only (Javed Mallick and Bharath 2008; Myint et al., 2013; Nichol and To, 2012).

The increase in the heat storage capacity of urban surfaces creates so called Urban Heat Island (UHI), in which built-up areas are hotter than nearby rural areas (Tran et al., 2017). This local difference in temperatures negatively impacts human beings and the environment because it hampers air quality, increases energy consumption, loses biological control, and affects human health. Advances in thermal remote sensing, Geographical Information Systems (GIS), and statistical methods have enabled the research community to characterize and examine UHI versus landscape relationships. Many studies deal with UHI analysis, providing effective feedback to policy-makers and researchers.

Heat waves can be exacerbated by UHI, increasing the heat burden on urban dwellers (Tan et al., 2010). Moreover, high heat waves will be more frequent and intense in future due to climate change. Heat stress will be more common among city dwellers, reducing human thermal comfort and increasing the risk of heat-related diseases. Studies on UHI in the recent years (such as geographical and temporal patterns, driving variables, and mitigation techniques) have grown and gained much attention (Phelan et al., 2015). The first step in these subjects is to quantify UHI intensity (UHII) accurately. The most commonly utilized methodologies for studying UHI include in-situ observation, remote sensing observation, and numerical modelling (Li et al., 2019).



A phenomenon of Urban Cool Island (UCI) is observed in some cities where the temperature in the urban area is cooler than the surrounding rural area. UCI phenomenon usually occurs during the daytime and is common in arid and semi-arid climatic regions (Yang et al., 2017). Many researchers have characterized the cooling effect of water bodies and green spaces. However, Surface Urban Cool Island (SUCI) investigation on the urban area is limited (Rasul et al., 2017).

Land Surface Temperature (LST) is one of the most critical environmental variables monitored by Earth-observing remote sensing systems (Bendib et al., 2017). Compared to air temperatures collected from weather stations, thermal imagery provides temperature anomaly at different spatial and temporal scales (Myint et al., 2013). LST derived from satellite imagery is a distinctive source of information to define surface urban heat islands. Satellite based thermal infrared image has been widely used as an indicator for UHI research.

In addition, land surface temperature derived from remote sensing imagery is better to understand the hottest and coolest areas than temperature collected from the urban weather station, which is located in the tree park-like surroundings (Nichol and To 2012). The Land Use Land Cover (LULC) characteristics also directly impact surface temperature. Urbanization leads to the expansion of built-up areas and impervious surfaces, increasing land surface temperature. Therefore, the analysis of the relationship between land use land cover and land surface temperature is crucial to understand the effects of urbanization.

### **1.3 URBANIZATION IN INDIA**

India is now confronting the rise of more than 35 cities with populations of one million or more, and it is expected to contain 14% of the World's urban population by 2025 (Sankhe et al., 2010). The number of urban agglomerations were 1827 in 1901 and it has increased to 7935 in 2011. The overall population increased fivefold from 238.4 million in 1901 to 1210.2 million in 2011, while the urban population increased nearly

fifteenfold from 25.85 million in 1901 to 377.1 million in 2011 (Franco et al., 2017).

Figure 1.1 depicts the trend of urbanization in India.

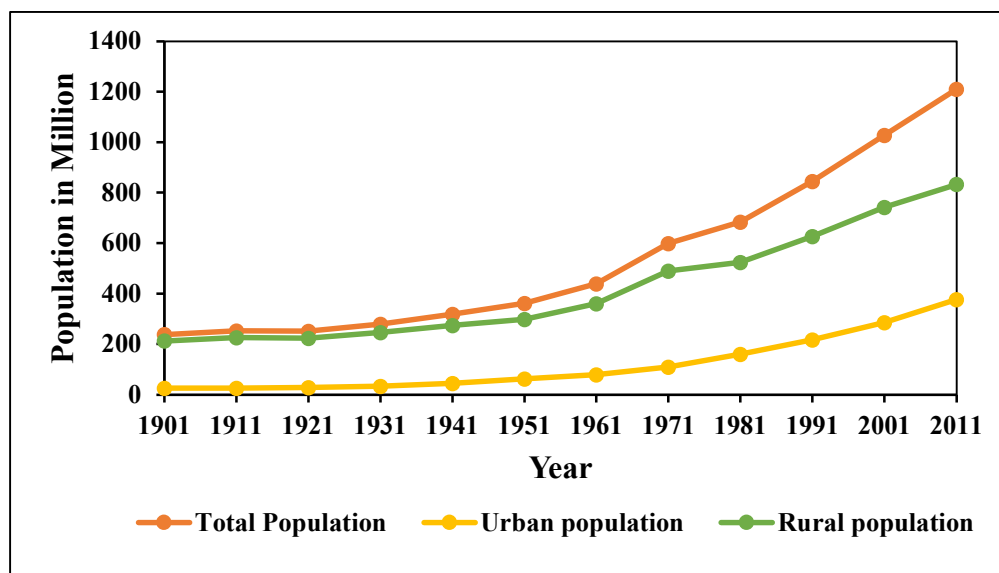


Figure 1.1 Urbanization trends in India (Source: Franco et al., 2017)

Delhi is the World's second most populous metropolitan agglomeration, with 22.7 million people, whereas Mumbai and Kolkata rank seventh and tenth, respectively, with 19.7 million and 14.4 million citizens. By 2025, the populations of Bangalore, Chennai, and Hyderabad are likely to approach 10 million (UN-DESA, 2012).

According to United Nations Department of Economic and Social Affairs 2014, India's urban population is expected to increase to around 800 million people in the year 2050. Also, based on researchers' analysis, two-thirds of India's buildings in 2030 will be built after 2010, mainly in metropolitan areas, to handle the increase in population. Between 1990 and 2014, the built environment is expected to have grown by 95 percent, exceeding population growth and municipal planning initiatives (Khosla and Bhardwaj, 2019). Megacities, multiple medium-sized cities, and tiny urban clusters will be among the new urban formations (Denis and Zerah, 2017). According to most industrialized World's historical experience, urbanization is a necessary component of modernization and progress. Indian cities are becoming economic hubs due to rapid urbanization (Ahmed et al., 2020).

Though population growth within the administrative bounds of large metropolitan areas have slowed in recent years. It has accelerated in their peripheries due to the expansion of census towns. The interplay between the core city and the periphery is critical for both sorts of entities growth and development (Pradhan, 2017). Contemporary urban studies in India make a concerted attempt to comprehend migration and migrants. The presence of a vast number of rural villages with urban features, on the other hand, is not widely recognized, and their economic significance is under appreciated (Jain and Jehling, 2020).

Rapid urbanization and urban development have diminished green cover and made cities vulnerable to climate change. Urbanization significantly impacts energy consumption and carbon dioxide emissions, although the impact varies depending on the region's economic development stage (Franco et al., 2017). The living environment is deteriorating due to the creation of UHIs, declining urban green cover, increased carbon emissions, and air pollution. Heat stress-related mortality and rising urban temperatures are still serious problems. Although the national aims of "improved energy efficiency" and "green India" are emphasized in the National Action Plan on Climate Change, the thermal climate of Indian towns is worsening due to an imbalance between constructed and natural spaces (Imam and Banerjee, 2016).

The Southwest Indian Subcontinent Monsoon is changing, seasonal swings are becoming more severe, and temperature anomalies are becoming more common. Furthermore, poor air quality and a severe water deficit exacerbate the situation. In cities, susceptibility of children to respiratory infections, and pavement dwellers' vulnerability to extreme climate conditions has increased dramatically. Around 2330 people died due to the 2015 summer heat wave (Imam and Banerjee, 2016). As a result, a study of climate change in urban areas of India and the development of commercially feasible avenues for its mitigation is critical, and it remains a worldwide concern.

#### **1.4 SCOPE OF THE RESEARCH WORK**

India has been facing a high rate of urbanization for the past few decades. As the population increases, people migrate from rural areas to cities, searching for employment and a better standard of living. Due to this, most of the metropolitan cities in India are becoming urban jungles. The rapid urbanization in the cities like Mumbai, Delhi, Kolkata, Chennai and Bengaluru has led to severe environmental issues in the respective regions. Bengaluru district marked a significant growth rate of 47.18 percent during 2001-2011. Urbanization will lead to tremendous pressure to provide civic amenities such as water supply, sewerage, drainage and housing. The expansion occurring presently in these areas is not planned growth, and hence the ecological balance of the area has affected. Due to this urbanization and the changing land use patterns, there is a notable change in the climate of the region.

From the previous studies, it is clear that many studies have been conducted to study the effect of urbanization on climate change. Nevertheless, only a few studies have been conducted in the Bengaluru region relating to the effect of urbanization on climate change using remote sensing techniques. This study mainly focuses on the impact of urbanization on the temperature, particularly using remote sensing data. Assessing the spatial and temporal distribution of LST and LULC in the region is the need of the hour. Previous studies mainly focused on Greater Bengaluru, a small part of the Bengaluru urban district (Ramachandra & Uttam, 2009; Ramachandra et al., 2013). None of the studies considers the whole of the Bengaluru Urban district. Considering the district as a whole help in understanding the spatiotemporal patterns of LULC and LST.

#### **1.5 RESEARCH OBJECTIVES**

The urban cool island effect in the study area is very less explored. Very few studies have been reported on UCI in a semi-arid environment. Bengaluru is one of the fast-growing metropolitan cities of India with a semi-arid tropical climate. Considering the district as a whole help in understanding the spatio-temporal patterns of LULC and LST in a better way as there are agricultural activities by farmers and urban area is surrounded by barren mountains with shrubs. This study focusses on the

characterisation of UCI based on hot spot analysis which is one of a kind in the study area. The major contribution of this study being the investigation of UCI in Bengaluru urban district and identification of statistically significant hot and cold spots in the region.

The objectives of the research work are listed below:

1. To assess the spatio-temporal patterns in land surface temperature and land cover in the context of urban cool island.
2. To model the land cover and land surface temperature interaction in the Bengaluru urban district region.
3. To explore the variation of urban surface characteristics and urban heat anomaly of the Bengaluru urban district area.

## **1.6 ORGANIZATION OF THESIS**

The thesis report comprises eight chapters as listed below:

**Chapter 1** presents the overview of urbanization in global and national perspective, the basis of the research and objectives set for the research work.

**Chapter 2** presents a detailed review of the past literature related to the impact of land cover change due to urbanization on LST, state-of-the art, tools and methodologies used by different authors across the globe. Summary of research gaps were also presented based on thorough literature survey.

**Chapter 3** describes the physiography and climate of the Bengaluru Urban district located in southern India considered as study area in this research. The urbanization experienced by Bengaluru over the years and its impact on the environment is also discussed in this section.

**Chapter 4** explains the various data sources and the detailed methodology used in the research study. One of the widely used machine learning algorithm, support vector

machines and popular meta-heuristic optimization technique particle swarm optimization which is employed in this research is discussed in detail

**Chapter 5** deals with the spatio-temporal patterns of LULC and LST from 1989 to 2017. The techniques employed to analyse the spatial and temporal patterns of LST and LULC is discussed in detail. The results obtained from this analysis and its discussion followed by the conclusions drawn from the analysis is enumerated.

**Chapter 6** deals with the modelling of land cover and the LST relationship. The spatial distribution of urban area and LST are characterised followed by modelling the interaction between land cover and LST. The algorithms employed for the modelling and its efficiency is explained. A detailed discussion on the outcomes of the model and the inferences are elaborated.

**Chapter 7** describes the variation of urban surface characteristics and urban heat anomaly of the region. The spatial variation of urban surface characteristics over the years from 1989 to 2017 and its interaction with LST is modelled. Future LST is predicted using a machine learning algorithm and the impact of change in surface cover on LST is analysed by formulating hypothetical scenarios. The variation of urban heat anomaly of the region is also investigated.

**Chapter 8** presents the summary and significant conclusions drawn from the research work. A brief summary of the study is provided. The general conclusions from the research and objective specific conclusions are presented. The limitation of the study and the scope for future research is also listed.



### LITERATURE REVIEW

---

---

#### 2.1 GENERAL

This chapter attempts to critically review the various techniques for LST retrieval from Landsat images and the impact of land cover change on LST. This chapter also discusses the studies on SUHI and SUCI. The applications of support vector machine algorithms in remote sensing are explored and the studies on the impact of urbanization on Bengaluru are described. Further, the gaps identified from the review of literature are detailed.

#### 2.2 LAND SURFACE TEMPERATURE RETRIEVAL

LST can be easily obtained from remote sensing data by using the thermal infrared band at different spatial and temporal scales which gives a better perception of the temperature distribution compared to the in-situ observation data. To estimate LST from remotely sensed data, three types of approaches have been developed: the single channel algorithm, split window algorithm, and a day-night MODIS LST method (Li et al. 2013).

To estimate LST from Landsat TM6 data, Qin et al. (2001) devised a mono window technique. According to the algorithm's sensitivity study, the hypothetical inaccuracy in ground emissivity has a negligible influence on the likely LST prediction. Sobrino et al. (2004) suggested a generalised single channel method that relies solely on the overall atmospheric water vapour concentration and the effective wavelength of the channel. The key benefit of this approach over previous single channel techniques is that it does not need effective mean ambient temperature measurements and can be applied to a variety of thermal sensors using the same equation and coefficients.



The single channel approach, two channel method, and temperature emissivity separation method were examined by Benmecheta et al. (2013) for LST retrieval. It simplifies the process of selecting and implementing these algorithms based on the image and set of parameters accessible to the user. By entering mean atmospheric water vapour concentration, temperature, and land surface emissivity, Song et al. (2014b) refined the mono window technique and applied it to Landsat TM or ETM+ data.

LST was calculated from Landsat 8 TIRS using the mono window technique from spectral radiance of band 10, and the surface emissivity was calculated using the Normalised Difference Vegetation Index (NDVI), which was calculated using OLI bands 5 and 4 (Bendib et al. 2017). The results were compared to MODIS products and found to be in good agreement. For Landsat images, Dai et al. (2016) refined the mono window technique by including mixed pixel categorization and subpixel mapping. LST results derived with the Radiative Transfer Equation (RTE) utilising atmospheric profile data and the MODTRAN model were compared to validate the technique. The modified mono window approach is able to offer more accurate LST than the original algorithm for Landsat TM/ETM+ imagery, according to validation.

Eswar et al. (2016) used the DisTrad thermal sharpening model to compare the relative performance of five different vegetation indices for thermal sharpening over agricultural and natural landscapes in India, namely NDVI, Fraction Vegetation Cover (FVC), Normalised Difference Water Index (NDWI), soil adjusted vegetation index, and modified soil adjusted vegetation index. The study relied on multi-temporal LST data from the Landsat-7 Enhanced Thematic Mapper Plus (ETM+) and MODIS sensors collected over two distinct agro-climatic grids in India. It was discovered that NDVI and FVC worked better only in wet situations, however, NDWI outperformed other indices and delivered correct findings in dry conditions.

Shi and Zhang (2018) used a mono window approach with ground emissivity and atmospheric transmittance estimate methods to get the Urban LST. When compared to field data, the error was determined to be  $0.1^{\circ}\text{C}$ , indicating that the approach may be employed for LST retrieval in hot humid regions. Within 250m and 350m, respectively,

the cooling effects of water and vegetation on adjoining urban sites were effective. LST can be retrieved from thermal infrared bands of different types of Landsat images (band 6 of Landsat 5 TM, Landsat 7 ETM+ and band 10 of Landsat 8) based on RTE by applying atmospheric correction values from the Atmospheric Correction Parameter Calculator online tool (Tran et al 2017). The change in LST patterns can be effectively analysed using Getis Ord  $G_i^*$  statistics.

Numerous approaches and algorithms have been proposed by researchers to derive LST from satellite images (Li et al. 2013). Low and medium spatial resolution spaceborne remote sensing images are usually used for deriving LST from satellite images (Zhou et al. 2014; Liu et al. 2016). Various complex interactions drive the temporal variation of LST, and its underlying mechanism can be explained by analyzing the temporal patterns of LST at different time scales (Chaudhuri and Mishra 2016; Wiesner et al. 2018; Zullo et al. 2019). The distribution of LST along the radial and circumferential direction in a city has not been adequately explored in previous studies. The mitigation and enhancement of LST significantly depend on the land use characteristics of an area and the permeability of the soil surface (Deng et al. 2018; Solangi et al. 2019; Tran et al. 2017).

### **2.3 IMPACT OF LAND USE LAND COVER CHANGE ON LAND SURFACE TEMPERATURE**

Land Use Land Cover (LULC) is identified as one of the key aspects of environmental change in both global and regional level. The multifaceted interactions between human and physical environments lead to the process of LULC change (Manandhar et al. 2010; Huang et al. 2012). Quantification of the causes and effects of LULC change is very crucial in the efficient utilization and management of natural resources. Understanding the trends of LULC change will be very helpful in the land use planning and environment management of a region (Zhao et al. 2013; Li et al.2018).

With the recent developments in Geographical Information Science (GIS) and remote sensing, the researchers can effectively characterize and examine the dynamic changes

in LULC (Chaudhuri and Mishra 2016; Tran et al. 2017). The availability of spatio-temporal consistent satellite images and ingenious image processing techniques has improved the efficiency of monitoring these LULC changes.

Urbanization is one of the most significant factors that cause LULC change. It is the rise in the population of cities in comparison to the rural population of the region. Urbanization is caused by the transformation of natural land surfaces comprising of vegetation and pervious surface into built-up and impervious surfaces due to the growth in economy and population (Tan et al. 2010; Mathew et al. 2016; Pal and Ziaul 2017). The uncontrolled and unplanned urban growth has led to serious issues on climate and local environment. (Bhat et al. 2017). The rapid urban growth directly or indirectly affects various environmental variables like land cover, temperature, rainfall and so on. India is facing a high rate of urbanization due to which most of its metropolitan cities are becoming urban jungles. The rapid urbanization in the cities like Mumbai, Delhi, Kolkata, Chennai, and Bengaluru has led to serious environmental issues in the respective regions.

In addition to LULC, LST is another imperative parameter which has a significant impact on the environment due to rapid urbanization. The LST patterns give useful information regarding surface physical properties and climate. Assessing the distribution of LST can be helpful in understanding various subjects like evapotranspiration, climate change and urban climate (Arnfield 2003; Bendib et al. 2017). Similar to LULC, LST also has dynamic spatial and temporal variations.

The relationship between urban land covers and LST changes is a crucial factor in the field of urban climate change (Guo et al. 2015; Li et al. 2017; Morabito et al. 2016; Song et al. 2014a). The response of LST to indices such as NDVI, NDWI, Normalized Difference Built-up Index (NDBI) and Normalized Difference Bareness Index (NDBAI) has been investigated using correlation and regression analysis (Zha et al. 2003; X. L. Chen et al. 2006; Rinner and Hussain 2011; Zhang et al. 2013; Estoque and Murayama 2017). Sun et al. (2012) reported that LST decreased with an increase in

vegetative cover and increased with an increase in the density of urban land in Guangzhou, China.

A study conducted in Dohuk city in Iraq has proved that NDBI and NDBAI correlate positively with high LST while NDVI and NDWI correlate negatively with low LST (Ibrahim 2017). Chen and Zhang (2017) noted that NDVI-MNDWI (Modified Normalized Difference Water Index) are better indicators of LST in comparison to NDBI and NDVI-MNDWI. In the present study, a linear relationship of LST with surface area ratio of different land cover types is formulated.

A lot of studies have been carried out to assess the impact of LULC on LST in various parts of India. LST has been extensively used as a significant parameter in understanding the impacts of LULC change on the environment. The studies on impact of urbanization on LST in various cities of India like Chennai (Devadas and Rose 2009), Delhi (Ogawa et al. 2012; Babazadeh and Kumar 2015; Grover and Singh 2015), Hyderabad (Franco et al. 2015), Mumbai (Grover and Singh 2015), Nagpur (Kotharkar and Surawar 2015), and Jaipur (Jalan and Sharma 2014) have been carried out by researchers. Most of the cities in India experience a heating effect with the development of urban areas, and the LST increases with increase in urban area and a decrease in vegetative cover (Chakraborty et al. 2015; Ziaul and Pal 2018).

## **2.4 STUDIES ON SURFACE URBAN HEAT ISLAND AND SURFACE URBAN COOL ISLAND**

One of the major impacts of urbanization is the development of a temperature anomaly called the Surface Urban Heat Island (SUHI) or Surface Urban Cool Island (SUCI) wherein there is a difference between the temperature of the urban and surrounding rural area. UHI is a phenomenon in which the urban area is hotter compared to the surrounding rural area while UCI is observed when the urban area is cooler compared to the surrounding rural area.

Luke Howard introduced the phenomenon of UHI in 1833, and it is mainly caused by the land surface manipulations generated by the impervious surfaces (Kolokotroni et al. 2006; Voogt and Oke 2003). Numerous studies have been carried out on UHI phenomenon which verified its close relationship with LULC and LST (Asgarian et al. 2015; Bokaie et al. 2016; Bozorgi et al. 2018; He 2018; He et al. 2019; Sabet Sarvestani et al. 2011; Santamouris et al. 2017; Stewart and Oke 2012; Zhao et al. 2017).

The thermal environment of Delhi was mapped by Pandey et al. (2009) and it was compared with the Aerosol Optical Depth (AOD). During summer season, the regions with lower AOD values tend to have higher temperature compared to higher AOD values. It was inferred from the study that the distribution of surface temperature during daytime depends on the aerosol distribution and a major water body located in the region.

During summer season, the buildings will become overheated, causing discomfort to the residents. This in turn leads to more air conditioners being installed causing an increase in energy use and carbon emissions (Levermore et al. 2018). During the day, an inverse or negative SUHI effect has been found over Jaipur, whereas a moderate or very weak SUHI effect has been observed over Ahmedabad, and a strong SUHI effect has been observed over both cities at night (Mathew et al. 2018). Soil has a faster rate of heating and cooling than manmade materials like roads and concrete, as measured by in-situ temperature measurements. The efficacy of remote sensing data for analysing the surface temperature fluctuations and surface urban heat island studies depends on the time of acquisition of the data.

Local Climate Zone (LCZ) classification is a useful tool to precisely determine the impact of urban factors, such as sky view factor, height of buildings, building surface fraction on the magnitude of UHI (Kotharkar and Bagade 2018; Stewart and Oke 2012). Literature on South Asian cities has thoroughly explored specific elements, such as urban LULC shifts and their related variations in vegetation cover, utilising various techniques to determine their impact on UHI development (Kotharkar et al. 2018).

UHI has also been measured using statistical methods and machine learning techniques (Rajasekar and Weng 2009). A Gaussian surface model has been used the most in these investigations since it can offer not only the intensity of the UHI but also its spatial distribution and point of concentration. UHI effects can also be examined using the kernel approach as it is effective in characterizing temperature values spatially on a continuous surface (Rajasekar and Weng 2009). Chun and Guldmann (2014) used two-dimensional and three-dimensional urban datasets as input for spatial statistical models to investigate the urban causes of UHI. The findings reveal that open spaces, solar radiation, vegetation, water and building roof-top areas, all have a significant impact on surface temperatures and that spatial regressions are required to account for the impacts of nearby factors.

Li et al. (2018) recently published a study on LST and regionalized ISA, linear regression functions were used to estimate UHI intensity. These statistical models eliminate the errors caused by defining the urban and rural boundaries or the selection of sample pixels, making comparisons of UHI between cities easier. The difficulties in the application of remote sensing data and derivatives in UHI modelling were reported by Szymanowski and Kryza (2011). The importance of remotely sensed data in modelling urban air temperature heat islands has been emphasised in literature (Shi et al. 2021). However, such models exhibited low performance in cities regularly shrouded by clouds and dry landscapes. Few researchers have quantified the air-surface UHI comparison (Gaur et al. 2018) and UHI attribution analysis (Akbari et al. 2016; Cai et al. 2018), by employing small numbers of sample pixels in urban and reference regions as an alternative to the area-weighted mean value.

In semi-arid regions, a phenomenon of urban cooling effect is experienced due to urbanization. The built-up areas in the semi-arid regions experience lesser temperature compared to the surrounding non-urbanized areas. This phenomenon is termed the urban cool island effect (Frey et al. 2009). Urban cool island effect on the semi-arid environment is a very less explored area. Very few researches have been carried out on urban cool island effect, its characterization and quantification (Rasul et al. 2015; Rasul et al. 2017). By connecting a conceptual boundary-layer model to a land-surface model,

Theeuwes et al. (2015) established a broad physical explanation for the urban cool island effect. The difference in the early morning mixed-layer depth over the city (deeper) and over the rural area causes UCI, according to the study. One of the primary elements that define the duration and magnitude of UCI is urban morphology. According to Rasul et al. (2017), imminent studies should be directed toward SUHI archipelagos since it has a significant effect on temperature, moisture and precipitation of the region.

Several researchers have quantified Urban Heat Island (UHI) and Urban Cool Island (UCI) in green spaces and water bodies within cities however the studies on UCI across a whole urban area are in their infancy and require better apprehensions (Li et al. 2011; Balzter et al. 2017). Research in UCI will provide opportunities for urban planners and policymakers to implement adaptive management strategies for sustainable cities in an uncertain climate future (Fan et al. 2017).

Yang et al. (2017) used a lumped urban air temperature model to investigate the phenomena of UCI in a high-rise compact metropolis. A novel concept of urban cool island degree hours was used to assess the intensity and duration of UCI. When anthropogenic heat is low, a high-rise and high-density city see a large daytime UCI, which is owing to increased heat storage capacity and lower solar radiation gain on urban surfaces. When there is no anthropogenic heat in a low-rise, low-density city, the UCI exists, but it quickly vanishes when there is minimal anthropogenic heat, and the UHI phenomena take over.

An urban cool island effect is observed in some parts of Central India during the winter season as reported in few studies (Ghosh et al. 2017). Majority of urban areas in India have negative SUHI during the daylight during the pre-monsoon summer season, and this is linked to low vegetation in non-urban areas during this period, resulting in less evapotranspiration (Ghosh et al. 2017). Heat waves in non-urban regions are more intense during pre-monsoon summer days due to greater LST leading to positive SUHI. These findings indicate the need for Surface Urban Heat Island Intensity (SUHII) to be

re-evaluated in India for climate adaptation, heat stress alleviation, and urban microclimate study.

## **2.5 STUDIES ON IMPACT OF URBANIZATION ON BENGALURU**

Sudhira et al. (2007) reported the city profile of Bengaluru with focus on urban settings and urban fabric. The challenges in planning for better management of basic services in the city were detailed. From 1973 to 2007, an increase of 466 percent paved surface has resulted in a 2% rise in LST, validating the occurrence of urban heat island in Greater Bengaluru (Ramachandra and Kumar 2009).

LSTs were found to be lower in vegetation and water bodies than in other land cover categories. The mean air temperature of the city centre is found to be substantially lower than that of the expansion zones due to the presence of water bodies and vegetation (Ambinakudige 2011). The temperature of the city centre, on the other hand, has fluctuated dramatically among different land cover classifications.

The existing clumped urbanization at the city centre with minimal headroom for additional urban densification implies that greater Bengaluru's future development will be in the peri-urban environments (Aithal et al. 2013). Urban simulation modelling combined with spatial metrics is helpful in capturing and displaying the spatio-temporal patterns of urbanization, as well as providing insights into the trajectory of urban expansion, for city planning.

Leapfrog development in core regions and ribbon development and cluster-based development in the buffer zones was observed in a time series analysis of land use change (Aithal et al. 2018). Urban sprawl was concentrated in places with better connectivity (Bharath et al. 2018).



## **2.6 APPLICATION OF SUPPORT VECTOR MACHINE ALGORITHM IN REMOTE SENSING**

Vapnik (1995) introduced the Support Vector Machine (SVM) approach, which is based on statistical learning theory and has lately been employed in various remote sensing applications. SVMs are supervised classifiers and scientists have enhanced SVMs to function with limited quantity and quality of training samples (Mountrakis et al. 2011).

Blanzieri and Melgani (2008) examined how to develop localised SVM techniques using a local k-nearest neighbour adaption. Their findings showed significant gains, particularly when non-linear kernel functions were used. Tuia and Camps-Valls (2009) proposed a regularisation approach for identifying kernel structure using unlabelled data to solve the issue of kernel predetermination. Using the Hilbert–Schmidt independence criterion, Camps-valls et al. (2010) provided an improved technique for testing kernel independence in diverse picture forms. Marconcini et al. (2009) investigated the inclusion of geographical information using composite kernels, finding significant gains but at a higher cost of computation.

Ghoggali and Melgani (2008) tested the performance of combination of genetic algorithm and SVM for remote sensing categorization using a restricted number of training data. The experimental findings demonstrated that even with a minimal training sample size, it is possible to enhance classification accuracy. For unsupervised change detection, Bovolo et al. (2008) used an SVM with a selective Bayesian thresholding technique. Dixon and Candade (2008) compared the algorithms: MLC, backpropagation neural network, and an SVM-based classifier for medium resolution imaging (15–30 m pixel size). A statistical analysis of a Landsat landscape revealed evident flaws in the MLC approach, although the findings for neural network and SVM classifiers were identical. Kaheil et al. (2008) created a wavelet and SVM-based synthetic method to estimate evapotranspiration at the input data's finest spatial resolution based on input variables such as MODIS LAI, MODIS emissivity, and spectral data from Landsat TM and ASTER.

Durbha et al. (2007) adopted a modified support vector regression method which involved parameter regularization for the retrieval of leaf area index from multiangle imaging spectroradiometer data and the validation of the results with field data offers a fairly good agreement. Moser and Serpico( 2009) estimated the land and sea surface temperatures using an automated parameter optimization approach for SVM regression. The proposed technique was more efficient compared to traditional grid-search based optimization methods like cross-validation and hold-out employing To sharpen multispectral bands utilising a higher resolution panchromatic band, Zhang and Ma (2008) developed a multiscale mapped least squares SVM (LS-SVM). The studies employed QuickBird data and included multiscale Gaussian radial basis function kernels. The approach was compared to various fusion methods such as curvelet transform, discrete wavelet transform, extended fast IHS and atrous wavelet transform and it was discovered that the proposed method and atrous wavelet transform performed the best.

SVR has been used in a wide variety of remote sensing problems like biomass estimations (Gleason and Im 2012), urban land cover determination from imaging spectrometer data (Okujeni et al. 2013) and bio-physical parameters from satellite reflectance measurements (Verrelst et al. 2012). The maximum night time urban heat island was predicted using SVM regression models based on the following variables: NDVI, surface albedo, atmospheric aerosol optical depth, relative aerosol optical depth, humidity, sunlight hour, and precipitation (Zhou et al. 2011).

The scale dependency of regression algorithm: Partial least square regression, gradient boosting machine, and support vector machine for the prediction of LST was analysed by Ghosh and Joshi (2014). Gradient boosting machine and SVM performed better for sharpening the image compared to partial least square regression. Piri et al. (2015) reported the accuracy of the SVR approach in estimating solar radiation using meteorological factors: Sunlight hours, maximum temperature, minimum temperature, average relative humidity, and daily solar radiation. The results of the statistical indicators coefficient of determination ( $R^2$ ) and Root Mean Square Error (RMSE)

indicate the superiority of the SVR model over the empirical models based on sunshine duration.

Moosavi et al. (2016) reported that PSO-SVR model furnished better results with an RMSE of 1.29 and  $R^2$  value of 0.93 compared to Particle Swarm Optimization with Adaptive Neuro Fuzzy Inference System (PSO-ANFIS) at 100 spatial resolution. Mathew et al. (2016) predicted the LST of Chandigarh city using an SVR model. The model was developed with input parameters road density, enhanced vegetation index, elevation and LST of the previous three years. SVR model performed better compared to artificial neural network model for the prediction of LST.

Abu Awad et al. (2017) employed nu-SVR, which involves nonlinear terms and higher-order interactions, as well as proper regularisation of parameter estimates for modelling the short and long-term black carbon exposures across Massachusetts, Rhode Island, and New Hampshire. SVR with improved particle swarm optimization (IPSO) method performed better in comparison to M5 tree model and multivariate adaptive regression model for the prediction of solar radiation as reported by Ghazvinian et al. (2019). Combination of sophisticated meta-heuristic optimization methods and SVR should be explored since it will improve the accuracy of prediction of solar radiation.

Groundwater potential map was created using SVR and metaheuristic optimization methods such as grey wolf optimization and Particle Swarm Optimization (PSO) for the Gangneung-si region, based on 13 groundwater-related characteristics (Fadhillah et al. 2021). The performance of SVR algorithm improved by the introduction of meta-heuristic optimization approach for fine tuning its parameters. PSO is useful for solving nonlinear problems since it converges quickly and requires minimal calculations (Fadhillah et al. 2021). The statistical calculation of next-day night-time SUHI by combining satellite data and in-situ meteorological data of a few selected cities in China using SVR was reported Lai et al. (2021).

## **2.7 SUMMARY OF LITERATURE**

A lot of studies have been carried out in the past relating to the effect of urbanization on the environment. Urbanization is a continuous process, and its impacts are also aggravating day by day. SUHI/SUCI are the two major impacts of urbanization. Researchers have quantified the impact of LULC on LST using different approaches in an urban heat island, but very few studies have been carried out on urban cool island. The research on urban cool island is in its infancy and should be quantified in detail to identify the causes and effects of the same. Remote sensing techniques can be used as an effective tool in monitoring the various effects of urbanization.

A thorough review of the various algorithms used for retrieval of land surface temperature from satellite images was carried out. Many researchers have studied and quantified the impact of land use land cover change on the land surface temperature. But very few works of literature are available in which a model is formulated to establish the relationship between the various land use and land surface temperature. Therefore, developing a new model for the region will be vital to understanding the spatiotemporal patterns of UHI and help in predicting the impact of land cover on land surface temperature in the future. An area of intense research in UHI monitoring is the techniques for data analysis and interpretation that integrate the temporal variations. The surface temperatures of urban agglomerations and cities with different climate conditions and ecosystems can be investigated using remote sensing. Micro and local level UHI research based on statistical regression models should be encouraged. Recently, artificial intelligence and machine learning algorithms are widely used for UHI studies.

SVR produced better results in comparison to multiple linear regression and artificial neural network with backpropagation. SVM has great generalisation ability when compared to other nonlinear machine learning techniques, such as the artificial neural network and is recognised as one of the best learning algorithms for low sample counts. The performance of SVR models can be improved by tuning the parameters with optimization algorithms. PSO algorithms have better results for tuning SVR parameters compared to other optimization algorithms for different applications. Integration of

machine learning algorithms and remote sensing data facilitates a comprehensive study of surface temperature of a region.

From the literature reviewed it is clear that many studies have been conducted to study the effect of urbanization on climate change. Nevertheless, only a few studies have been conducted in the Bengaluru region relating to the effect of urbanization on climate change using remote sensing techniques. This study mainly focuses on the impact of urbanization on the temperature, in particular, using remote sensing data.

## **2.8 RESEARCH GAPS**

From the above mentioned observations, a detailed study regarding the effect of urbanization on temperature is very crucial in climate change studies of a particular region. Future predictions will be possible by establishing a relationship between these parameters. Hence the proposed study aims at establishing a relationship between land surface temperature and major land cover classes in an urban environment. The study aims at exploring various remote sensing techniques for quantifying the anomalies in the surface temperature

Earlier studies on Bengaluru are mainly focussed on the UHI of the region since it is carried out in Greater Bengaluru. This study considers the whole of Bengaluru urban district which facilitates the exploration of the phenomenon of UCI. Hot spot analysis helps in the identification of statistically significant hot and cold spots which is a distinctive finding in the region. Another contribution of the research work being, the future prediction of LST exploiting the relationship between land cover types and LST through time.

## CHAPTER 3

### STUDY AREA

---

---

#### 3.1 INTRODUCTION

The study area selected is the Bengaluru urban district in Karnataka state, India. Bengaluru is popularly known as the 'Garden city of India' and the information technology capital of India. It is famous for its cultural heritage and industries encompassing Information Technology (IT), aerospace, manufacturing, and other sectors. Kempe Gauda, a scion of the Yelahanka dynasty who eventually established himself in Magadi, is credited with the creation of modern Bengaluru in 1537 A.D. During his governance, four watchtowers were installed at the four cardinal points predicting the expansion of Bengaluru in the course of time. Bengaluru has preserved its unique cultural linkages keeping up with its tradition, culture and history, despite the hype around IT based and other commercial activities.

#### 3.2 PHYSIOGRAPHY AND CLIMATE

The Bengaluru urban district is geographically located between 77°34'19" E - 12°59'34" N and 77°38'13" E - 12°56'38" N, respectively, as shown in Figure 3.1. The Bengaluru urban district has a geographical area of 2,196 km<sup>2</sup> and is located at an altitude of about 900 m above mean sea level. It is situated midway between the eastern and western coast of the Indian peninsula. The maximum distance between the eastern and western tip of the district is approximately 50 kilometers and the northern to southern tip extends to about 58 kilometers.

Bengaluru urban district is constituted by four taluks: Bengaluru East, Bengaluru North, Bengaluru South and Anekal. Anekal taluk, Bengaluru South and Bengaluru East are characterised by an uneven landscape with a combination of hills and valleys. The elevation of Bengaluru South ranges from 717 to 973 metres while for Bengaluru East taluk it is between 860 to 928 metres. Bengaluru North is a level plateau with elevation

ranging from 839 to 963 metres above mean sea level. A prominent ridge runs between north-easterly to south-westerly in the middle of the taluk. The state of Tamil Nadu bounds the Bengaluru urban district in the southeast, the Ramanagara district in the southwest, and the Bengaluru rural district in the northeast and northwest.

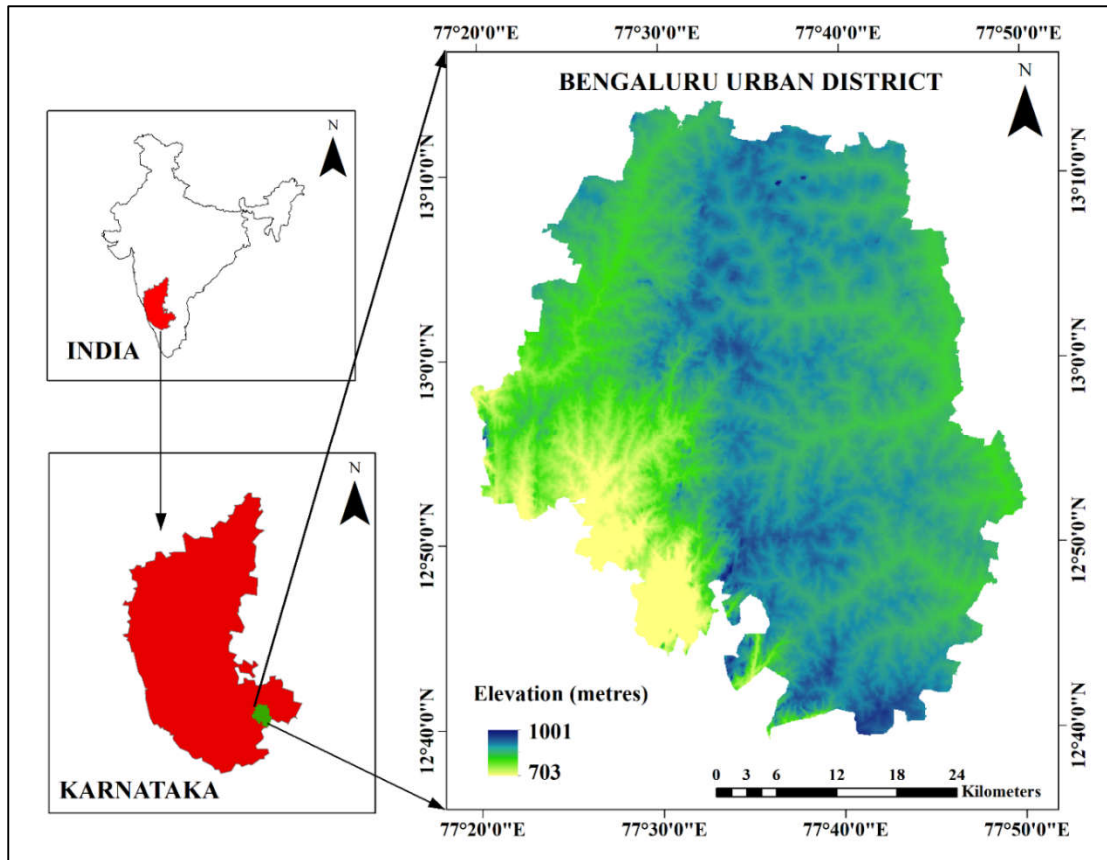


**Figure 3.1** Location map of the study area

The district receives a mean annual total rainfall of 880 mm. No major rivers are flowing in the district except Arkavati and South Pinakini rivers. The rivers are seasonal rivers and Arkavati is presently polluted with sewage. A series of tanks with different sizes are located in the eastern parts of Bengaluru South taluk and Bengaluru East taluk.

### 3.2.1 Geomorphology

Granite and gneisses are the chief rock types present in Bengaluru North taluk. This is exposed in the middle of the taluk as a ridge running north-north easterly and south-

south westerly. The granitic gneisses are crisscrossed by pegmatitic and aplitic veins. Basic xenolithic patches are common and banding is prominent (Directorate of Census operations 2011). The rocks are characterized by sheet jointing parallel to the exposed surface, which is a unique property of Bengaluru gneisses. The longitudinal joints are predominantly seen providing an appearance of tilted beds, on weathered surface.

### 3.2.2 Climate

The study area experiences a seasonal dry tropical savanna climate. There are four main seasons: the summer season from March to May, the southwest monsoon from June to September, the retreating monsoon in October and November and the dry season from December to February.

#### 3.2.2.1 Rainfall Pattern

Bengaluru is bestowed with two rainy seasons corresponding to southwest and northeast monsoons from June to September and October to November, preceding one another but with opposite wind regimes. The rainfall pattern of the study area from 1901 to 2011 is presented in Figure 3.2.

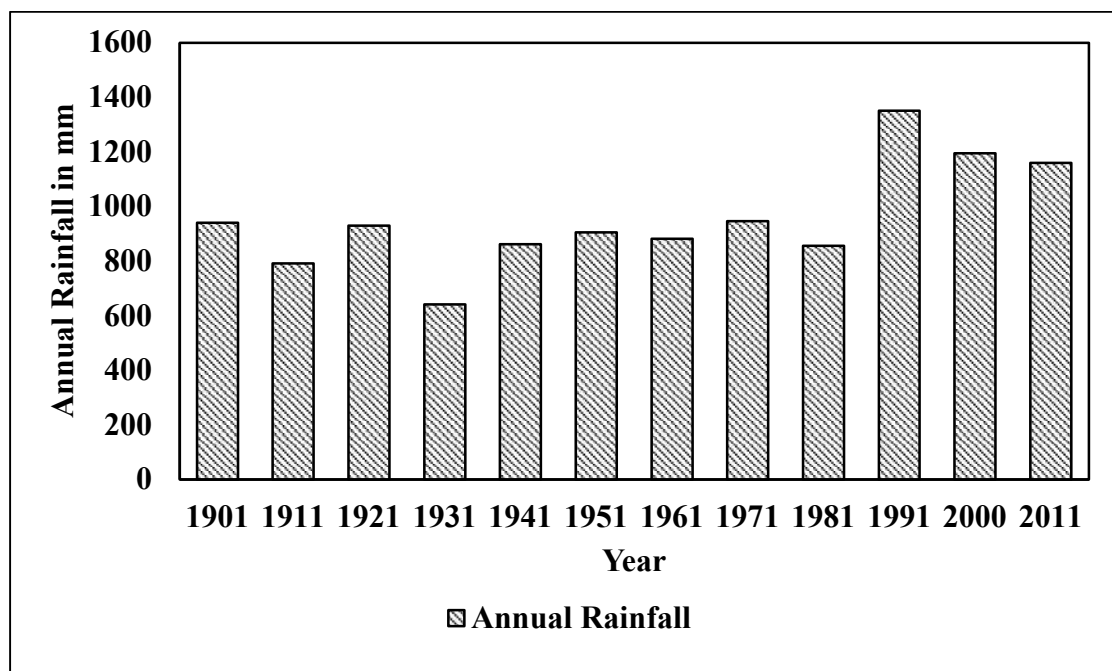


Figure 3.2 Distribution of annual rainfall in the region from 1901 to 2011



The pre-monsoon rainfall accounts for 19 to 20 percentage of the annual rainfall, north east monsoon contributes 25 to 28 percentage and south west monsoon contributes 52 to 56 percentage of the annual rainfall. A relatively high variability of rainfall is experienced by Anekal taluk.

### 3.2.2.2 Temperature

One of the significant aspects of the climate of the district is the agreeable range of temperature, from the lowest maximum of 14°C in January to the highest maximum of 33°C in April. The winter temperature of the district varies from 12°C to 25°C, while the summer temperature ranges from 18°C to 38°C. From the analysis of monthly temperature and rainfall data from 1901 to 2000, it can be understood that the highest value of the maximum and minimum temperature is recorded in April and May months, while the mean rainfall is highest during September and October (Figure 3.3).

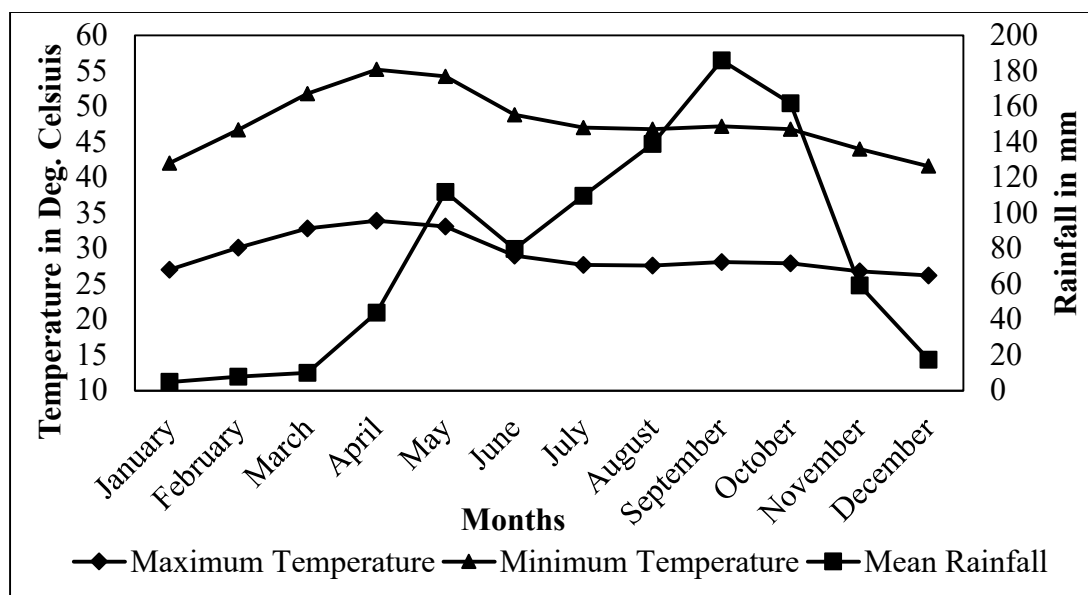


**Figure 3.3 Variation of monthly mean temperature and rainfall of Bengaluru district based on 1900-2000 data.**

### 3.2.2.3 Wind Pattern

The winds are west-south westerly to westerly in period from May to September and easterly-north easterly to easterly-south easterly during the period from November to

March. The transition of the wind regime from easterly to the westerly and vice versa take place during the months April and October.

### **3.2.3 Soil**

Red fine loamy to clay soils and red laterite are the main soil types in Bengaluru urban district. The laterite soil is characterized by red and pale-yellow colour and very low base exchange capacity. It is easy to cultivate when moist and the crops grown include jowar, ragi and groundnut. The red loams are porous and friable with light texture. The texture of the soils varies from gravel to sandy loam to clay loam. The clay fractions of the red soils are rich in Kaolinitic type of minerals (Directorate of Census operations 2011).

## **3.3 URBANIZATION**

Presently, Bengaluru has become one of the swiftly growing cities in the World from a tiny village way back in the 12<sup>th</sup> century. It has been branded as the 'Silicon Valley' of India and is one of the leading technological innovation hubs with a high technological achievement index of 13 as per the Human Development Report (Sudhira et al., 2007).

### **3.3.1 Demography**

From 2001 to 2011, Bengaluru urban district recorded a population growth rate of 47.18 percent. The decadal growth rate increased by 12.10 percent compared to the previous growth rate. The decadal growth rate of rural areas is 12.16 percent, and that of urban areas is 51.91 percent which is considerably more than the rate registered in rural areas. The annual rainfall received also exhibits an increasing trend. The extent of urbanization in the study area can be acknowledged by a tremendous increase in population in the past few years. Since 1970, there has been a steep increase in the region's population (Figure 3.4). Similarly, the plot of annual rainfall exhibits a prominent increase after 1980.

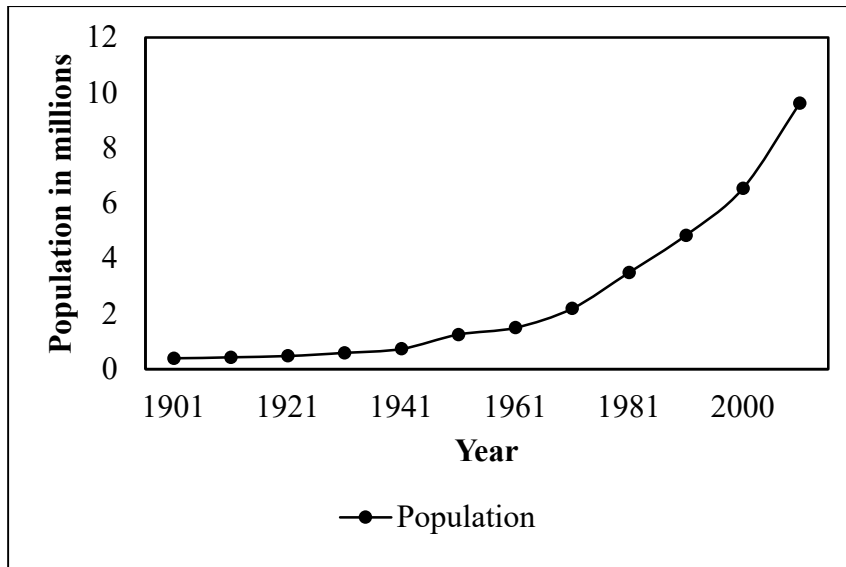


**Figure. 3.4 Distribution of the population in the region from 1901 to 2011**

### 3.3.2 Impact of Urbanization on Climate

The temperature of Bengaluru has increased by about 2°C from 1973 to 2007, confirming the urban heat island phenomenon (Ramachandra & Kumar, 2009).

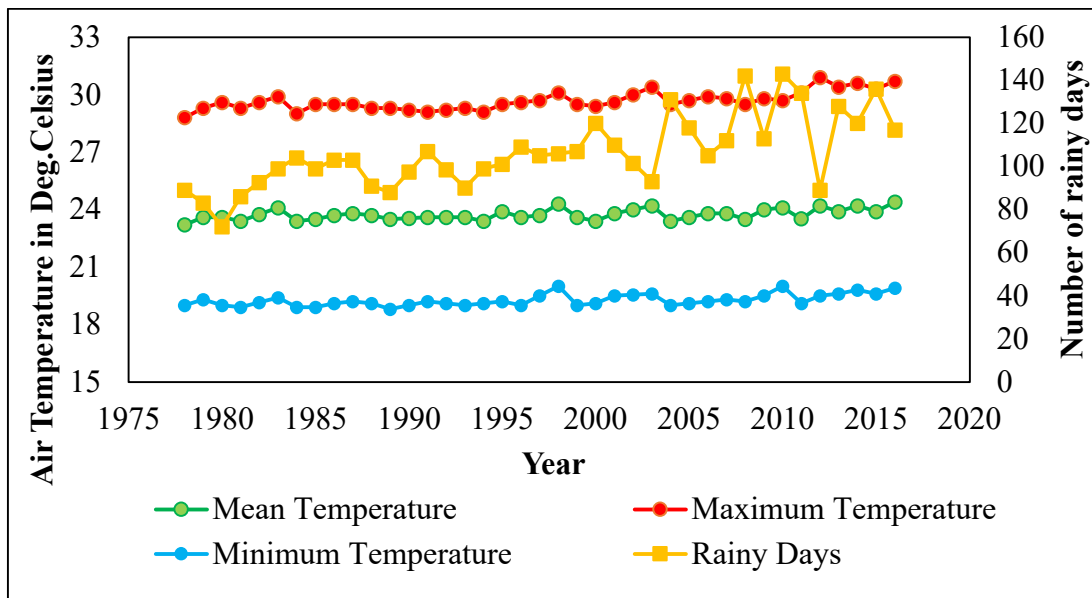


**Figure 3.5 Annual Temperature variation with number of rainy days in the Bengaluru region from 1978 to 2016**

From the analysis of climate variables for the past few decades, it was observed that there is an increase in the region's minimum, maximum and average temperature and an increase in the number of rainy days was also spotted during the same period (Figure 3.5).

Over the years there has been a sharp decline in the number of water bodies in the region. Another main issue of the study area is the frequently occurring flash floods. It poses a threat to the life and property of the inhabitants in the area. Recently, flash floods have become very common in the region. Within just few hours of rain most of the low lying areas in Bengaluru will be under water. The storm water drains will not be able to take the load resulting in water overflowing in several roads.

The increase in precipitation and the rainy days can be attributed to the region's change in temperature and land use land cover. According to previous studies, there has been a significant change in the land use land cover of the region. Therefore, a detailed study on the spatial and temporal variation of LULC and LST and their interrelationship by considering the Bengaluru district as a whole is pertinent at this point in time.



### DATA AND METHODS

---

---

The study employs cloud-free satellite images to analyse the LST and LULC change patterns. This chapter mainly discusses the data sets, detailed methodology and the computational tools employed for this study.

#### 4.1 DATA

The study is mainly focused on the dry season and employs Landsat 5 Thematic Mapper (TM), Landsat 8 Operational Land Imager (OLI), and Moderate Resolution Imaging Spectroradiometer (MODIS) images. Table 4.1 illustrates the details of the data used in the study. The images were acquired at around 10.00 A.M Indian Standard Time. The Landsat images were used for LULC mapping and LST retrieval during the daytime, while MODIS data were used for LST validation and for acquiring night-time LST. The study uses various remote sensing methods to estimate the LST and LULC of the study area for the years 1989, 1994, 2001, 2005, 2014 and 2017. The study used toposheets from the Survey of India to prepare a base map: 57G8, 57G12, 57G15, 57G16, 57H5, 57H6, 57H9, 57H10, 57H13 and 57H14.

#### 4.2 COMPUTATIONAL TOOLS

The study used two complementary computational software tools: ArcGIS10.1<sup>©</sup> and ERDAS Imagine 14<sup>©</sup>, along with R 4.1.0 and MATLAB 2015a<sup>©</sup>.

##### 4.2.1 ArcGIS 10.1

ArcGIS developed by Environmental Systems Research Institute (ESRI) was first released in 1999. ArcGIS is a GIS software used to support field workflow, analyse and visualize data. The maps were created to facilitate the identification of spatial patterns for better planning and decision-making. ArcGIS is developed around a geodatabase in

which spatial data is stored using an object-relational database approach. It provides tools to manage and extract information from remotely sensed datasets. The study employs ArcGIS version 10.1 to analyse the land cover patterns and land surface temperature and to prepare various maps.

**Table 4.1 Specifications of the remote sensing data used in the study**

Sensors	Date of Acquisition	Path /Row	Bands/Product used	Resolution (m)	Source
Landsat 5 TM	22-02-1989	144/51	5,4,3,2 6	30 120*(30)	earthexplorer.usgs.gov
Landsat 5 TM	20-02-1994	144/51	5,4,3,2 6	30 120*(30)	earthexplorer.usgs.gov
Landsat 5 TM	27-03-2001	144/51	5,4,3,2 6	30 120*(30)	earthexplorer.usgs.gov
Landsat 5 TM	18-02-2005	144/51	5,4,3,2 6	30 120*(30)	earthexplorer.usgs.gov
Landsat 8 OLI	15-03-2014	144/51	6,5,4,3 10	30 100*(30)	earthexplorer.usgs.gov
Landsat 8 OLI	23-03-2017	144/51	6,5,4,3 10	30 100*(30)	earthexplorer.usgs.gov
Landsat 8 OLI	31-03-2020	144/51	6,5,4,3 10	30 100*(30)	earthexplorer.usgs.gov
MODIS (MYD11A1)	18-02-2005	25/7	LST	1000	ladswb.nascom.nasa.gov
MODIS (MYD11A1)	15-03-2014	25/7	LST	1000	ladswb.nascom.nasa.gov
MODIS (MYD11A1)	23-03-2017	25/7	LST	1000	ladswb.nascom.nasa.gov

\*Thermal band is acquired at different resolution, but products were resampled to 30m pixels by NASA

#### **4.2.2 ERDAS IMAGINE 14**

ERDAS IMAGINE is a satellite image processing tool developed for analysing geospatial data in both vector and raster formats. The software could explore various datasets including optical panchromatic, multispectral, hyperspectral imagery, radar, and LiDAR data. ERDAS IMAGINE powered by Intergraph Corporation is a comprehensive package supporting multiple workflows including orthorectification, terrain creation, editing and analysis. The study uses ERDAS IMAGINE 14 software for land cover classification and land surface temperature retrieval from Landsat data.

#### **4.2.3 R 4.1.0**

R tool developed by Ross Ihaka and Robert Gentleman, is an open-source software environment for statistical computing and graphics. It includes a well-developed, simple and effective programming language for data manipulation and calculations. The software's capabilities are extended by the user created packages, including statistical techniques, reporting, etc. One of the main advantages of R is the ease of installation and user-friendly interface. It has an extensive, intelligible, comprehensive collection of intermediate tools and graphical facilities for data analysis. R 4.1.0 was employed in the study to analyse the land cover and land surface temperature data based on the concentric ring approach and multiple linear regression.

#### **4.2.4 MATLAB 2015a**

MATLAB (MATrix LABoratory) developed by MathWorks is a registered fourth-generation programming language to analyse data, develop algorithms and create models. The main capabilities of the software include data analyses, programming, external language interfaces and parallel computing. It can be employed for various image processing and machine learning applications. It facilitates graphics for visualizing data, matrix manipulations, implementation of algorithms and interfaces to Python, Java, C/C++, .NET, SQL, and Microsoft Excel, etc. MATLAB has add-on toolboxes that are application specific in advance research activities. The study employs



MATLAB R2015a for coding of Hybrid PSO-SVR algorithm. LIBSVM toolbox was used for coding the model.

### 4.3 OVERALL METHODOLOGY

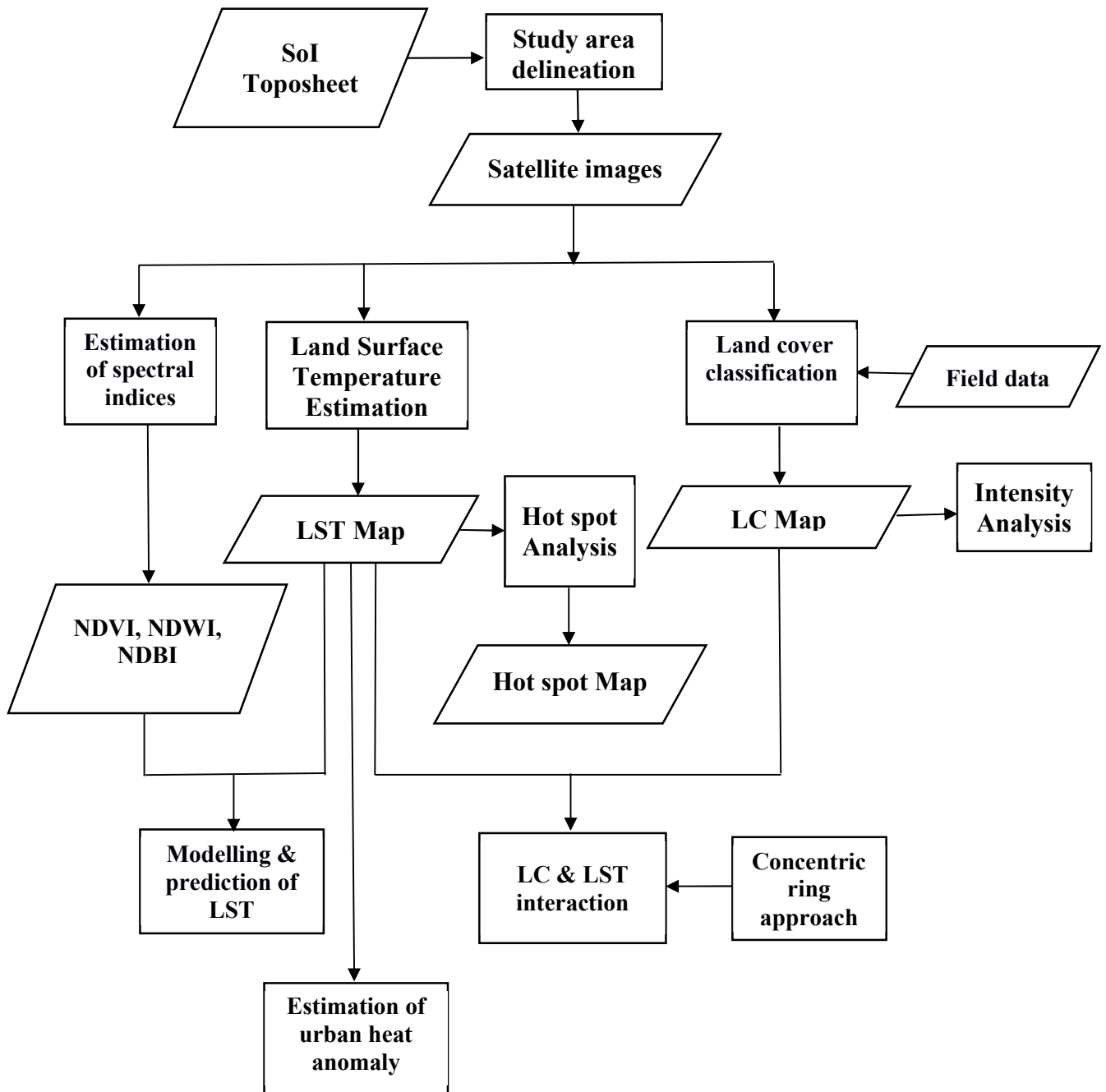


Figure 4.1 Overall methodology of the research work

The overall methodology of the study is described in Figure 4.1. The first step includes data collection. The data required comprises satellite images and various ground truth data. The Survey of India (SoI) toposheet was used to delineate the study area. Land Surface Temperature was retrieved from Landsat images by employing a radiative transfer equation. The land cover classification was conducted using the Maximum likelihood algorithm. The spatio-temporal land cover patterns were analysed using Intensity analysis, while the spatio-temporal variation of LST is quantized by employing hot spot analysis.

Land cover and LST interaction were explored using the concentric ring approach. Linear and non-linear relationship between LST and surface area ratios was analysed for the years 1989, 2001, 2005 and 2017 by employing multiple linear regression and Hybrid PSO-SVR model respectively. Multiple linear regression and Hybrid PSO-SVR model was adopted to quantify the interrelationship between urban surface characteristics and LST, the future LST was predicted using Hybrid PSO-SVR model. Further, the temporal patterns of urban heat anomaly in the study area were investigated.

#### **4.4 ALGORITHMS**

This section explores the significant algorithms employed in this study. This research work uses multiple linear regression, support vector regression, and particle swarm optimization for linear and non-linear analysis.

##### **4.4.1 Multiple Linear Regression**

In simple linear regression, the relationship between two variables is modelled where,  $x$  is the predictor or independent variable and  $y$  is the response or dependent variable. The response  $y$  is usually controlled by more than one independent variable. A linear model represents the relationship between a continuous random variable  $y$  and different predictors, which has the form:

$$y = \beta_0 + \beta_1x_1 + \beta_2x_2 + \dots + \beta_kx_k + e \quad (4.1)$$

Where  $\beta_0, \beta_1, \dots, \beta_k$  are the regression coefficients,  $e$  describes the random variation of  $y$  not defined by  $x$  variables, which may be due to the effect of other variables on  $y$  which are not observed or not known (Vogt and Johnson, 2015).

Regression models can be used for various purposes such as prediction, data description, parameter estimation, variable screening and control of the output.

The model for  $i^{th}$  observation is given by:

$$y_i = \beta_0 + \beta_1 x_{i1} + \beta_2 x_{i2} + \dots + \beta_k x_{ik} + e_i \quad (4.2)$$

Assumptions for  $e_i$  or  $y_i$  is as follows:

For  $i = 1, 2, \dots, n$

- (i)  $E(e_i) = 0$  or, equivalently,  $E(y_i) = \beta_0 + \beta_1 x_{i1} + \beta_2 x_{i2} + \dots + \beta_k x_{ik}$
- (ii)  $var(e_i) = \sigma^2$  or, equivalently,  $var(y_i) = \sigma^2$
- (iii)  $cov(e_i, e_j) = 0$  for all  $i \neq j$  or, equivalently,  $cov(y_i, y_j) = 0$

- Assumption 1 specifies that all relevant independent variables ‘ $x$ ’ are included in the model and is linear.
- Assumption 2 states that the response variance ‘ $y$ ’ is constant and does not depend on the values of predictor variables ‘ $x$ ’.
- Assumption 3 asserts that the values of the dependent variable ‘ $y$ ’ are uncorrelated with each other.

The model eq. (4.2) is framed based on these assumptions. Regression coefficients can be determined by employing the least-squares approach. Least-squares method is based on the principle that the sum of squares of deviations is minimum.

#### 4.4.2 Support Vector Regression

Support Vector Machines (SVM) proposed by (Vapnik, 1995) is a popular machine learning algorithm for identifying patterns and evaluating data that can be used for classification, prediction and regression analysis. It is one of the popular techniques for analysing sophisticated patterns of data (Rajabi-Kiasari and Hasanlou, 2020). SVM is

a non-probabilistic binary classifier, separates the data using linear boundaries. The SVM concept fits a hyperplane to a set of data points such that the distance of the closest points to the hyperplane is maximum. The closest points are called the support vectors and the distance of the support vectors from the hyperplane is termed as margin. The basic assumption is that the positive and negative points are linearly separable by a linear decision surface. Non-linear classification and regression are implemented by mapping the input features into higher dimensional feature space using the kernel trick (Mathew et al., 2019). Support Vector Classification (SVC) and Support Vector Regression (SVR) are two subclasses of SVM.

Vapnik (1995) introduced SVR with a few minor differences in the principle of SVM classification. The most common type of SVR model that uses  $\varepsilon$  – insensitive loss function to solve linear and non-linear regression problems in higher dimensional feature space called as  $\varepsilon$ -SVR.

Consider a training dataset:

$$D = \{(x_i, y_i) | x_i \in R^d, y_i \in \{-1, 1\}\}_{i=1}^n \quad (4.3)$$

Where  $x_i$  is the input value with  $n$  as the dimension of input space and  $y_i$  is the output value.

SVR method is applied by defining a linear regression function

$$y = f(x) = w^T \varphi(x) + b \quad (4.4)$$

Where  $f(x)$  represents the forecasted value.  $\Phi(x)$  is the non-linear function in terms of input variable  $x$ . Hyperplane bias parameter and weight factor are given by  $b$  and  $w$  respectively.

These coefficients can be estimated by solving the following minimization problem.

$$\min(R(c)) = \frac{1}{2} \|w\|^2 + c \cdot \frac{1}{n} \sum_{i=1}^n |y_i - f(x)|_\varepsilon \quad (4.5)$$

$$|y_i - f(x)|_\varepsilon = \begin{cases} 0 & \text{if } |y_i - f(x)| \leq \varepsilon \\ |y_i - f(x)| - \varepsilon & \text{Otherwise} \end{cases} \quad (4.6)$$

Where,  $\varepsilon$  is the insensitive loss function. The loss function will be zero if the predicted data lie within the tube of radius  $\varepsilon$  (Figure 4.2). Slack variable  $\xi$ ,  $\xi^*$  are defined as the deviation on both sides of the decision surface (Figure 4.3).  $C$  is the regularization parameter defining the trade-off between model flatness and empirical risk.

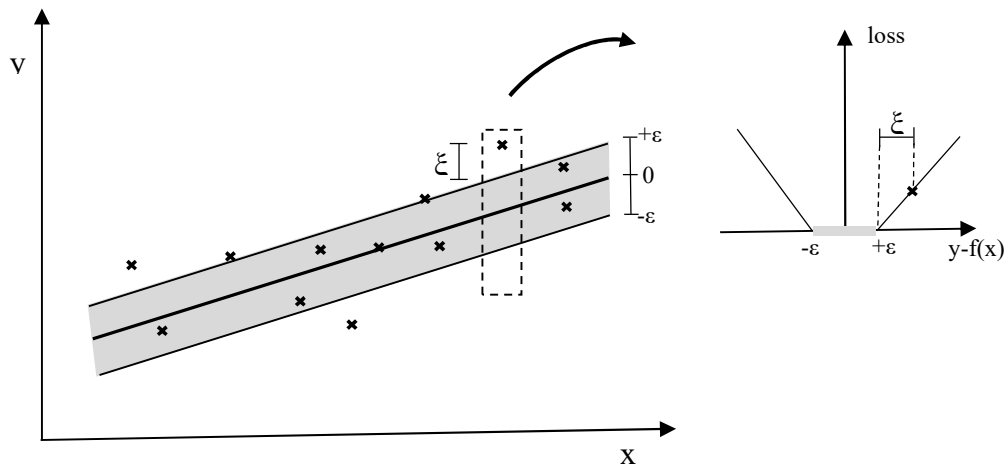


**Figure 4.2 Solution of SVR problem in graphical form (Source: Smola and Schölkopf, 2004)**

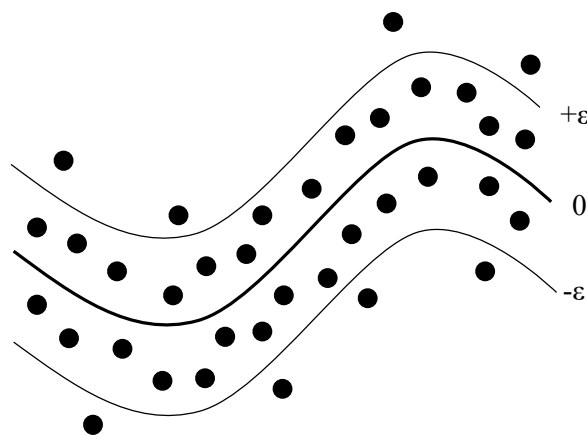


**Figure 4.3 The tube of radius  $\varepsilon$  defined by SVR algorithm within which the forecasted value must lie (Source: Panahi et al., (2021)).**

Equation 4.5 can be rewritten as:

$$\text{Min } R(w, \xi, \xi^*) = |w|^2 + C(\sum_{i=1}^N(\xi + \xi^*_i)) \quad (4.7)$$

With constraints,

$$w\varphi(x_i) + b_i - d_i \leq \xi_i + \xi^*_i \quad \text{for } i=1,2,3 \dots N \quad (4.8)$$

$$d_i - w\varphi(x_i) - b_i \leq \xi_i + \xi^*_i \quad \text{for } i=1,2,3 \dots N \quad (4.9)$$

$$\xi_i, \xi^*_i \geq 0 \quad \text{for } i=1,2,3 \dots N \quad (4.10)$$

The Primal Lagrangian equation can solve the constrained optimization problem. The SVR function can be represented in terms of Lagrangian multipliers  $\alpha_i$  and  $\alpha_i^*$  and kernel function  $k(x_i, x_j) = (\Phi(x_i), \Phi(x_j))$  (Smola and Schölkopf, 2004) as:

$$f(x) = \sum_{i=1}^n(\alpha_i - \alpha_i^*)k(x_i, x_j) + b \quad (4.11)$$

The kernel function transforms the input dataset into feature space (higher dimensionality space) through non-linear transformation. In order to achieve maximum accuracy, precise estimation of  $C$ ,  $\varepsilon$ , type of kernel function and optimal value for the kernel function parameter is necessary (Panahi et al., 2021)

Researchers have proposed different kernel functions (Pillonetto et al., 2014) and the most commonly used kernels are the polynomial functions and the Radial Bias Function (RBF) of the Gaussian kernel function. The kernel function to be employed depends on the problem and dataset, but RBF performs efficiently for a wide range of datasets.

The RBF function is given by:

$$k(x, x_i) = \exp(-\gamma|x - x_i|^2) \quad (4.12)$$

Where,  $\gamma$  is the bandwidth of RBF.

The combination of  $C$ ,  $\varepsilon$  and kernel function parameter  $\gamma$  determines the optimal generalization performance of SVR. Therefore, an optimization algorithm capable of

identifying this optimum combination of hyperparameters of SVR will result in a robust model.

#### 4.4.3 Particle Swarm Optimization

Particle Swarm Optimization (PSO), a nature inspired algorithm developed by (Kennedy & Eberhart, 1995) can be used for optimizing diverse engineering problems. PSO is a popular population-based optimization algorithm motivated by animal's social behaviour, such as schooling fish and flocking birds. Each particle termed as a candidate solution which moves in a trajectory defined by its own best position and velocity in the parameter space. Particles shift their position in the multidimensional search space until a global optimum is achieved, wherein cognitive and social learning forms the basis of the search experience. Cognitive learning involves focusing on each individual learning experience and exclusion of neighbour's experience, while social learning particle depends on its neighbors for guidance and ignores its own experience. The combination of these two models determines the change in position of particles by balancing the exploitation-exploration trade-off (Akande et al., 2017).

PSO begins with a randomly generated swarm of particles in a search space with its position and velocity constantly changing.  $\vec{X}_{P_{best}}$  stored in the particle's memory is the best position the particle occupies in the search space.  $\vec{X}_{G_{best}}$  is the best position (minimum error) attained by all the particles in the search process. Each particle shifts towards its best position compared with the group's best position and move towards that position, finally converging to a single point (Panahi et al., 2021).

In the PSO method a particle in D-dimensional search space constitutes two vectors,  $i^{th}$  particle position ( $\vec{X}_i = \{X_{i1}, X_{i2}, X_{i3}, \dots, X_{iD}\}$ ) and particle velocity ( $\vec{V}_i = \{V_{i1}, V_{i2}, V_{i3}, \dots, V_{iD}\}$ ).

The particles in the swarm change their position and velocity based on the following functions:

$$\vec{V}_i(t + 1) = w\vec{V}_i(t) + c_1r_1 \times [\vec{X}_{P_{best_i}} - \vec{X}_i(t)] + c_2r_2 \times [\vec{X}_{G_{best}} - \vec{X}_i(t)] \quad (4.13)$$

$$\vec{X}_i(t + 1) = \vec{X}_i(t) + \vec{V}_i(t + 1) \quad (4.14)$$

Where,  $\vec{X}_i(t+1)$  and  $\vec{V}_i(t+1)$  are the  $i^{th}$  particle position and velocity at  $(t+1)$  iteration respectively. The balance between global exploration and local exploitation is indicated by the optimal value of inertia weight,  $w$ . The optimal solution can be obtained with fewer iterations if the value of  $w$  is suitably selected. However, if the value of  $w$  is greater than one, then there is an increase in the particle velocity leading to a wider search space and unstable algorithm.  $c_1$  and  $c_2$  are the acceleration constant and learning factor respectively. The experiences of the individual particle are reflected by a cognitive parameter ( $c_1$ ), while the experiences of all particles is indicated by social parameter ( $c_2$ ). The values of these parameters have a notable impact on the movement of particles in each iteration, the optimal value of which aids convergence, avoids early convergence at local optima (Sheng et al., 2015).  $g_{best}$  refers to the fittest position of the entire swarm and  $p_{best}$  represents the best position  $i^{th}$  particle has ever reached in the  $t^{th}$  iteration.  $r_1$  and  $r_2$  are random vectors used to diversify the population with values ranging from 0 to 1 (Campana et al., 2013).

Eq. (4.13) can be divided into three parts: current velocity of the particles, cognitive component, which indicates the individual particle's behavior and social component which represents a collaboration among particles (Kennedy & Eberhart, 1995). If the first part is excluded, the algorithm searches only in the neighborhood of the best particle and does not explore the rest of the search space. At the same time, the exclusion of the second and third parts will result in a blind global search. To achieve the optimal results, balance between local and global search must be maintained by employing all three parts of the algorithm. The algorithm stops when no significant advancement occurs in the fitness function or when a specified number of iterations have conceded. Compared to other metaheuristic algorithms like genetic algorithms, the implementation of PSO algorithm is more straightforward, includes fewer calculations and operations, with higher convergence rates (Shi & Eberhart, 1998).





### **SPATIO-TEMPORAL PATTERNS OF LAND COVER AND LST**

---

---

#### **5.1 INTRODUCTION**

The present study aims to analyse the spatial and temporal distribution of LC and LST for the Bengaluru urban district in the urban cool island effect context. Assessing the spatial and temporal distribution of LST and LULC in the region is the need of the hour. Bengaluru is one of the fast-growing metropolitan cities of India with a semi-arid tropical climate. This study focuses on the characterization of UCI based on hot spot analysis, which is one of a kind in the study area. The analysis was performed from 1989 to 2017. The main objectives of this section are to: quantify the land cover change patterns and identify the driving factors, explore the spatio-temporal variation of LST, and assess the impact of LC change on LST using hot spot analysis for the period 1989-2017.

#### **5.2 METHODOLOGY**

The study uses various remote sensing methods to estimate the LST and LC of the study area for the years 1989, 1994, 2001, 2005, 2014 and 2017. The methodology of this chapter is described in Figure 5.1. Survey of India (SoI) toposheets were used to delineate the study area. The study area delineated from the Landsat images was used for land cover mapping and LST retrieval. The land cover pattern of the region during the period of study was analysed using intensity analysis. The spatio-temporal pattern of LST in the study area was explored based on hot spot analysis.

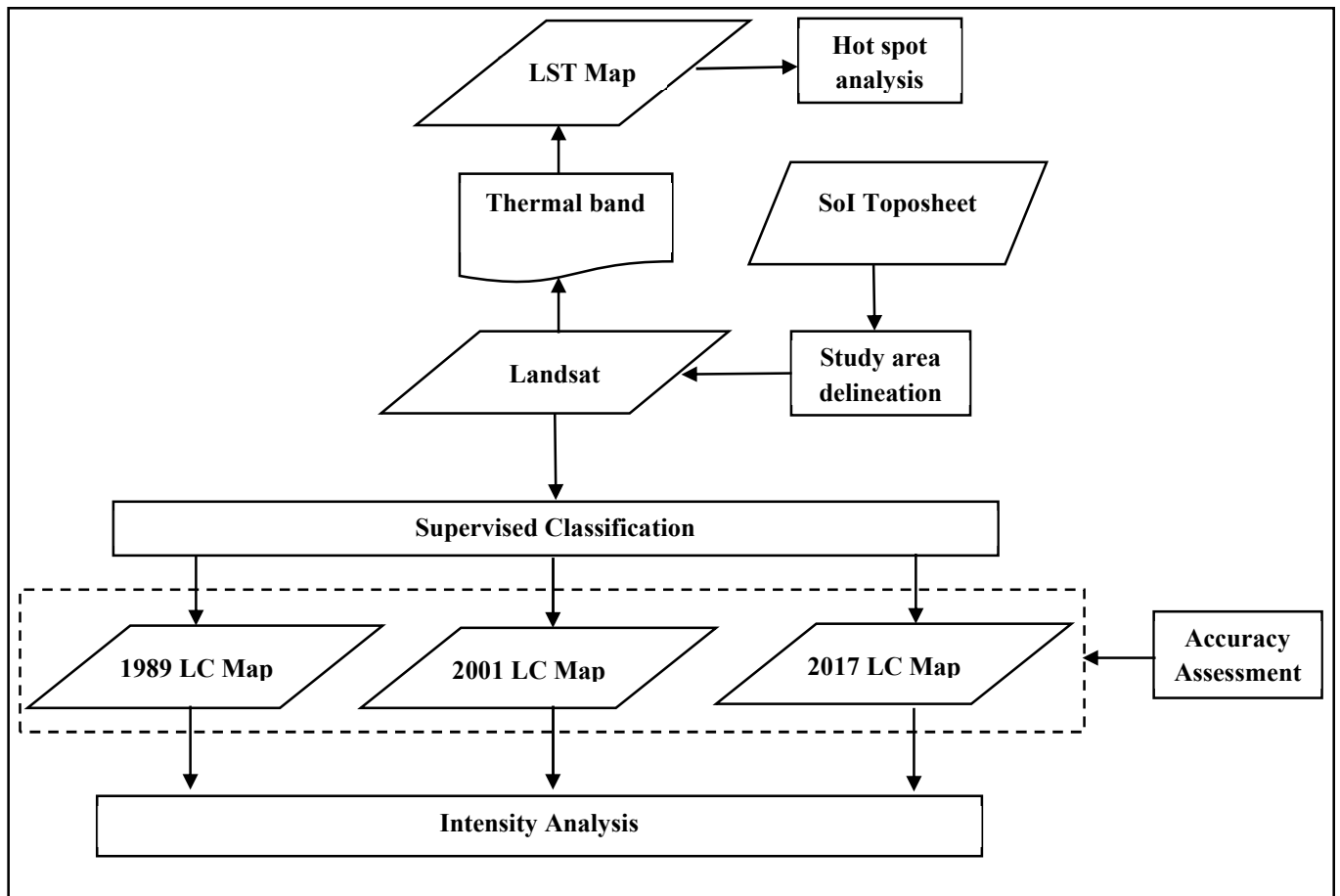


**Figure 5.1 Flowchart of methodology**

### 5.2.1 Land Use Land Cover Mapping

Land cover refers to the sort of features on the earth's surface and land use refers to the human activity or economic purpose that a piece of land serves. Land use and land cover information play a vital role in land planning and management activities. Land cover mapping is achieved by classifying the pixel in an image through different image classification techniques. Normally, multispectral data are used for classification. The numerical basis for categorization is the spectral pattern existing within the data for each pixel. i.e., various feature types express different combinations of digital numbers based on their inherent spectrum reflectance and radiometric characteristics. For each pixel, the term pattern indicates the radiance measurements recorded in different wavelength bands. The classification algorithms known as spectral pattern recognition

uses this pixel-by-pixel spectral information as the basis for automated land cover classification (Lillesand & Chipman, 2012).

The land cover classification is carried out based on supervised classification technique using Maximum likelihood algorithm. In supervised classification, the image analyst monitors the pixel categorization process by providing numerical descriptors of the various land cover types to the computer algorithm. Training areas include representative sample sites of known land cover types that are used to compose a numerical interpretation key that characterizes the spatial attributes for each feature type of interest. The supervised classification includes a training phase followed by a classification phase. Maximum likelihood classifier is based on the assumption that the data points in the training set is normally distributed. An unknown pixel is classified based on the probability density function by evaluating the probability of the pixel value fitting to each category. Maximum likelihood classifier exhibits good performance over a range of land cover types, conditions and satellite systems. It can readily handle covarying data which is very common in satellite images (Bolstad and Lillesand 1991).

Land Cover map of the region was prepared for the years 1989,1994, 2001, 2005, 2014 and 2017. It was prepared based on supervised classification by employing the maximum likelihood algorithm. Four broad Land Cover (LC) classes were identified: vegetation, water, barren and urban. The urban class includes commercial and industrial land, residential area, and impervious surface. The area of each land cover class was calculated for comparison.

### **5.2.2 Accuracy assessment**

An unbiased representation of the land cover of a region can be proved by the accuracy of the Land Use Land Cover (LULC) map. The accuracy of the LULC map is usually measured in terms of a confusion matrix. The rows and columns of the confusion matrix consist of sample points (pixels) allotted to a particular category relative to the actual category obtained from the ground (Congalton, 1991). The rows usually indicate the classified data from satellite images and the columns represent the reference data. The map's overall accuracy and each class's accuracy are obtained from the confusion

matrix. The overall accuracy is obtained by dividing the total correct pixels by the total number of pixels. The individual accuracy is measured using the user's accuracy (error of commission), based on classified data and the producer's accuracy (error of omission), based on reference data (Smits et al., 1999).

Kappa coefficient is another multivariate technique commonly used in accuracy assessment (Cohen, 1960) of classified image. It assesses whether the confusion matrix is significantly different from a random result. The Kappa analysis can be used to estimate if a classifier result is better than the other by comparing the two matrices (Smits et al., 1999). The Kappa coefficient ( $K$ ) is given by equation 5.1 (Congalton, 1991).

$$K = \frac{N \sum_{i=1}^r x_{ii} - \sum_{i=1}^r (x_{i+} * x_{+i})}{N^2 - \sum_{i=1}^r (x_{i+} * x_{+i})} \quad (5.1)$$

Where  $r$  is the number of rows in the matrix,  $x_{ii}$  is the number of observations in row  $i$  and column  $i$ ,  $x_{i+}$  and  $x_{+i}$  are the marginal totals of row  $i$  and column  $i$  respectively and  $N$  is the total number of observations. The value of  $K$  ranges from 0 to 1 where 1 represents the complete agreement between the classified and reference data (Pal and Ziaul, 2017).

This study used 230 ground-truth points from Google Earth and the field using Global Positioning System (GPS). The overall accuracy, individual accuracies and Kappa coefficient were determined. An overall accuracy higher than 85% indicates the best agreement between the classified and the ground-truth data (Foody, 2002).

### 5.2.3 Intensity Analysis

Intensity analysis was carried out to analyse the pattern of LC change. Based on the preliminary studies conducted in the study area, it is observed that major private sector companies were established around the year 2000, which led to the urban growth of

Bengaluru. Therefore, the duration of analysis was divided into two periods: period -1 from 1989 to 2001 and period-2 from 2001 to 2017 based on the availability of cloud-free satellite data. The intensity analysis was performed for these two periods.

The extent and rate of LC change for the periods in the entire area and in each category are examined using Intensity Analysis (Aldwaik and Pontius, 2012). The intensity analysis can be broken down into three levels: interval, category, and transition (Table 5.1). At the interval level, the variation in the rate of LC change in the study area was studied by estimating the annual change intensity of each period. The intensity analysis is based on the assumption that the annual changes are distributed uniformly across the entire period and it is called uniform intensity.

The annual change rates obtained are compared with the uniform intensity value. The results from the intensity analysis determined which period experienced a faster rate of LC change compared to the other. In the category level analysis, the intensity of gross gains and gross losses in each LC class were estimated for both periods. The intensity of gain/loss obtained for each class of LC was then compared with the uniform intensity. At the category level analysis, uniform intensity is the annual change that would occur if the variation within each interval were scattered uniformly across the entire spatial extent. Thus, the dormant and active land use classes and the constancy of their pattern of change over both the periods were assessed using category level analysis. At the transition level, the transition rate from one LC class to another was analysed for both periods. The observed transitions were compared with the uniform transition intensities to and from land use classes to examine which LC classes were avoided or targeted in a given period (Chaudhuri and Mishra, 2016).

**Table 5.1. Equations for intensity analysis (Aldwaik and Pontius, 2012)**

$$S_t = 100\% \times (\{ \sum_{j=1}^J [ ( \sum_{i=1}^J C_{tij} ) - C_{tij} ] \} / [ \sum_{j=1}^J ( \sum_{i=1}^J C_{tij} ) ]) / (Y_{t+1} - Y_t) \quad (5.2)$$

$$U = 100\% \times (\sum_{t=1}^{T-1} \{ \sum_{j=1}^J [ ( \sum_{i=1}^J C_{tij} ) - C_{tij} ] \} / [ \sum_{j=1}^J ( \sum_{i=1}^J C_{tij} ) ]) / (Y_T - Y_1) \quad (5.3)$$

$$G_{tj} = 100\% \times \{ [ ( \sum_{i=1}^J C_{tij} ) - C_{tij} ] / (Y_{t+1} - Y_t) \} / \sum_{i=1}^J C_{tij} \quad (5.4)$$

$$L_{ti} = 100\% \times \{ [ ( \sum_{j=1}^J C_{tij} ) - C_{tii} ] / (Y_{t+1} - Y_t) \} / \sum_{j=1}^J C_{tij} \quad (5.5)$$

$$R_{tin} = 100\% \times [ C_{tin} / (Y_{t+1} - Y_t) ] / \sum_{j=1}^J C_{tij} \quad (5.6)$$

$$W_{tn} = 100\% \times \{ [ ( \sum_{i=1}^J C_{tin} ) - C_{tmm} ] / (Y_{t+1} - Y_t) \} / \sum_{j=1}^J [ ( \sum_{i=1}^J C_{tij} ) - C_{tmj} ] \quad (5.7)$$

$$Q_{tmj} = 100\% \times [ C_{tmj} / (Y_{t+1} - Y_t) ] / \sum_{j=1}^J C_{tmj} \quad (5.8)$$

$$V_{tm} = 100\% \times \{ [ ( \sum_{i=1}^J C_{tmj} ) - C_{tmm} ] / (Y_{t+1} - Y_t) \} / \sum_{j=1}^J [ ( \sum_{i=1}^J C_{tij} ) - C_{tmj} ] \quad (5.9)$$

---

Where  $J$  = number of classes;  $i$  = index of a class at the initial time point for a particular time interval;  $j$  = index for a class at the final time point;  $m$  = index for the losing class in the transition of interest;  $n$  = index for the gaining class in the transition of interest;  $T$  = number of time points;  $t$  = index for the initial time point of interval ( $Y_t, Y_{t+1}$ ), where  $t$  ranges from 1 to  $T-1$ ;  $Y_t$  = year at time point  $t$ ;  $C_{tij}$  = number of pixels that transition from class  $i$  at time  $Y_t$  to class  $j$  at time  $Y_{t+1}$ ;  $S_t$  = annual intensity of change for time interval ( $Y_t, Y_{t+1}$ );  $U$  = value of uniform line for time intensity analysis;  $G_{tj}$  = annual intensity of gross gain of class  $j$  for time interval ( $Y_t, Y_{t+1}$ );  $L_{ti}$  = annual intensity of gross loss of class  $i$  for time interval ( $Y_t, Y_{t+1}$ );  $R_{tin}$  = annual intensity of transition from class  $i$  to class  $n$  during the time interval ( $Y_t, Y_{t+1}$ ) where  $i \neq n$ ;  $W_{tn}$  = value of uniform intensity of transition to category  $n$  from all non- $n$  classes at time  $Y_t$  during the time interval ( $Y_t, Y_{t+1}$ );  $Q_{tmj}$  = annual intensity of transition from class  $m$  to class  $j$  during the time interval ( $Y_t, Y_{t+1}$ ) where  $j \neq m$ ;  $V_{tm}$  = value of uniform intensity of transition from class  $m$  to all non- $m$  classes at time  $Y_{t+1}$  during the time interval ( $Y_t, Y_{t+1}$ ).

---

At first, a cross-tabulation matrix is prepared for both periods. Table 5.2 & 5.3 demonstrates the cross-tabulation matrix for the period -1 (1989-2001) and period-2 (2001-2017) respectively. The first matrix is obtained by overlaying LC maps of 1989

and 2001, while the second matrix is obtained by overlaying maps of 2001 and 2017. The values in the matrices are the area of the corresponding land cover class in square kilometers. The total column in right of the matrix is the area of each class in the initial year of period, while the total row is the area of each class in the subsequent year. The column in the far right gives gross losses in each class during the period, while the row in the bottom gives gross gains during the period.

**Table 5.2. Land transition matrix of the study area for period-1(1989-2001) in sq. km**

Category	2001				Total	Gross Loss
	Vegetation	Water	Urban	Barren		
<b>1989</b>						
<b>Vegetation</b>	417.31	9.87	120.16	281.09	828.43	411.12
<b>Water</b>	24.62	17.37	7.23	8.59	57.82	40.44
<b>Urban</b>	10.38	0.51	75.44	9.64	95.97	20.53
<b>Barren</b>	191.66	1.31	212.16	813.61	1218.74	405.13
<b>Total</b>	643.97	29.06	414.98	1112.94		
<b>Gross gain</b>	226.66	11.69	339.54	299.33		

At interval level analysis, the LC change experienced during both periods are analyzed and the period in which the land transition is faster is identified. At the category level, the four categories, namely vegetation, water, urban and barren, were examined. The active and dormant categories were determined. At the transition level, the analysis was carried out in two sub-levels: firstly, the transition rate from urban to other classes and secondly, the transition rate from vegetation to other classes was determined in both periods. The LC class which is intensively avoided or targeted is identified in this level of analysis.



**Table 5.3. Land transition matrix of the study area for period-2 (2001-2017) in sq.km**

Category	2017				Total	Gross Loss
	Vegetation	Water	Urban	Barren		
<b>2001</b>						
<b>Vegetation</b>	203.06	11.44	231.57	190.53	636.60	433.54
<b>Water</b>	8.57	9.34	5.45	5.41	28.77	19.44
<b>Urban</b>	48.32	0.58	267.86	97.53	414.29	146.43
<b>Barren</b>	87.21	0.82	446.47	574.73	1109.22	534.49
<b>Total</b>	347.16	22.18	951.35	868.20		
<b>Gross gain</b>	144.10	12.84	683.50	293.47		

#### 5.2.4 LST Retrieval

Land Surface Temperature of the study area was retrieved from the thermal infrared band of Landsat images. The approach used in this study for LST retrieval is a simple single-channel algorithm that can be employed for coarse resolution images. The method incorporates atmospheric profile values and emissivity obtained from NDVI, thereby improving the accuracy of the extraction. Since the period considered for the study is from 1989 to 2017 and the dataset used is Landsat data, an LST extraction method that can be applied to sensors with single thermal band data was adapted for the study.

The conversion of pixel value of the Landsat images to LST comprises of the following steps. (Landsat 7, 2011; Landsat 8, 2015)

(1) Conversion of pixel values to Spectral Radiance (Landsat 5 TM)

$$L_{\lambda} = G_{\text{rescaled}} \cdot Q_{\text{Cal}} + B_{\text{rescaled}} \quad (5.10)$$

In the case of Landsat 8,

$$L_{\lambda} = M_L \cdot Q_{\text{Cal}} + \Delta_L \quad (5.11)$$

Where,  $L_{\lambda}$  – spectral at-sensor radiance in watts/(m<sup>2</sup>\*ster\*μm);  $G_{\text{rescaled}}$  - rescaled gain;  $B_{\text{rescaled}}$  - rescaled bias;  $Q_{\text{Cal}}$  - quantized calibrated pixel value;  $M_L$ - radiance

multiplicative scaling factor for the band;  $\Delta_L$  - radiance additive scaling factor for the band

For 1989, the spectral radiance is directly converted to LST in Kelvin (due to the absence of atmospheric corrections values), while for the years 2001, 2005 and 2017, atmospheric corrections are applied to the spectral radiance obtained. NDVI threshold method introduced by Valor and Caselles (1996) was employed to estimate ground surface emissivity. The method uses a green coverage ratio and NDVI to assess surface emissivity.

The green coverage ratio ( $P_v$ ) of each pixel was estimated using the following eq. (5.12) proposed by (Shi and Zhang, 2018)

$$P_v = \frac{NDVI - NDVI_{\min}}{NDVI_{\max} - NDVI_{\min}} \quad (5.12)$$

Where  $NDVI_{\max}$  is the maximum value of NDVI, which corresponds to thick vegetation and  $NDVI_{\min}$  is the minimum value of NDVI corresponding to the soil.

The ground emissivity ( $\varepsilon$ ) of each pixel for the urban land surface was assessed using eq. (5.13):

$$\varepsilon = 0.9589 + 0.086P_v - 0.0671P_v^2 \quad (5.13)$$

In the case of Landsat ETM+ and Landsat 8 images, atmospheric corrections are applied to the spectral radiance obtained, while for Landsat 5 TM the spectral radiance is directly converted to LST in Kelvin (due to the absence of atmospheric corrections values).

(2) Application of atmospheric corrections values to spectral radiance for Landsat 7 ETM+ and Landsat 8 images (McCarville et al., 2011, Tran et al., 2017)

$$L_T = L_\lambda - L_u - \tau(1 - \varepsilon)L_d) / (\tau \cdot \varepsilon) \quad (5.14)$$

Where  $L_T$  – surface leaving radiance;  $L_u$  - upwelling radiance;  $L_d$  - downwelling radiance;  $\tau$  - atmospheric transmission;  $\varepsilon$  - surface emissivity

The values of  $L_u$ ,  $L_d$  and  $\tau$ , were evaluated using the Atmospheric Correction Parameter Calculator online tool (<http://atmcorr.gsfc.nasa.gov>; viewed on January 2018).

### (3) Conversion of Spectral Radiance to LST

$$T = K_2 / [\ln (K_1/L_T + 1)] \quad (5.15)$$

Where  $L_T$  – surface leaving radiance in watts/(m<sup>2</sup>\*ster\* $\mu$ m) (For Landsat 5 TM image,  $L_T = L_\lambda$ );  $K_1$ ,  $K_2$  - calibration constants of Landsat images ( $K_1$  in watts/(m<sup>2</sup>\*ster\* $\mu$ m) and  $K_2$  in Kelvin); T- the surface temperature in Kelvin

The LST maps obtained were validated using MODIS LST data. One hundred random sample points were selected from extracted LST maps and MODIS data for each year and a scatterplot was created to determine the coefficient of correlation (Bendib et al., 2017). The value of the correlation coefficient indicates the accuracy of the prepared LST map.

### 5.2.5 Hot Spot Analysis

The spatial correlation of LST in the study area was examined using an optimized hot spot analysis tool (Getis-Ord  $G_i^*$ ) in the ArcGIS software. The optimized hot spot analysis tool interrogates the data to obtain the settings that will yield optimal hot spot results. The presence of hot spots and cold spots over the entire area was characterized by comparing each feature (LST value) with its neighboring features (Ord & Getis, 1995). Comparing the value of a given feature with its neighboring features is essential in characterizing the spatial relationship of features (Nelson and Boots, 2008). Hot spots are regions where the maximum value of the feature is clustered, while cold spots are regions where the minimum value of the feature is clustered. Other features should bound a feature with a high value with high value to become a statistically significant

hot spot. This technique can effectively be used to quantify and characterize spatial autocorrelation of remotely sensed imagery. The spatial dependence for each pixel is measured, and the relative magnitude of the digital numbers in the pixel's neighborhood is indicated. The Getis-Ord  $G_i^*$  local statistics is calculated using (ESRI, 2017) eq. (5.16).

$$G_i^* = \frac{\sum_{j=1}^n w_{ij} x_j - \bar{X} \sum_{j=1}^n w_{ij}}{s \sqrt{\frac{n \sum_{j=1}^n w_{ij}^2 - (\sum_{j=1}^n w_{ij})^2}{n-1}}} \quad (5.16)$$

Where,  $x_j$  – attribute value of the feature;  $w_{ij}$  – spatial weight between feature  $i$  and  $j$ ;  $n$  – total number of features and

$$\bar{X} = \frac{\sum_{j=1}^n x_j}{n} \quad (5.17)$$

and

$$s = \sqrt{\frac{\sum_{j=1}^n x_j^2}{n} - \bar{X}^2} \quad (5.18)$$

The  $G_i^*$  statistic value obtained for each feature in the dataset is a *z-score*. Clustering high values result in higher positive *z-scores* (hotspot), and clustering of smaller values results in smaller negative *z-scores* (cold spot). The statistical significance of clustering for a specified distance is indicated by *z-score* value (99% significant: >2.58 or <-2.58; 95% significant: >1.96 or <-1.96; 90% significant: >1.65 or <-1.65). To be statistically significant, at a significance level of 0.01(99%), a *z-score* would have to be less than -2.56 or greater than 2.56. Seven categories were identified from the statistical results: very cold spot, cold spot, cool spot, not statistically significant, warm spot, hot spot, and very hot spot. The LST pattern was linked with the change in LC to assess the impact of LC change on LST. This methodology gives a better insight into the impact

of LC change rather than concentrating only on certain high and low LST values. The hot spot maps were created for 1989, 2001 and 2017.

### 5.2.6 Pearson's Correlation Coefficient

Pearson's Correlation coefficient is introduced in this study to establish the relationship between LST and LC classes. It measures the degree of linear correlation between two variables, determined by the value of  $r$  (Zhang et al., 2019). It is a dimensionless measure, and the value ranges from -1 to +1, where -1 indicates the variables have a perfect negative correlation, +1 indicates the variables have a perfect positive correlation, whereas zero indicates there is no linear relationship between the two variables. Pearson's correlation coefficient  $r$  between two variables  $X$  and  $Y$  is given by eq. (5.19) (Asuero et al., 2006).

$$r = \frac{\sum_{i=1}^n (X_i - \bar{X})(Y_i - \bar{Y})}{\sqrt{\sum_{i=1}^n (X_i - \bar{X})^2} \sqrt{\sum_{i=1}^n (Y_i - \bar{Y})^2}} \quad (5.19)$$

Where  $\bar{X}$  and  $\bar{Y}$  are the mean of the variables  $X$  and  $Y$  respectively;  $n$  is the sample size.

## 5.3 RESULTS

Based on the analysis, the LC and LST maps were prepared for 1989, 1991, 2001, 2005, 2014 and 2017. The spatial and temporal patterns of LC and LST were analysed using intensity analysis and hot spot analysis respectively. The results prove that there is a significant change in land cover and LST of the region over the years.

### 5.3.1 Land Cover Classification

The two main classes observed from LC classification are urban and barren land. Water constitutes only a small portion of the study area. The accuracy of the land use map obtained was determined by comparing the ground-truth measurements with the classified data. Ground control points from each land cover class was collected from the field and used for accuracy assessment. The overall accuracy of the LC maps obtained from different years (1994, 2001, 2005, 2014 and 2017) ranges from 84% to

91%. The Kappa coefficient ranges from 0.85 to 0.91. In recent years, the LC map's overall accuracy has been better than in the earlier years since the spatial resolution of the recent images was improved using the pan-sharpening technique. The LC maps of the study are shown in figure 5.2. The values of overall accuracy and Kappa coefficient suggest that the classified map and the reference data have good agreement with one another. The LC change from 1989 to 2017 is analysed through Intensity Analysis. For the past 28 years, the urban area has increased by about 40%, while the other land cover classes like vegetation, water and barren have decreased. The urban area has increased from 4% to 43%, vegetation has considerably decreased from 38% to 16% and barren land has decreased from 55% to 40% of the total area from 1989 to 2017. This change was mainly due to the increase in information technology establishments which in turn accelerate real estate and infrastructural projects at a faster rate to cater to housing and other services. The two intervals considered for analysis are 1989 - 2001 and 2001 - 2017.

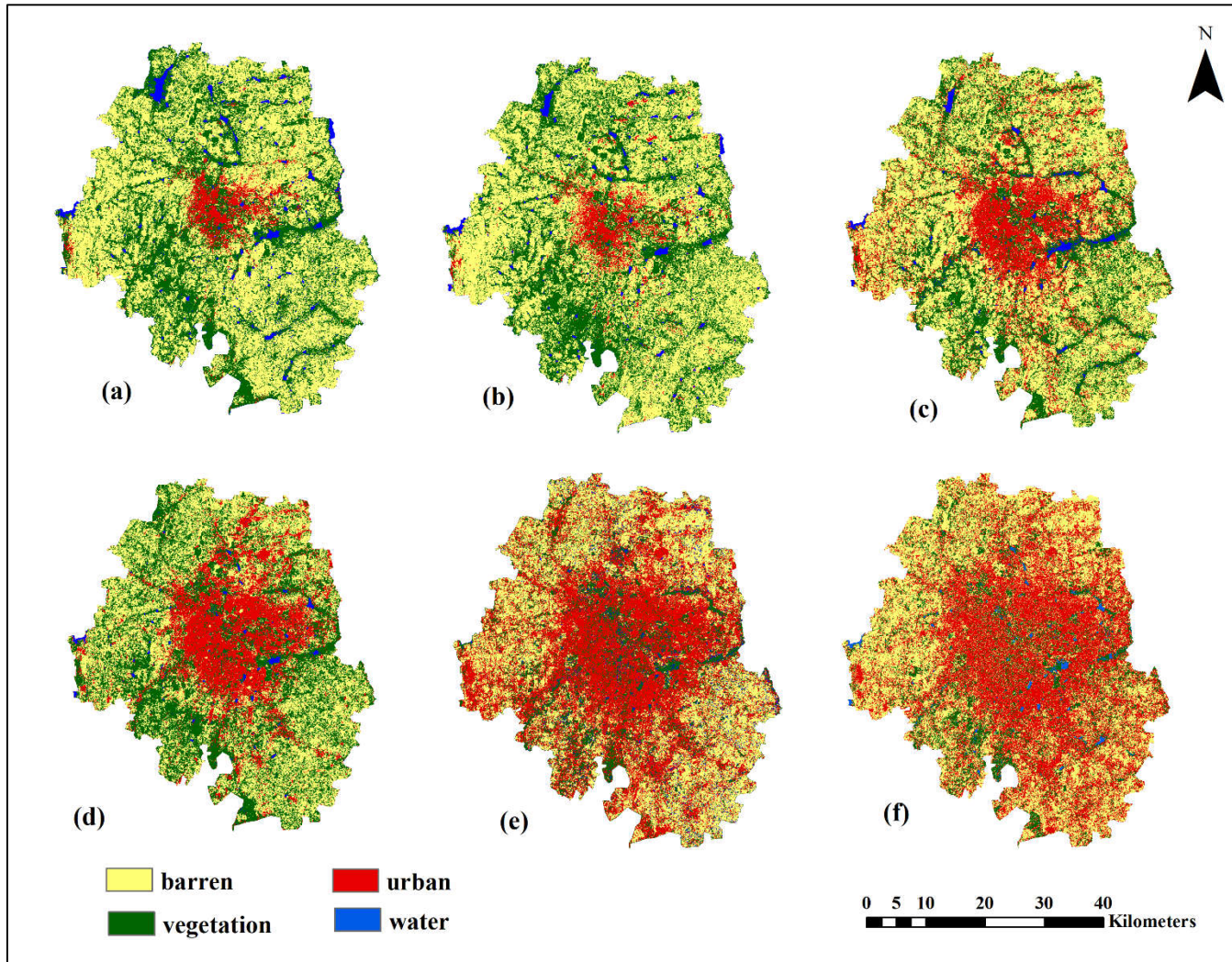


Figure 5.2. LC map of the study area for the years (a)1989 (b) 1994 (c) 2001 (d) 2005 (e) 2014 (f) 2017.

### 5.3.2 Intensity Analysis of Land Cover Change

Figure 5.3 illustrates the time interval analysis for the two periods. The bars that extend to the right side display indicate intensity of an annual area of change within each period. The bars to the left indicate the gross area of total changes in each period. The left-hand side of the figure shows that the change in area in the region during period-2 (2001-2017) is more and the reason for it being that the duration of period -1 is larger than the duration of period - 2. Analyzing the right-hand side of the figure, it is observed that the annual change in area is more prominent in 1989-2001. This is obtained from the value of uniform intensity. The uniform line is the vertical line drawn along the right side of the figure. The bars that extend beyond the uniform line indicate that the change is faster in that period. In this case, the annual change in the area for period-1 from 1989 to 2001 is faster, while slower in period-2 from 2001 to 2017. This indicates that the LC change is faster in 1989-2001 while it is slower in 2001-2017. After analysing each interval's rate of LC change, category level analysis for each period was carried out. This is because many multinational IT companies started operating from 1989 to 2001.

Figures 5.4 & 5.5 illustrate the category level analysis for 1989-2001 and 2001-2017 respectively. The bars that spread to the right side indicate the intensity of annual gains and losses within each category and that to the left side display the gross annual area of gains and losses in the study area. From the left side of Figure 5.4, it is clear that the urban area has the most significant gain during the period 1 while vegetation has the largest loss. In the case of Figure 5.5, the most significant gain is for the urban area, but the most considerable loss is shifted to barren land. Hence the behavior of urban area is similar in both the periods. The active and dormant classes could be identified by the uniform line drawn in the right side of the figure. For the period 1989-2001, the urban, vegetation and water classes are the active land use classes, while barren land is dormant during the period. Among the active land use classes, the urban area has experienced significant gain while vegetation and water experienced a significant loss. Similar behavior is observed for the period-2 (2001-2017), where the urban, vegetation and water are the active classes, and barren land is the dormant class. The study region exhibits similar behaviour for the category level analysis in both periods.



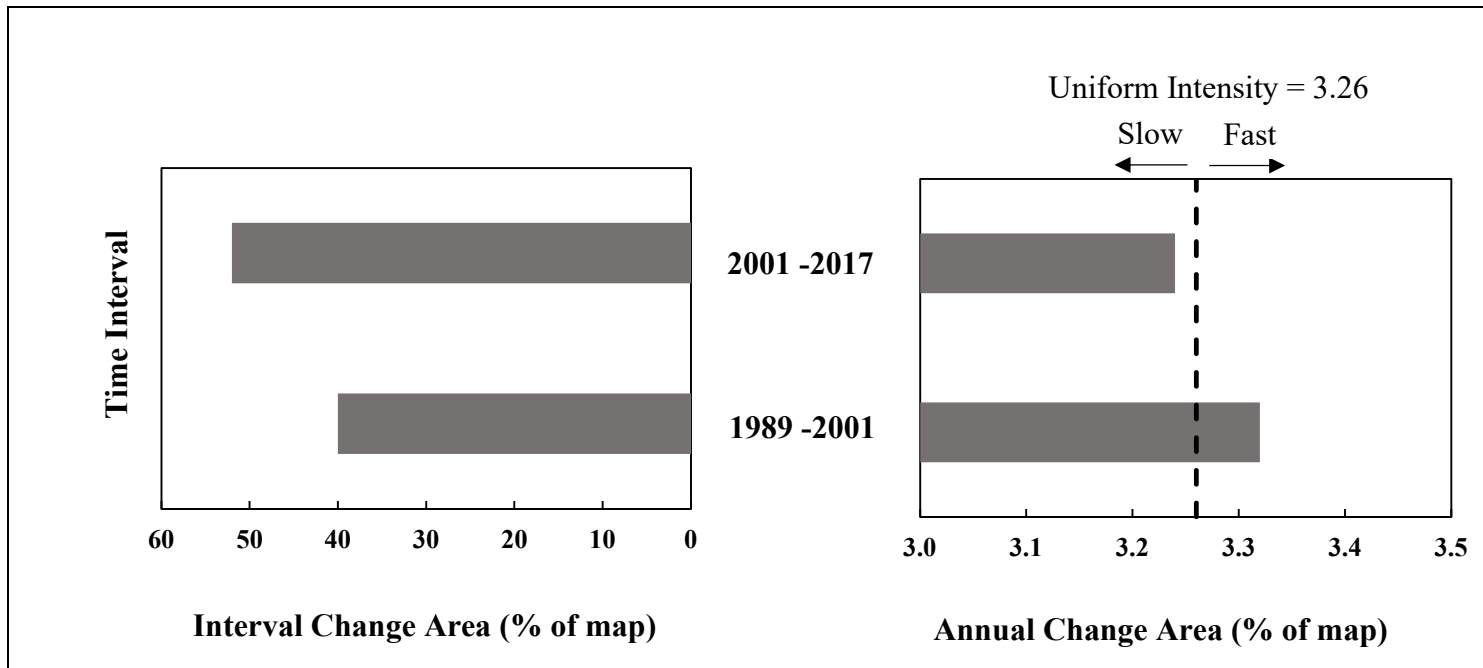


Figure 5.3. Time intensity analysis for two periods: 1989-2001 and 2001-2017.

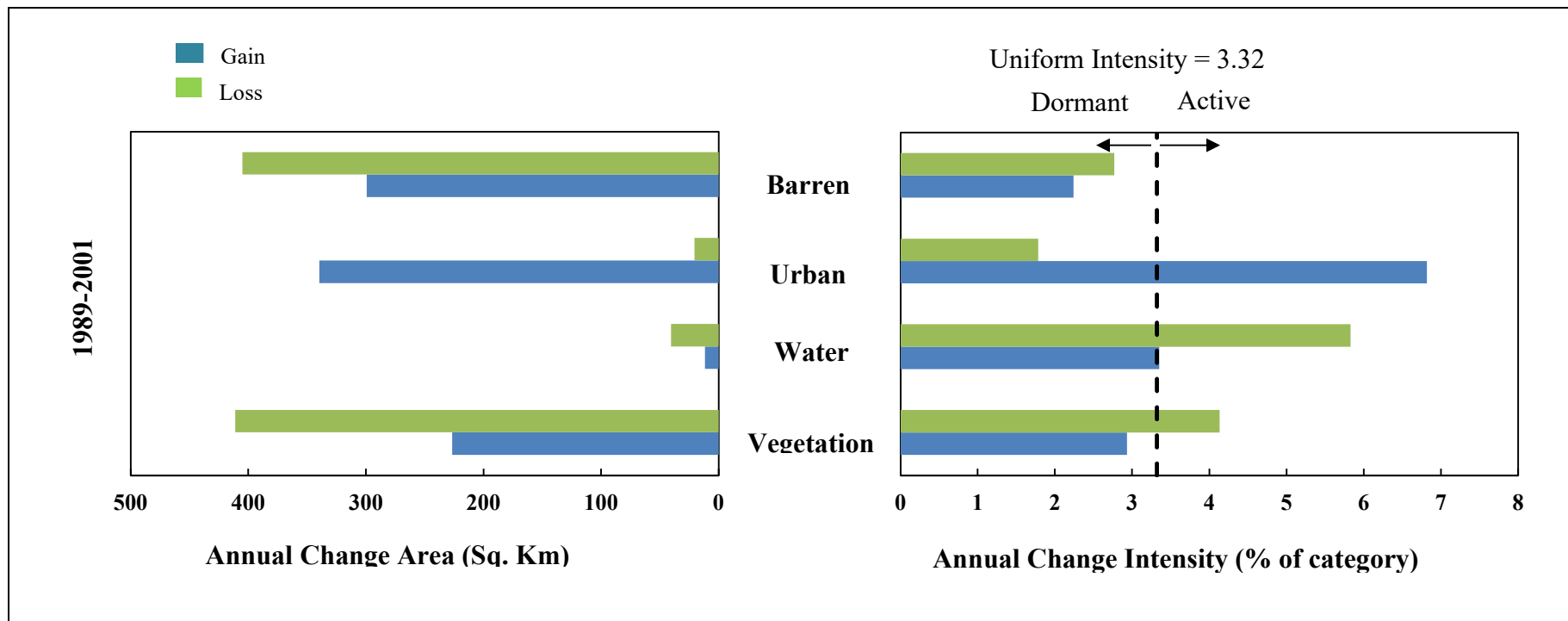


Figure 5.4. Category intensity analysis for the period-1, 1989-2001

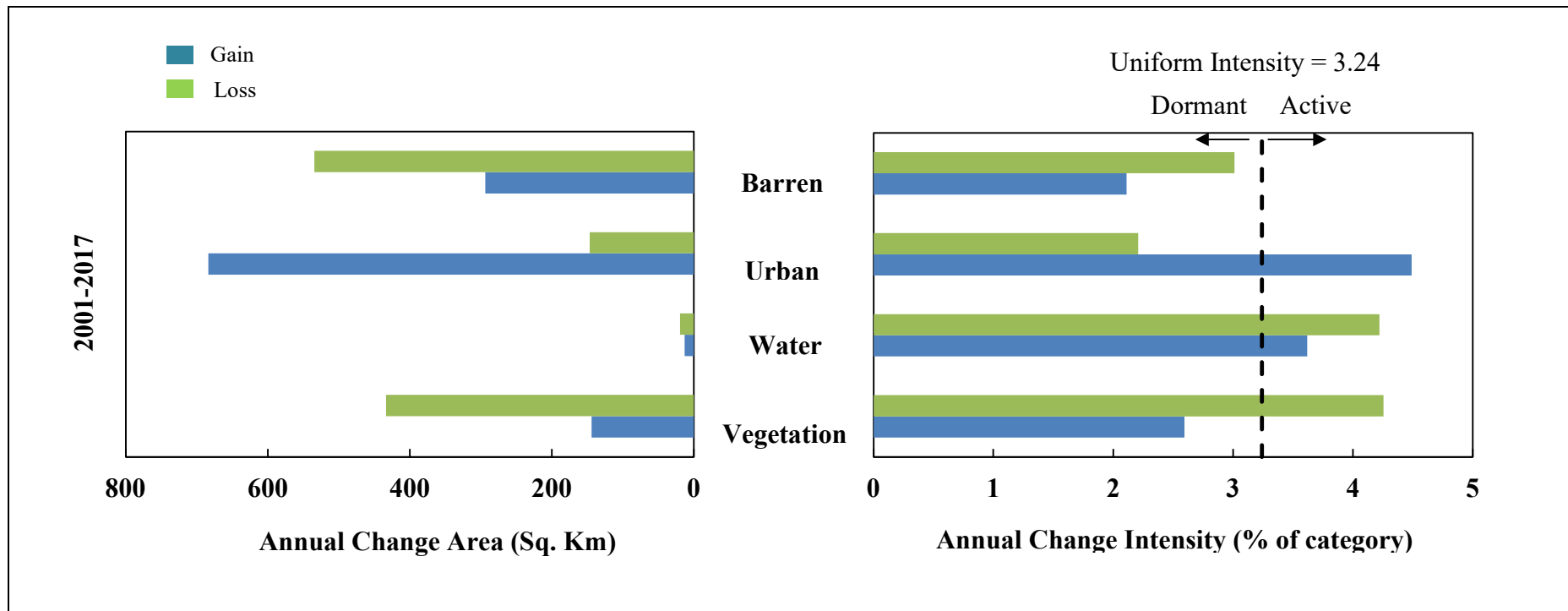


Figure 5.5. Category intensity analysis for the period-2, 2001-2017.

Figure 5.6 shows the transition intensity analysis to urban for period-1 (1989-2001). Figure 5.7 shows the transition intensity analysis to urban for period-2 (2001-2017). The bars that spread to the left imply a gross annual area of transitions to urban, and the bars to the right imply the intensity of annual transitions to urban within each non-urban category. The transition to urban from other non-urban classes is analysed. From the left side of Figure 5.6, it is observed that the major transition to the urban area has occurred from the barren land. The area of transition from barren to urban is more compared to the other two classes. Similar behavior is observed for the period-2, provided the transition from barren to urban is stationary. The uniform line on the right side of the figure determines whether the transition should be avoided or targeted. Since the barren land extends beyond the uniform line, it should be targeted. The transition from barren to urban land is prominent compared to the other non-urban classes. The transition from water and vegetation can be avoided, and the transition from barren land to urban should be focused. Figure 5.7 also exhibits a similar behavior where the major transition to the urban area has occurred from barren land. Thus, the transition from barren to urban is stationary according to the intensity analysis.

The transition intensity analysis from vegetation for 1989-2001 and 2001-2017 are shown in Figure 5.8 and Figure 5.9 respectively. The left side portion of the figure indicates the gross annual area of transitions from vegetation and the right side indicates the intensity of annual transitions from vegetation within each non-vegetation category. From the left side of Figure 5.8, it can be observed that the area of transition from vegetation to barren is high compared to urban and water. In the period shown in Figure 5.9, the most significant transition from vegetation to barren was noticed, while the transition from vegetation to urban is decreased and that of water has increased compared to period-1. The vertical uniform line to the right side of the figure determines whether the transition is targeted or avoided. In both periods, the transition intensity from vegetation to urban and water is high. These two transitions are targeted while the transition intensity to urban in period-2 is less compared to the previous period.

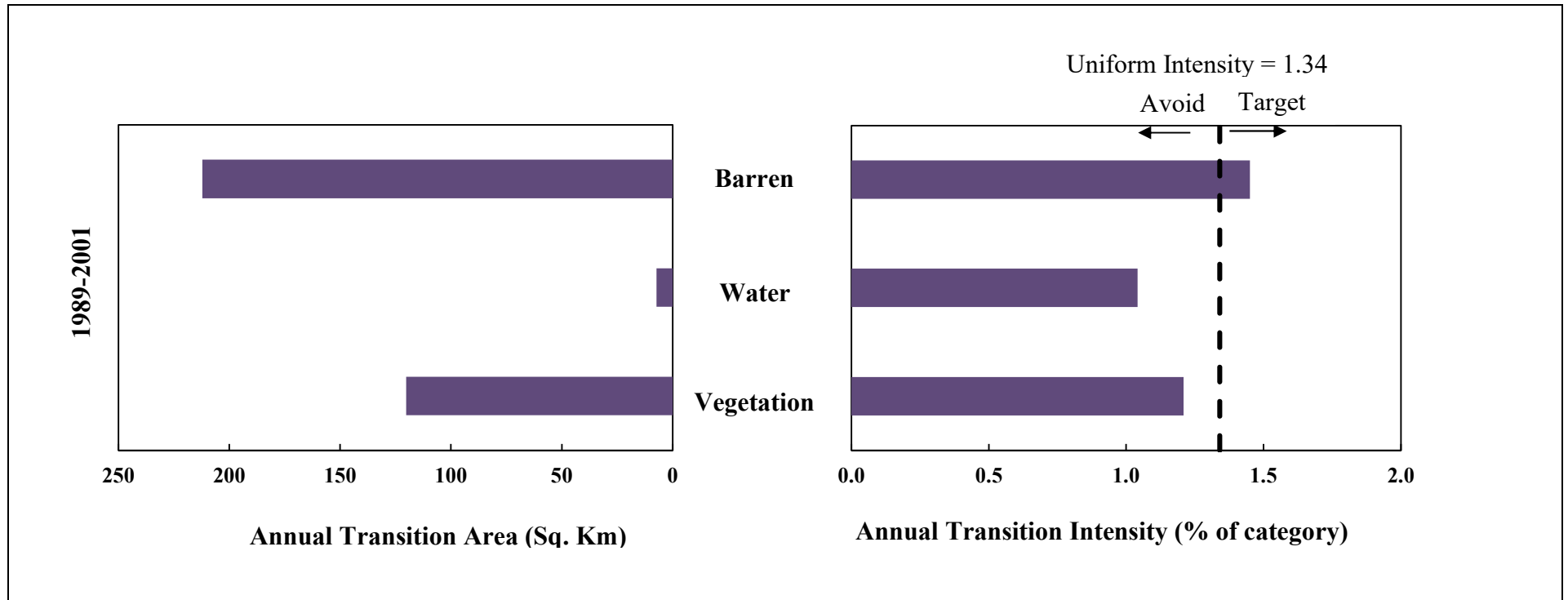


Figure 5.6. Transition intensity analysis to urban for 1989 -2001

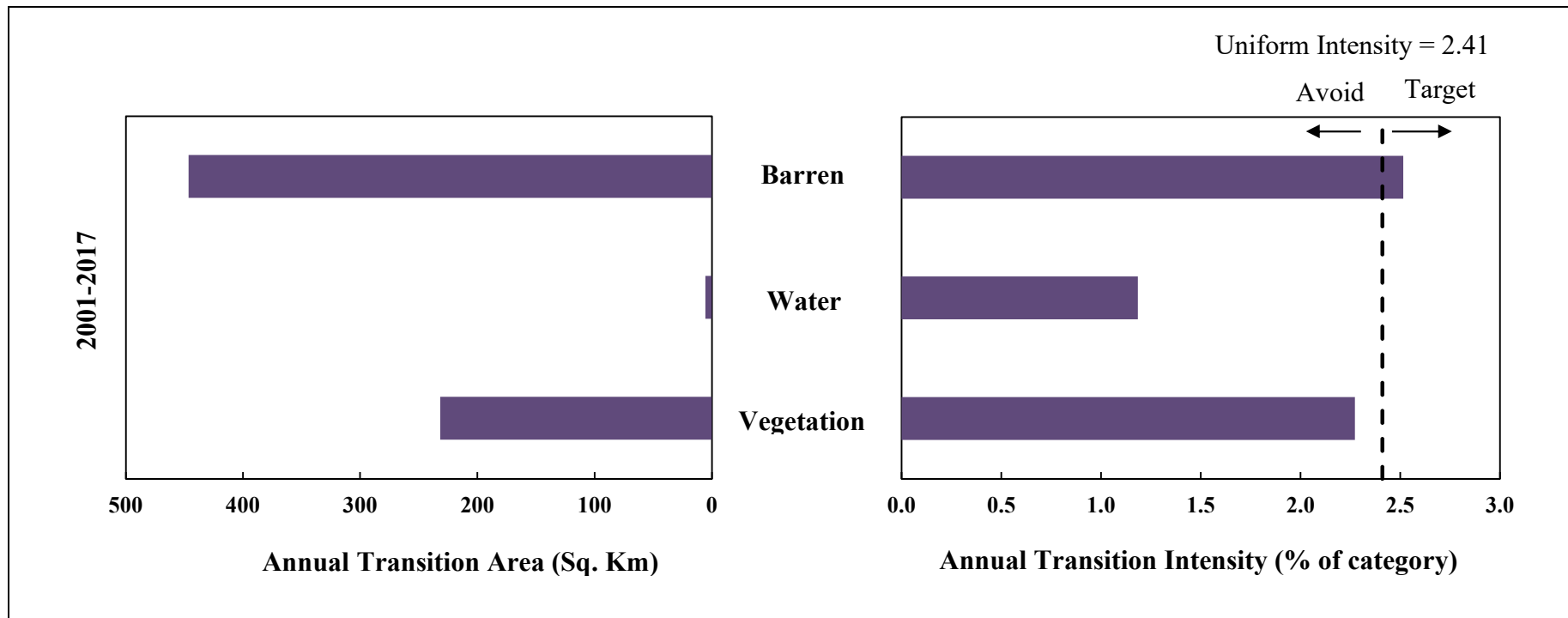


Figure 5.7. Transition intensity analysis to urban for 2001-2017

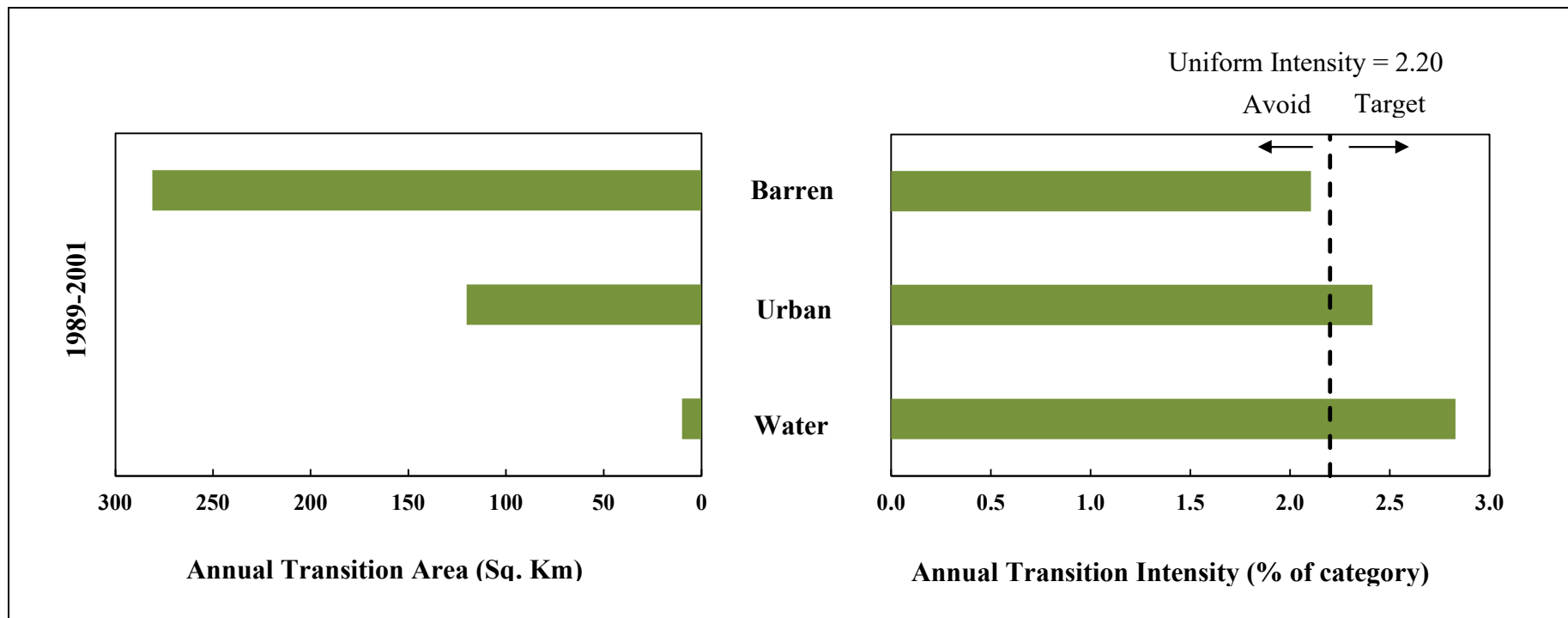


Figure 5.8 Transition intensity analysis from vegetation for 1989-2001

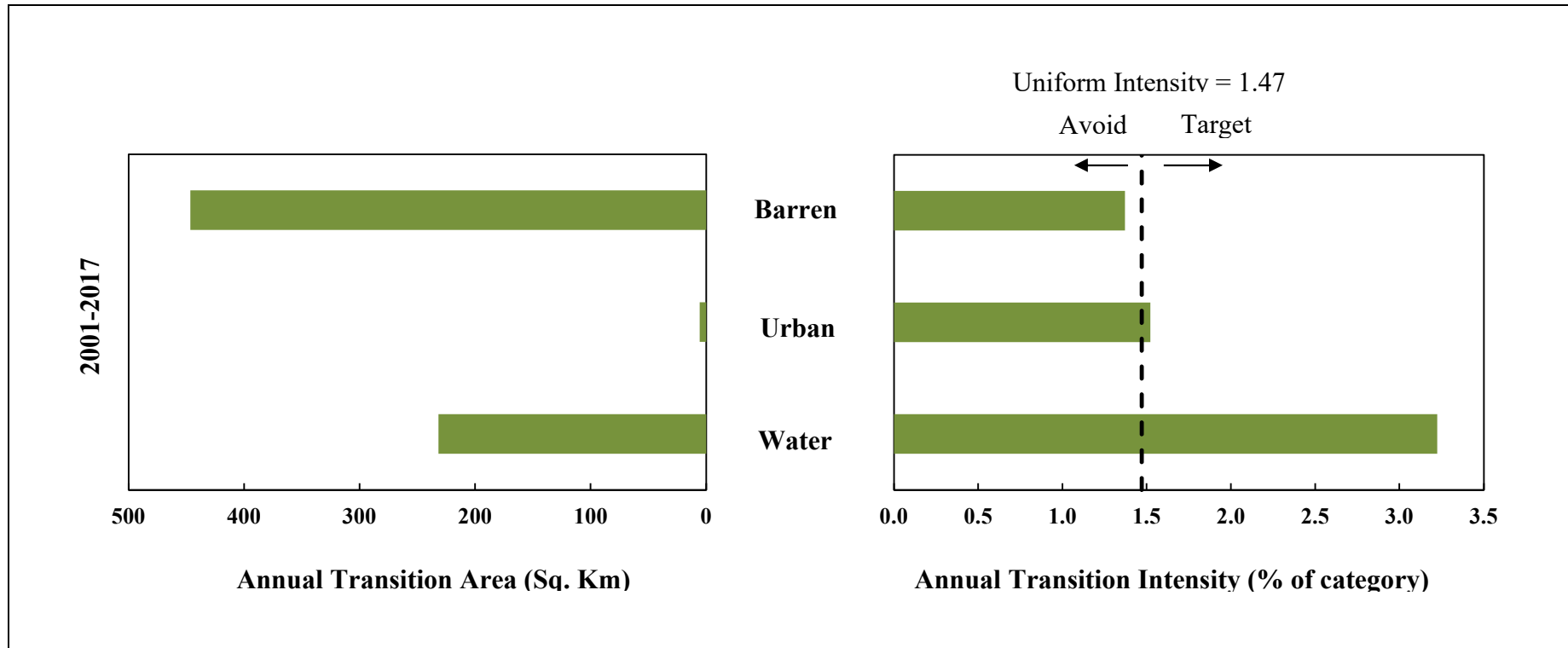


Figure 5.9 Transition intensity analysis from vegetation for 2001-2017.



Concisely, it revealed that the major change in land use occurred from 1989 to 2001 as compared to 2001 to 2017 considered. There is a major increase in the urban area in both periods. The vegetation and water have undergone a significant loss in both periods with vegetation experiencing a higher loss in period-2 compared to period-1. In both periods, it is seen that the transition from barren to urban is intensely targeted and the transition from vegetation to water is also moderately targeted.

### **5.3.3 Spatio-temporal variation of LST**

The LST patterns of the study area for the years 1989, 1994, 2001, 2005, 2014 and 2017 are shown in Figure 5.10. The LST obtained was validated using MODIS derived LST. The MODIS data used is MYD11A1 with a spatial resolution of 1 km. The spatial resolution of the LST retrieved from Landsat images was aggregated to 1 km for comparison. A significant positive correlation between the LST estimated from Landsat data and MODIS derived LST was obtained from the scatter plot with 100 random sample points. Correlation coefficients in the range of 0.70 to 0.74 were obtained for different years. This shows the accuracy and reliability of the method used for LST retrieval. There was a substantial increase in the LST of the region from 1989 to 2017. It can be observed that the region's maximum, minimum and mean LST have increased from 1989 to 2017.

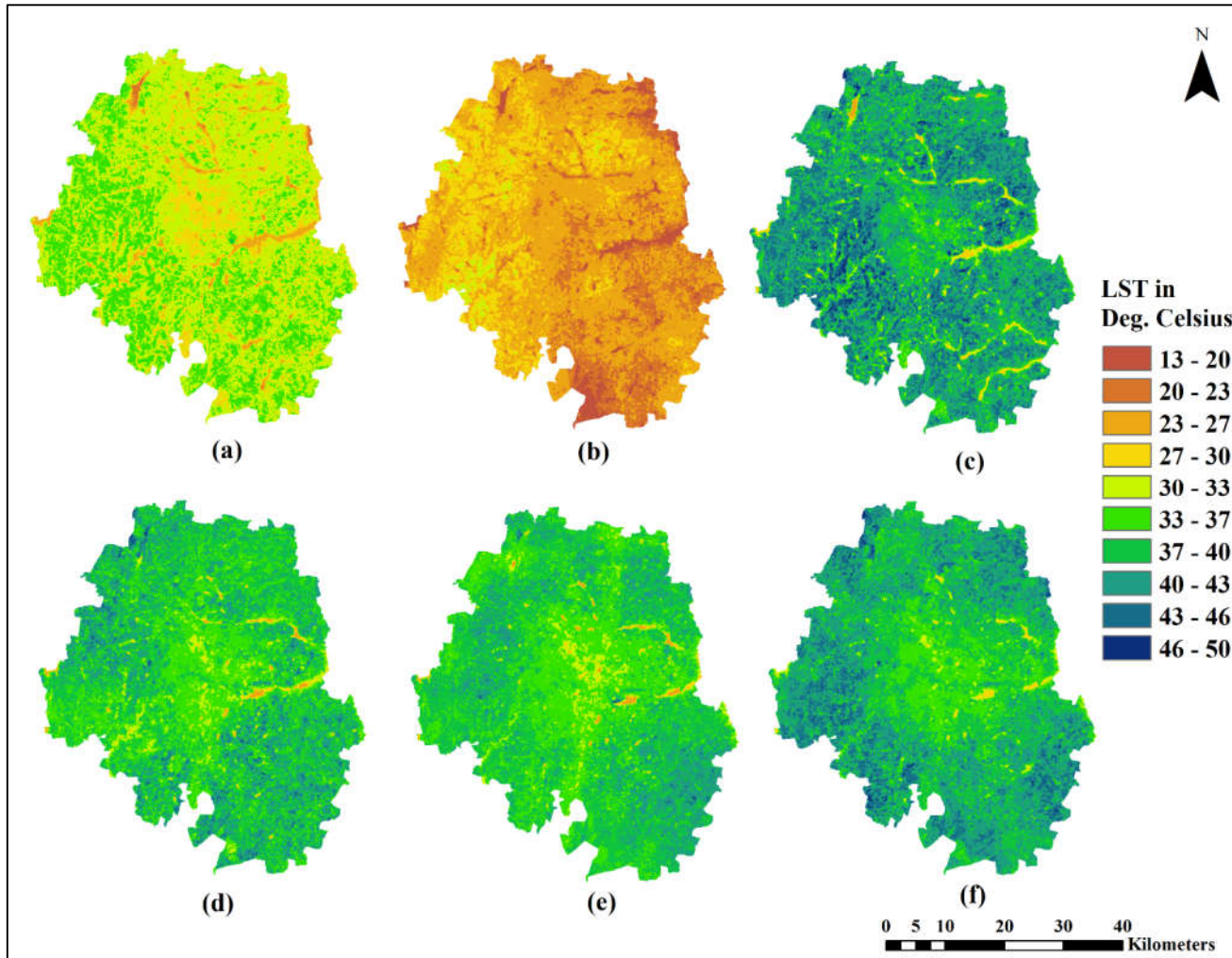
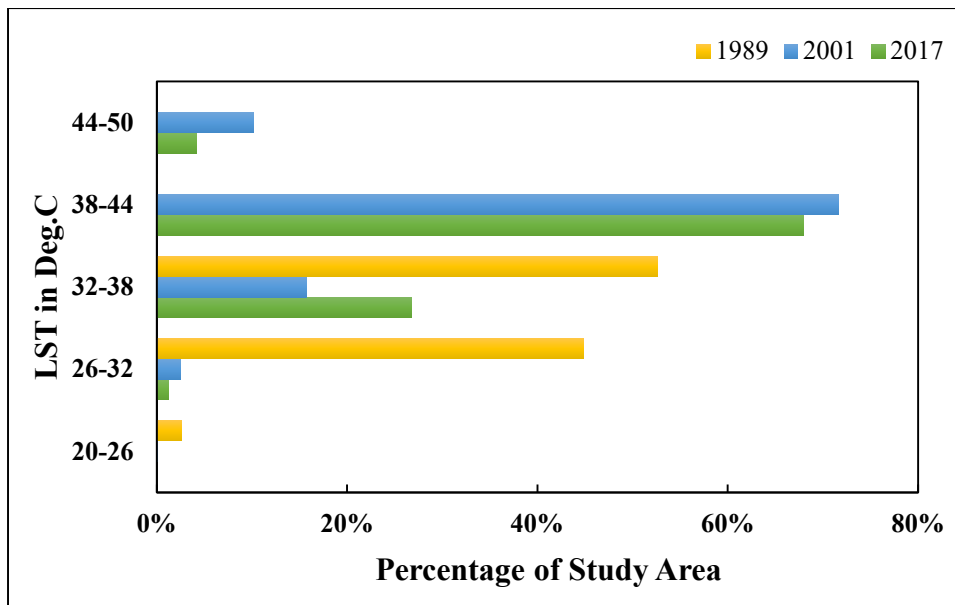


Figure 5.10. LST Map of the study area for the years (a)1989 (b) 1994 (c) 2001 (d) 2005 (e) 2014 (f) 2017.



**Figure 5.11 The variation of LST in the study area**

The variation of LST in the study area for 1989, 2001 and 2017 were plotted in Figure 5.11, examined to understand the change in LST patterns. In the year 1989, 53% of the study area was under LST range from 32°C to 38°C and 45% experiences LST range from 26°C to 32°C. In the year 2001, 72% of the study area experience an LST of 38°C to 44°C and 16% experiences LST of 32°C to 38°C. For the year 2017, 68% of the study area experience an LST of 38°C to 44°C and 27% experiences LST of 32°C to 38°C. Thus, it is evident that there is a clear shift in the range of LST from 1989 to 2017. In the year 1989, only a small percentage of the study area experienced LST of 38°C to 44°C whereas, in 2017, 68% of the area falls into this category. Over the years from 1989 to 2017, the mean LST has increased by about 7°C.

On analysing the pattern of LST for a particular year, it is observed that the lowest values of LST were traced towards the centre portion of the study area while the higher values were observed along the periphery of the study area. The centre part of the study area is cooler than the surrounding area. This was mainly due to large biological and recreational parks of more than 300 acres with many trees, lawns and water bodies in the study area as observed in LC map.

Apart from this, the LST derived from the satellite images was compared with the air temperature of the region. The maximum, minimum and mean values of LST and the air temperature was compared for the different years (Figure 5.12). A comparatively higher correlation was obtained for maximum temperature with a correlation coefficient of greater than 0.81, while 0.80 was obtained for minimum temperature. The reason is that the minimum air temperature is usually measured during the night, while the minimum LST is the minimum temperature observed at the time of acquisition of the satellite image.

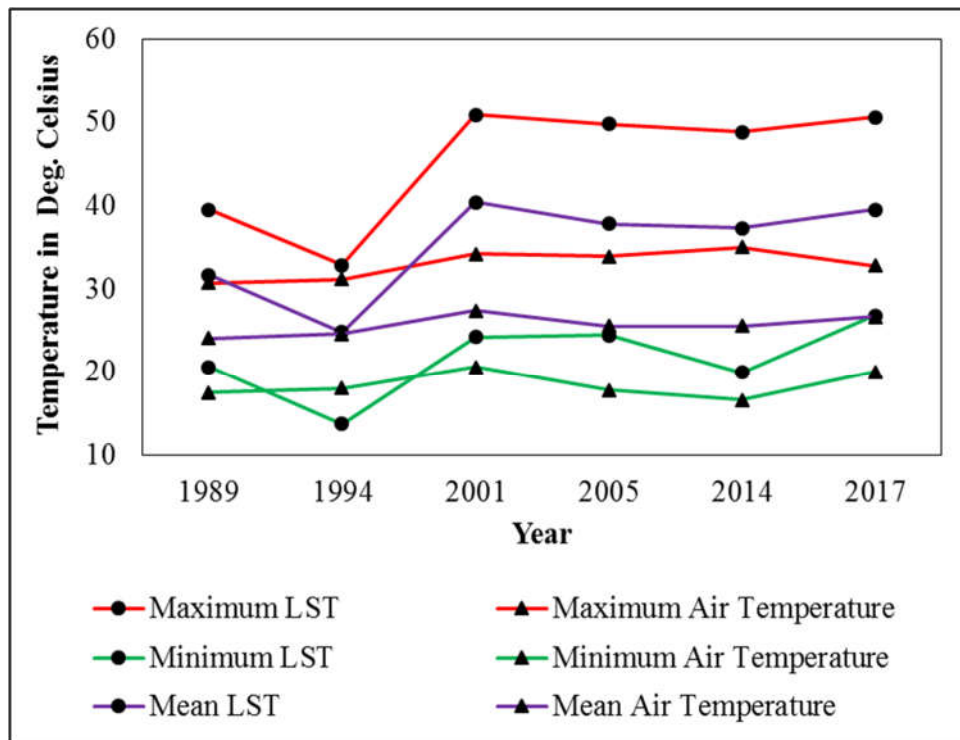


**Figure 5.12 Comparison of LST and Air temperature for the study area**

### 5.3.4 LST and LC relationship

The mean LST of each land use type is estimated for the years 1989,1994, 2001, 2005, 2014 and 2017. Table 5.4 demonstrates the change in the distribution of LST for different classes for the years 1989, 2001 and 2017. There is a sizeable increase in the mean LST for each land use type. From 1989 to 2017, the mean LST of vegetation and water increased by about 7°C and 6°C respectively. The LST of urban and barren land

increased by 8°C. Meanwhile, there is an increase in the urban land and a considerable decrease in the area of vegetation, water, and barren land. The change in LST occurred mainly during the period from 1989 to 2001. This was justified through the intensity analysis that the change is faster during this period (1989-2001).

The highest increase in LST is observed for built-up and barren land. The vegetation class in the study area mostly consist of urban vegetation, i.e., residential lawns, trees, shrubs and grasses along the paved surfaces. Due to this, some pixels (spatial resolution of 30m) will have a mixed land cover type. In the supervised classification with a maximum likelihood algorithm, a mixed pixel is classified into a particular class based on the proportion of the class. Hence, vegetation class exhibits a relatively equal increase in LST with urban in the study. Even though, there is an increase in LST of the region, the lower LST values are observed towards centre of an urban area. The higher LST values were observed along the periphery of city where barren land is accumulated. This might be due to the presence of several parks and water tanks situated in the area.

**Table 5.4. Mean LST and land cover area of the study region**

Land cover types	1989		2001		2017		Change during 2001-1989		Change during 2017-2001	
	Mean LST (°C)	Area (Sq.km)	Mean LST (°C)	Area (Sq.km)	Mean LST (°C)	Area (Sq.km)	LST (°C)	% of area	LST (°C)	% of area
	Vegetation	29.74	829.54	37.00	644.83	36.93	347.16	7.26	8.38	0.07
Water	24.90	57.89	29.07	29.1	31.06	22.18	4.17	1.31	1.99	0.31
Barren	31.58	1220.4	41.23	1114.4	40.06	862.3	9.65	4.81	1.17	10.91
Urban	29.43	96.09	39.18	415.53	37.94	951.71	9.75	14.49	1.24	24.62

There exists a prominent impact of LC change on the LST of the study region. The results show that urban area has increased by approximately 40%, with an LST of 8°C

from 1989 to 2017. Overall, the study shows a positive correlation between urban land and LST over the area. However, the increase in LST can be attributed to the rise in the impervious area of the region with modern building and construction materials at large and usage of HVAC, vehicular pollution etc. on a lighter scale which could be investigated separately.

The LST for the different LC classes for the period of interest was compared using the Pearson correlation coefficient. Figure 5.13 presents the mean LST experienced by the four land cover classes for the years 1989, 1994, 2001, 2005, 2014 and 2017. The correlation coefficient obtained for the classes: vegetation, water, barren and urban is 0.77, 0.88, 0.76 and 0.74 respectively. A relatively high value of correlation coefficient (greater than 0.6) indicates that there is a linear relationship between the LST of the different LC classes with time. There is a gradually increasing trend noticed in the mean LST of the LC classes. One of the limitations of this study is that only six images were used for determining the correlation coefficient due to which an exact picture cannot be established.

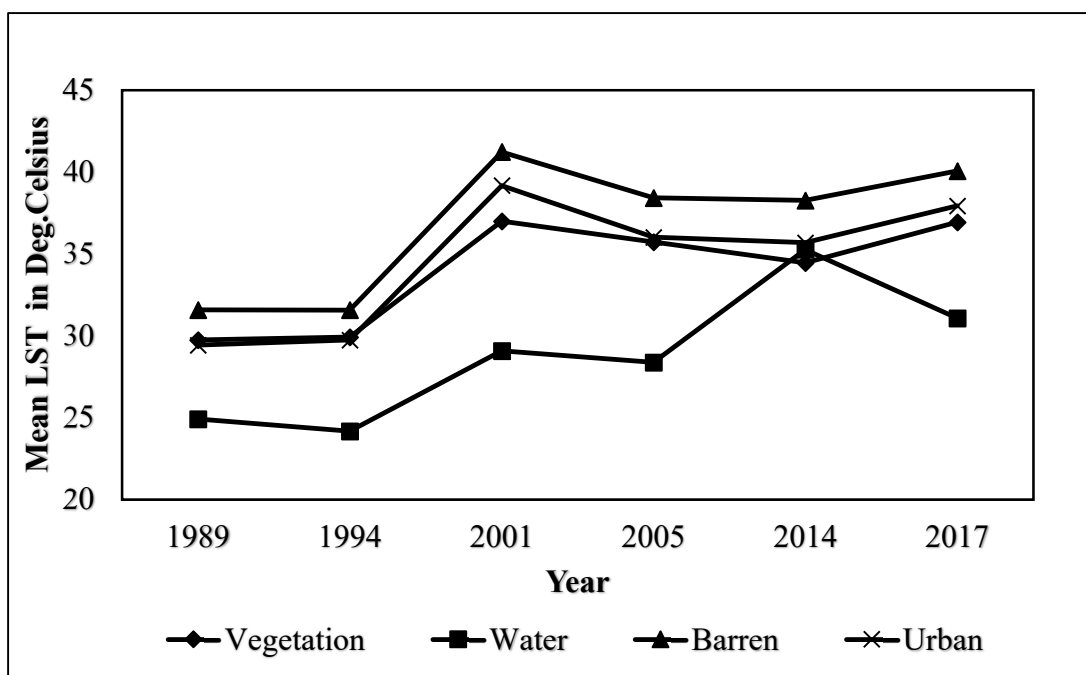


**Figure 5.13. Variation of mean LST for different land cover classes**



### 5.3.5 Impact of LC on LST

Hot spot identification using Getis-Ord  $G_i^*$  statistics is widely used in various research areas like natural disaster estimation (Harris et al., 2017), crime analysis (Craglia et al., 2000), road accident evaluation (Prasannakumar et al., 2011) and heat vulnerability assessment (Wolf & McGregor, 2013). This study examined the impact of LC change on LST using this method. The hot spot map of Bengaluru was created for three different dates (Figure 5.14). This provides a better understanding of the LST distribution in the area. Identifying hot and cold spots by this method does not depend on a single high or low LST value and hence provides a better picture of the hot and cold regions.

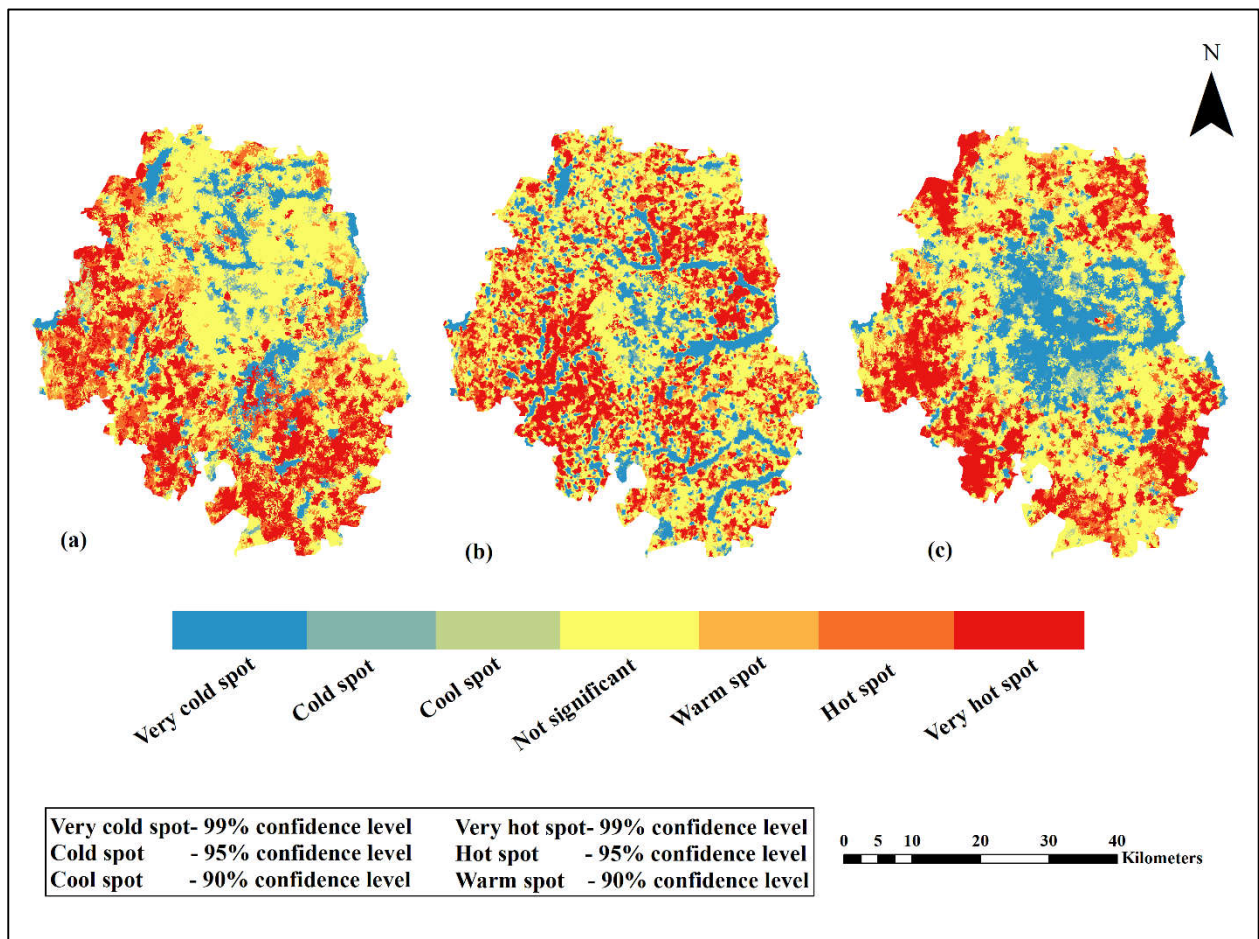


**Figure 5.14. Hot spot map of the study area for the years (a) 1989 (b) 2001 (c) 2017**

The cold spots are mainly clustered in and around the water bodies, and the hot spots are clustered in the barren land. Over time, some "insignificant" regions have become cold spots by the transformation of certain parks and water tanks in the centre part of the study area into cold spots. On the whole, hot spot regions are more than cold spot regions. Approximately 24% of the study area is warmer while 14% is cooler throughout the study period (28 years). The hottest land cover type is barren, and the coldest land cover type is water.

During the study period, hot spot regions tend to decrease (39.56% in 1989 to 35.04% in 2017) while cold spot regions tend to increase (14.36% in 1989 to 22.89% in 2017). In the years 1989 and 2001, waterbody contributed for more than 50% of the cold spots, while in 2017, the cold spots are mainly observed in the urban area. Over 28 years, a localization of cold spots has been observed in the central part of Bengaluru city, where the major land use type is urban. At the same time, hot spots are observed in the peripheral regions of Bengaluru, where the major land use type is barren land. As urban expansion occurs, the cold spots are clustered in the urban area. Hence it can be inferred that in recent years, urban area has become cooler than the surrounding rural area confirming the existence of an urban cool island in Bengaluru. Urban cool islands are regions where the urban area is cooler than the surrounding rural area.

#### **5.4 DISCUSSION**

The proposed research deals with LC change and its impact on surface heating patterns for the metropolitan city of Bengaluru. Monitoring and predicting LC change and its impact on the environment is a topic of growing interest in the present scenario.

The main objective of this study was to assess the spatio-temporal patterns of LC and LST and explore the impact of LC on LST from 1989 to 2017. Intensity analysis was employed to analyse the variations of LC and its driving forces, and the patterns of LST was investigated by employing hot spot analysis. This research can be replicated for other cities experiencing a significant change in land cover due to urbanization over the years.



The results show that Bengaluru experienced a significant increase in the urban area from 1989 to 2017. From 1989 to 2000, the land use change rate is faster than in 2001 to 2017 and the transition exhibited is barren to urban. For 28 years from 1989-2017, mean LST has increased by about 6°C and the urban area's mean LST has increased by almost 8°C. Another significant observation from the study is that the cold spots have increased, and it is mainly clustered in the urban area.

The findings of this research can be attributed to urbanization experienced in the study area during the past years. Numerous public and private sector companies were established after 1990 which led to the migration of people from different parts of the country to Bengaluru. The urban growth that started in the 1990s is still advancing in the region with the drastic increase in population and urban area. Due to urbanization, the impervious area has increased, leading to the area's surface heating effect. The daytime urban cool effect can be ascribed to different factors. Bengaluru urban district constitutes several parks like Cubbon Park, Lalbagh botanical garden being the two major spots and has several water tanks and lakes which affect the LST of the region. The daytime LST pattern of the area is due to the intense heat waves produced in the non-urban area during the summer season. In the summer season, the evapotranspiration in the city's outskirts will be much less due to low vegetation. At the same time, the evapotranspiration in the urban areas will be high due to the human population, planted trees and gardens leading to a cooling effect in the urban area compared to the surrounding (Ghosh et al., 2017).

The urban growth and surface warming effect of Bengaluru obtained from this study is in agreement with the previous studies (Ramachandra & Kumar, 2009; Ramachandra et al., 2013) reported in the region. However, the urban cool effect in Bengaluru is not reported in any of the previous literature as most of the studies focused on the Greater Bengaluru urban core. Studies carried out in other major Indian cities mainly focused on the urban heating patterns and their adverse effects on the human community by employing different methodologies. Grover and Singh (2015) reported that the urban heating effect in Delhi is observed to be less prominent due to the mixed land use type and vegetation cover. The LST pattern exhibits a negative correlation with vegetation

and a positive correlation with built-up in Indian cities: Chennai (Farris & Reddy, 2010) and Nagpur (Kotharkar & Surawar, 2015) while the temperature profile experiences a dip in areas with water bodies, lakes and parks as reported in Hyderabad (Franco et al., 2015).

## **5.5 CONCLUSION**

The study presents a comprehensive approach for analysing the spatio-temporal variation of LC and LST and the impacts of LC change on the environment. The LC change pattern is analysed using intensity analysis and the impact of LC on LST is quantified using hot spot analysis. Significant changes in the LC and LST pattern have been observed in the study area from 1989 to 2017. The LC change from 1989 to 2001 is faster than the period from 2001 to 2017. The major change witnessed by the study area during this period is the increase in urban, which is due to the transition from vegetation and barren to urban. The vegetative cover in the area is extensively affected during this transition. The growth of the urban region has been from centre to outwards. The LST pattern of the region has also changed during the study period. The mean LST of the study area has increased by 6°C during the period from 1989 to 2017. Over the years, there has been a shift in the range of maximum LST (experienced by more than 50% of area).

This change in LST can be attributed to the increased urban area of the region by the addition of a greater number of information technology companies. The impervious area has increased drastically from 1989 to 2017. In the past thirty years, the study area has undergone significant urban land use changes, one of the main reasons for this being the Information technology revolution in the region. Bengaluru has witnessed a tremendous increase in job opportunities in Information Technology, aerospace, manufacturing, and other sectors. This has led to the migration of a large population from different parts of the country to Bengaluru. There has been a significant increase in the number of buildings, houses, roads, metros, and other infrastructures, thereby widening the urban area.

It was found that examining LST patterns at different time frames can be effectively performed using hot spot analysis by Getis-Ord  $G_i^*$  statistics. The identification of hot spot and cold spot by this method does not depend on a single high or low LST value and hence provides a better picture of the hot and cold regions. Overall, hot spot regions (approximately 24%) are more than cold spot regions (approximately 14%). The analysis results during the study period showed that hot spots tend to decrease (39.56% in 1989 to 35.04% in 2017) while the cold spots tend to increase (14.36% in 1989 to 22.89% in 2017). As the urban expansion occurs, the cold spots have increased, and it is mainly clustered in the urban area. It confirms the presence of an urban cool island in Bengaluru urban district, where the surrounding rural area is warmer than the urban centre.

# MODELLING LST AND LAND COVER INTERACTION

---

---

## 6.1 INTRODUCTION

This chapter provides a detailed understanding of the distribution of LST in the study area and how the land cover correlates with LST in an urban cool environment. The aim is to characterize the study area's urban growth and LST patterns and explore the land cover and LST interaction in the context of UCI effect using the concentric ring approach. This is achieved by modelling the urban land density and LST as a function of distance from the urban centre. Further, the relationship between land cover types such as urban, vegetation, water and LST is determined for different years emphasizing the impact of land cover change on the daytime and night-time surface heating.

## 6.2 METHODOLOGY

The LST and land cover types of Bengaluru for the years 1989, 2001, 2005 and 2017 were estimated using various remote sensing methods. LST and surface area ratio of the land cover types were analysed using concentric ring-based approach. Figure 6.1 describes the overall methodology of this section.

### 6.2.1 Land Density Estimation

The urban land use type comprises commercial, industrial land, residential area, and impervious surfaces. The main urban area of a city is divided into three regions, urban core or urban centre, the suburban regions and the outskirts. In this study, the boundary was fixed based on the administrative border of the Bengaluru urban district. A city's spatial extent was defined based on the concentric ring approach, a standardized approach for urban growth studies (Jiao, 2015).

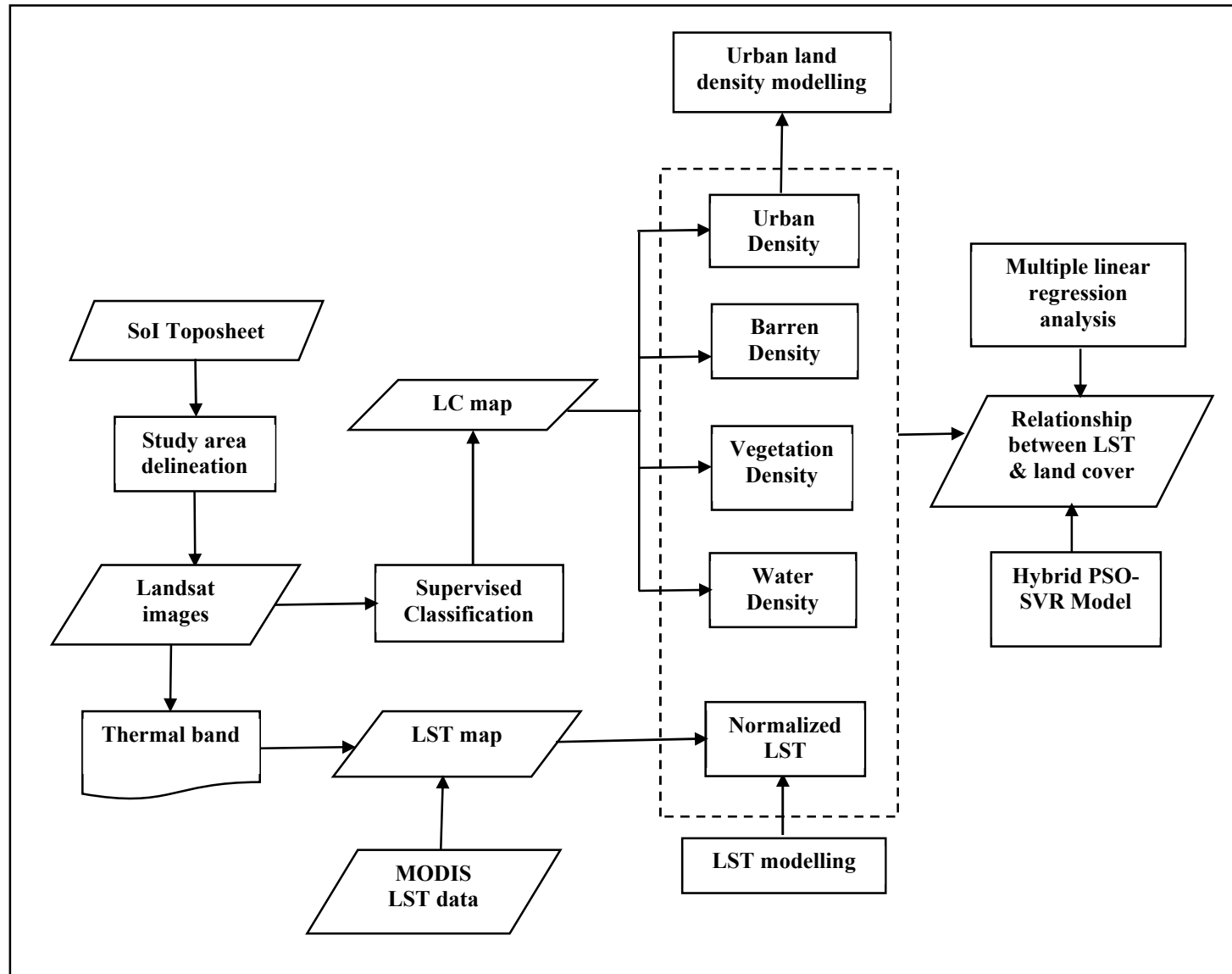
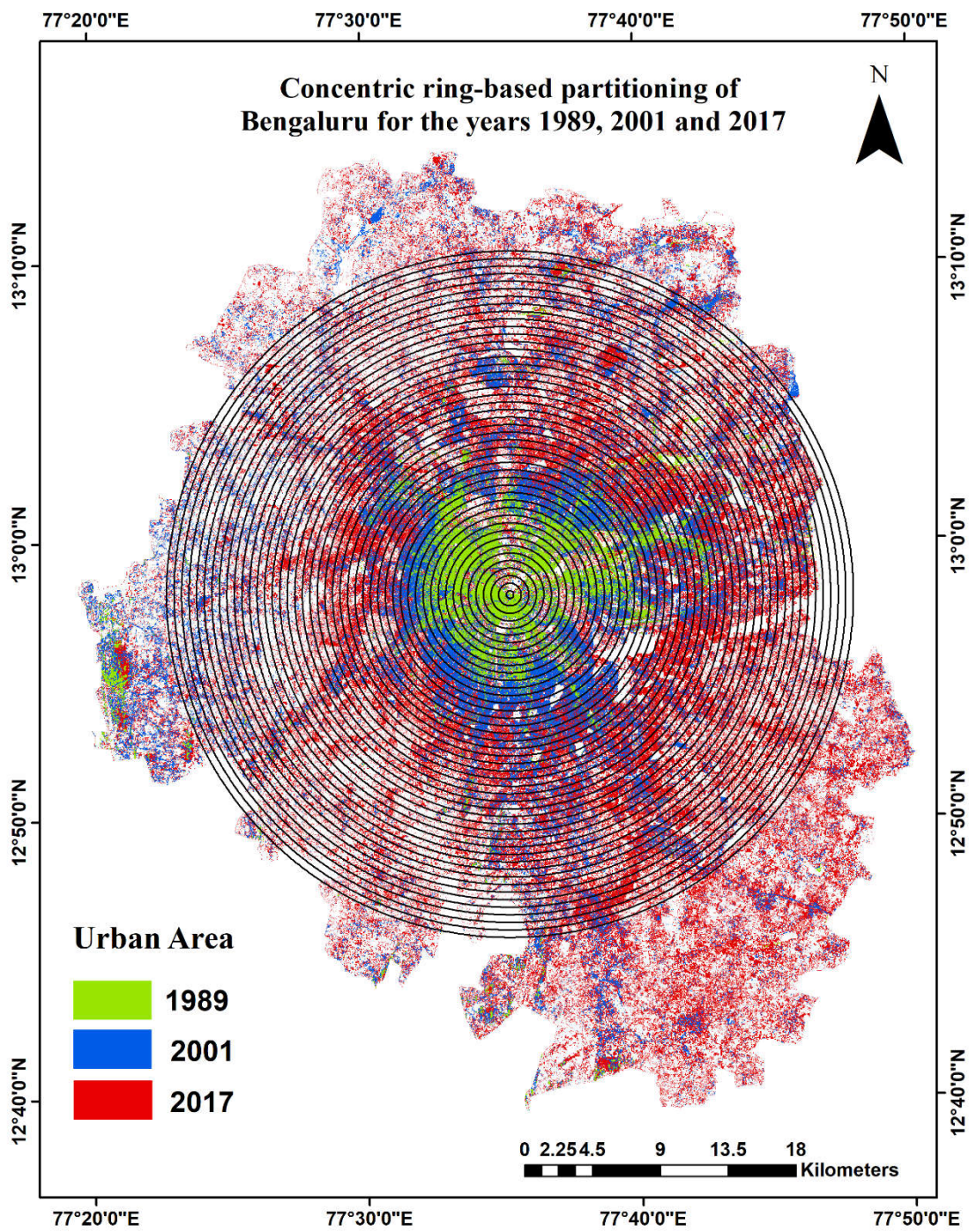


Figure 6.1 Data and methodology flowchart for LST modelling

The study area was divided into concentric rings of width 500 m, and the Urban Density (UD) of each ring was estimated. UD was determined based on the land cover map prepared from Landsat imagery. The urban land density was calculated by dividing the urban area in each ring by the total land area in the corresponding ring.

The procedure was implemented for the years 1989, 2001, 2005 and 2017. Similarly, the surface area ratio of the other three land cover classes corresponding to each ring referred to as Vegetation Density (VD), Water Density (WD) and Barren Density (BD) was estimated for the years 1989, 2001, 2005 and 2017. In the study area, the urban area exhibited a monocentric expansion from 1989 to 2017, as evidenced in Figure 6.2.

Based on the land cover map, the urban area of Bengaluru in the years 1989, 2001 and 2017 was superimposed with the concentric ring to obtain Figure 6.2. The urban area has grown spatially from centre to outwards. An integral part of the core city area, namely the Corporation circle, was selected as the centre point of the concentric rings. Urban features constitute 50% of the area of the centre ring from the year 1989.



**Figure 6.2 Concentric ring-based partitioning of Bengaluru illustrates the urban area in 1989, 2001 and 2017.**

### 6.2.2 Inverse S-shape Function

The spatial variation of urban land density with distance from the urban centre can be demonstrated by a modified sigmoid function providing an inverse S-shape curve given by equation 6.1 (Jiao, 2015).

$$f(r) = \frac{m - c}{1 + e^{\alpha(\frac{2r}{D} - 1)}} + c \quad (6.1)$$

Where  $f$  is the modified sigmoid function,  $r$  is the distance from the urban centre,  $m$  and  $c$  are asymptotes of function  $f$ , which provides the information related to the UD in the outskirts of the city. When there is a rise in the value of  $c$ , it means urban development has occurred in the outskirts or urban fringes.  $\alpha$  is a constant controlling the slope of the density function, and  $D$  determines the radius of the main urban area, an increase in the value of  $D$  suggests the urban area's expansion.

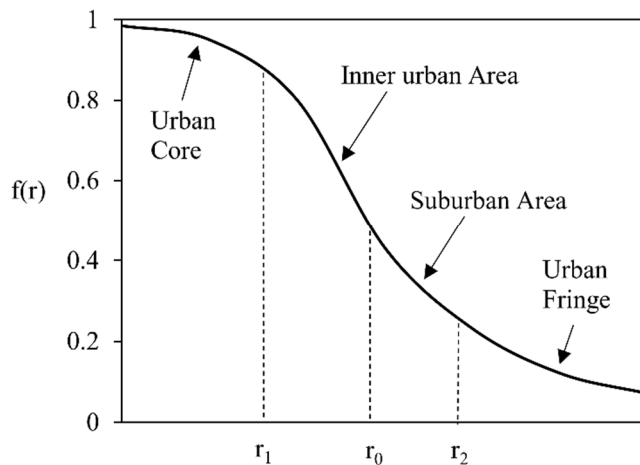


**Figure 6.3. Illustration of different zones of urban area from the urban centre (Source: (Jiao, 2015)).**

The results of the urban density function are reliable for cities that experience monocentric urban expansion. A city's urban growth pattern over time can be apprehended by the parameterization of the function. The decreasing rate of urban land density can be explained using the first derivation of the urban land density function



(Figure 6.3). The urban land density first increases to reach a maximum value and then decreases towards the periphery.

The condition in which UD is higher in the city core and comparatively significantly less in the surrounding is termed as the compactness of a city. Equation 6.2 can be used to determine the compactness of a city. Compact cities have a steep slope for the urban density function, while sprawling cities have comparatively less steep curves (Bonafoni and Keeratikasikorn, 2018). The slope of the function in the intermediate urban zone between urban core and urban fringe is defined by the parameter  $k_S$  as given in equation 6.2. When the city experiences expansive urban growth,  $k_S$  (1/km) value decreases.

$$k_S = \frac{0.57735(1-c)\alpha}{1.316957D} \quad (6.2)$$

### 6.2.3 Model Parameter Estimation

A non-linear least square fitting method was used to fit the function to the data sets by an iterative process of determining and refining the values of constants  $m$ ,  $c$ ,  $\alpha$  and  $D$ . This non-linear model is employed to fit the inverse S-shape function to the UD and normalized LST values.

The accuracy of the fitted model was evaluated using four different metrics: Coefficient of determination ( $R^2$ ), Correlation Coefficient ( $CC$ ), Root Mean Square Error ( $RMSE$ ) and Mean Absolute Error ( $MAE$ ).

### 6.2.4 Normalized LST

The concentric ring approach is employed to determine the mean LST at different distances from the city centre. The LST is normalized using maximum and minimum values to compare the images of different years. The LST for each pixel is scaled to obtain the normalized LST ( $LST_n$ ) given by equation 6.3.

$$LST_n = \frac{LST - LST_{\min}}{LST_{\max} - LST_{\min}} \quad (6.3)$$

Where  $LST_n$  is the land surface temperature value of each pixel,  $LST_{max}$  and  $LST_{min}$  are the maximum and minimum values of LST for a particular satellite image.  $LST_n$  is an index with a value ranging from 0 to 1 (similar to UD). It is a generalized measure of surface temperature, estimated to reduce the effect of atmospheric conditions while using multi-year images (Bonafoni & Keeratikasikorn, 2018).

In the present study, daytime LST is calculated from Landsat images, and corresponding night-time LST is obtained from MODIS data. Daytime LST maps are prepared for the years 1989, 2001, 2005, and 2017, and night-time LST maps of 2005 and 2017 (depending on the data availability) are used. The mean value of  $LST_n$  is estimated for each concentric ring (500 m wide), plotted as a function of distance from the urban centre. The inverse S-shape function is fitted to mean  $LST_n$  data to analyse LST variation with distance from the urban centre.

### **6.2.5 Multiple Linear Regression**

Multiple linear regression is applied to establish the relationship between LST and land cover types. LST, UD, VD and WD were employed to develop linear regression models of the study area for the years 1989, 2001, 2005 and 2017. These models could be employed to predict LST patterns with rapid urban expansion in the future.

UD and mean normalized LST are calculated for each concentric ring for 1989, 2001, 2005 and 2017. The variation of UD and mean  $LST_n$  with distance from the city centre is modelled, and the parameters are estimated to understand the behavior of urban growth and LST pattern over the years. The correlation between LST and different land cover types is reported by developing linear equations for day and night for the study period.

### **6.2.6 Establishment of proposed Hybrid PSO-SVR Model**

In this study, the parameters of the SVR model  $C$ ,  $\varepsilon$  and  $\gamma$  are tuned by PSO algorithm. This study uses an RBF kernel with only one parameter ( $\gamma$ ). The flowchart shown in figure 6.4 illustrates the entire process of the proposed model.

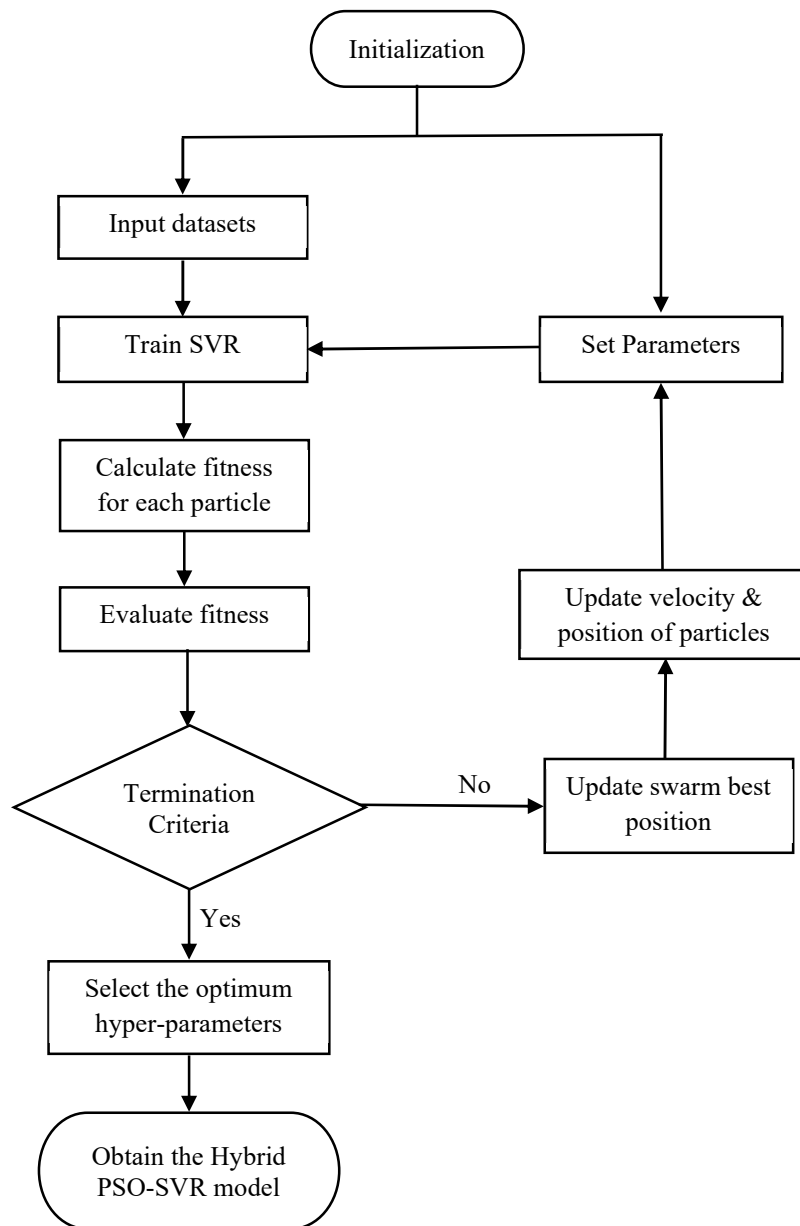


**Figure 6.4. Flowchart of the establishment of Hybrid PSO-SVR Model**

In the beginning, the lower and upper limits of the two SVR parameters  $C$  and  $\gamma$  are specified while the value of  $\varepsilon$  is kept constant. The randomly generated value of  $C$  and  $\gamma$  and the value of  $\varepsilon$  is given as the initial input to SVR model. Then fitness of the model in terms of Mean Squared Error (MSE) is estimated for identifying suitable parameters of SVR. The  $p_{best}$  value and the fitness evaluation of the particle are then compared.  $p_{best}$  value is set to current value if it is better than  $p_{best}$  and the location of  $p_{best}$  in the

dimensional space will be assigned to the current value. Then the current value is compared with the  $g_{best}$  value and if it is better,  $g_{best}$  is changed to the current value. The new position and velocity of the particle are estimated based on the equations 4.13 and 4.14 respectively. The MSE value is repetitively calculated until a specified number of iterations is passed. The critical parameters of SVR and PSO algorithm is specified in table 6.1.

The SVR model intends to develop a relationship of the form.

$$Q = f(p)$$

Where  $p$  is the input vector comprising of variables  $p_1, p_2, p_3$  and  $p_4$  and  $Q$  is the output vector. In this case the input variables are UD, VD, WD and BD while the output variable is LST. The proposed model is developed for the years 1989, 2001, 2005 and 2017 to evaluate the interaction between LST and land cover ratios. The dataset for each year is divided into two sets: 70% for training the model and 30% for testing.

**Table 6.1 PSO and SVR parameter values**

<b>Method</b>	<b>Parameters</b>	<b>Assigned values</b>
<b>PSO</b>	Cognitive Parameter	1.5
	Social Parameter	1.7
	Number of Iterations	100
	Inertia weight( $w$ )	0.6
	Swarm size	30
<b>SVR</b>	Regularization parameter ( $C$ )	0.1 - 20
	Parameter of kernel function( $\gamma$ )	0.01 - 10
	Insensitivity( $\epsilon$ )	0.1

### 6.3 RESULTS AND DISCUSSION

The distribution of the surface area ratio of the land cover types for the years 1989, 2001, 2005 and 2017 is presented with respect to the distance from the centre of the city (Tables provided in Appendix). From 1989 to 2017 urban area has increased tremendously while vegetation, water and barren land have decreased.

#### 6.3.1 Urban land density modelling

The urban land density for the years 1989, 2001, 2005 and 2017 was estimated based on a concentric ring approach. Figure 6.5 illustrates the variation of urban land density from the centre of the city to outwards. Urban land density was estimated using land cover map prepared from Landsat imagery, and it tends to decrease from the centre to outwards. The UD has increased with years, especially in the outskirts and intermediate urban areas, with an intense sprawl in the hinterland for the year 2017.

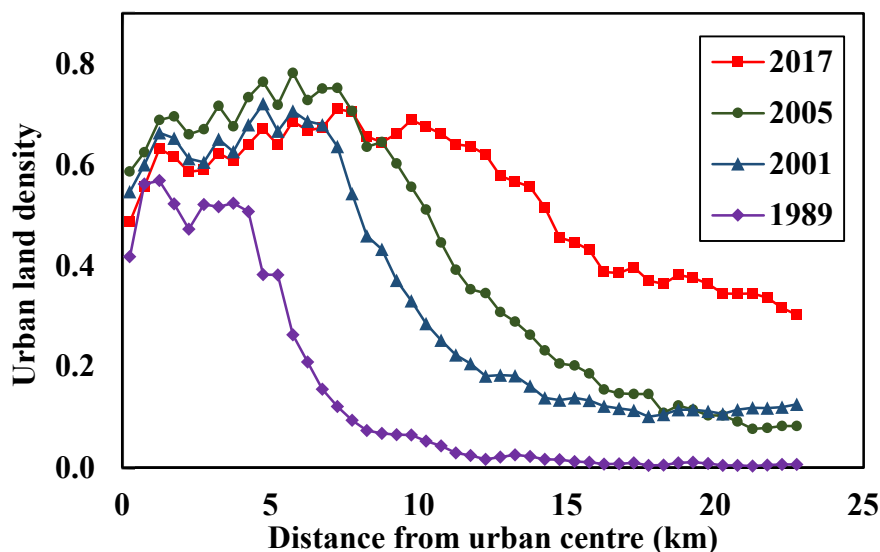
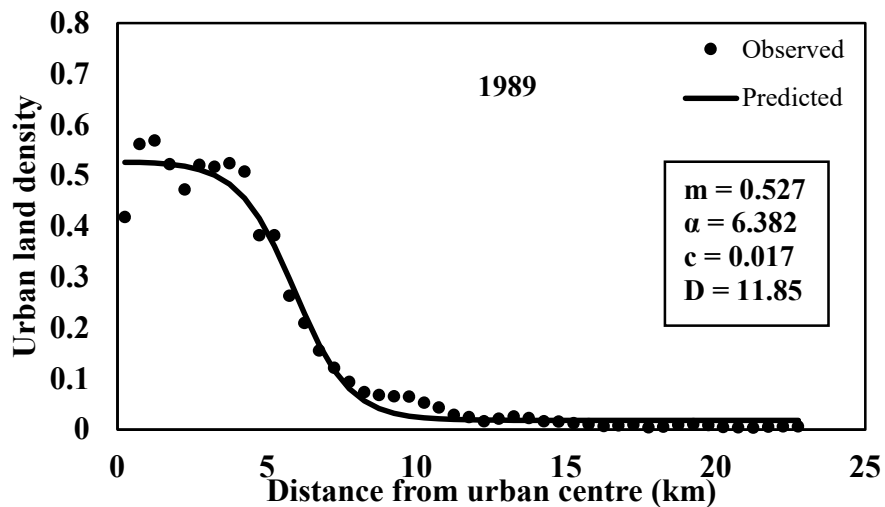


Figure 6.5. Urban land density from city centre for the years 1989, 2001, 2005, 2017.

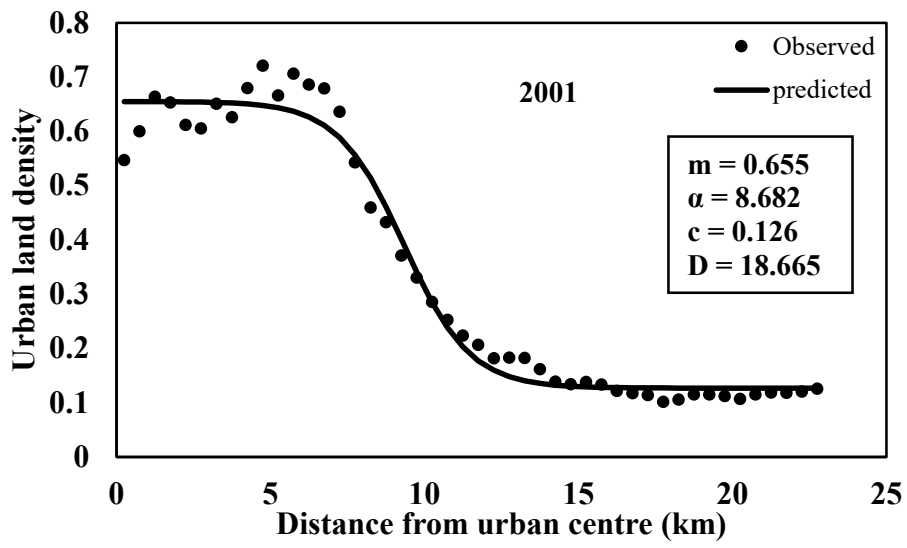
In the year 1989, the UD has higher values in the first 5 km from the centre while in the other three years the higher values are observed within 9 km from the centre. The urban density curve exhibits a significant progressive shift from the year 2001. The initial major dip in the curve could be attributed to the presence of an urban recreational park called Cubbon Park near the centre. The city core encompasses numerous green spaces

and lakes which explains the recurrent inundations in the curves. In the years 2001, 2005 and 2017, the urban core does not exhibit significant change while the UD in the suburban regions has increased during the years.

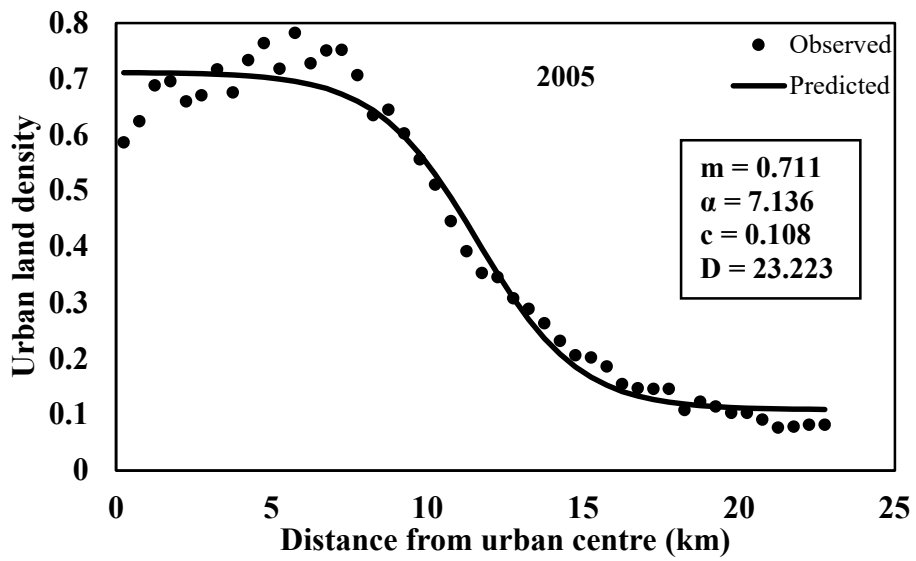
The variation of UD with distance from the city centre can be best represented using an inverse S-shape function. Figure 6.6 illustrates the fitting of urban land density function on the land density data estimated during the study period. The fitting parameters  $m$ ,  $c$ ,  $\alpha$  and  $D$  are estimated for the corresponding datasets. The reliability of the model function can be ascertained by using the values of the different metrics such as  $R^2$ ,  $CC$ ,  $RMSE$ ,  $MAE$ . Table 6.2 illustrates the accuracy metrics for the fitted model. The higher value of  $R^2$  and  $CC$  and lower values of  $RMSE$  and  $MAE$  prove the fitting of the model in the urban land density data.



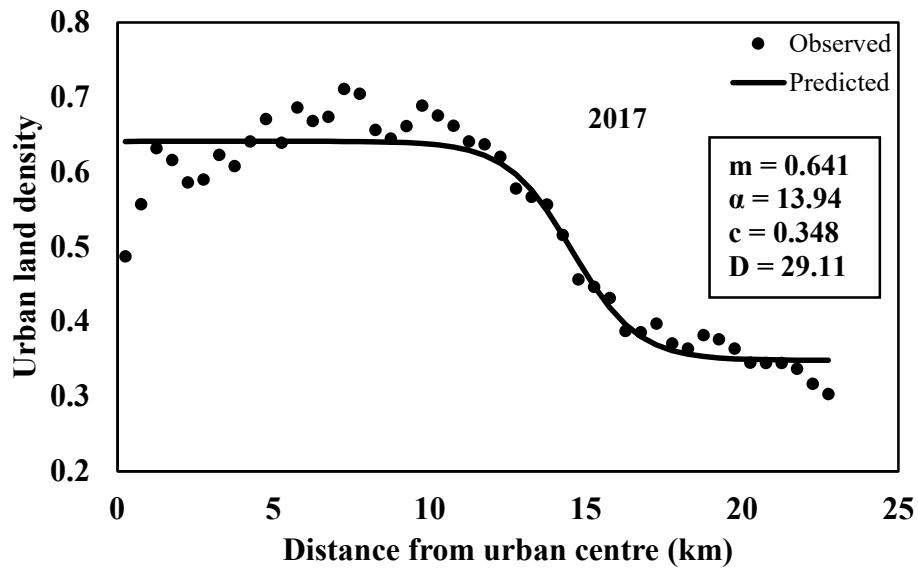
(a)



(b)



(c)



(d)

Figure 6.6. Fitting of urban land density function to the land density data for the years (a) 1989 (b) 2001 (c) 2005 (d) 2017.

Table 6.2. Model evaluation metrics for urban land density

	1989	2001	2005	2017
<b>R<sup>2</sup></b>	0.926	0.888	0.913	0.861
<b>CC</b>	0.9911	0.9892	0.9880	0.9582
<b>RMSE</b>	0.0039	0.0051	0.0059	0.0056
<b>MAE</b>	0.0189	0.0258	0.0307	0.0261

The parameter  $c$  has increased during the period from 1989 to 2017 with a significant increase in the year 2017, indicating the growth of urban area in the outskirts during period-2. The radius of main urban land has increased over the study period, which is indicated by increase in value of  $D$  over the years. The value of constant  $\alpha$  reports the slope of urban density function. The increasing value of  $\alpha$  suggests the expansive growth of urban core during the study period. The radius of the urban core was less than 5 km in 1989 and has grown up to 14 km in 2017.



The predicted curve for 1989 is very steep, suggesting the city's compactness during that period, while in 2017 it is less steep, signifying the urban area's sprawling. The overall density of the urban land can be illustrated by the slope of the urban density function (Bonafoni & Keeratikasikorn, 2018). The slope of the function is determined using the parameter  $k_s$ . The value of  $k_s$  shows a decreasing trend from 1989 to 2017, indicating an increase in suburban growth (Table 6.3). The urban area was initially concentrated in the city, and later it expanded to the outskirts. Since the year 2001, UD in suburban and urban fringe has expanded and is still growing as indicated by the curve of 2017.

**Table 6.3. Slope of the modified sigmoid function for urban land density**

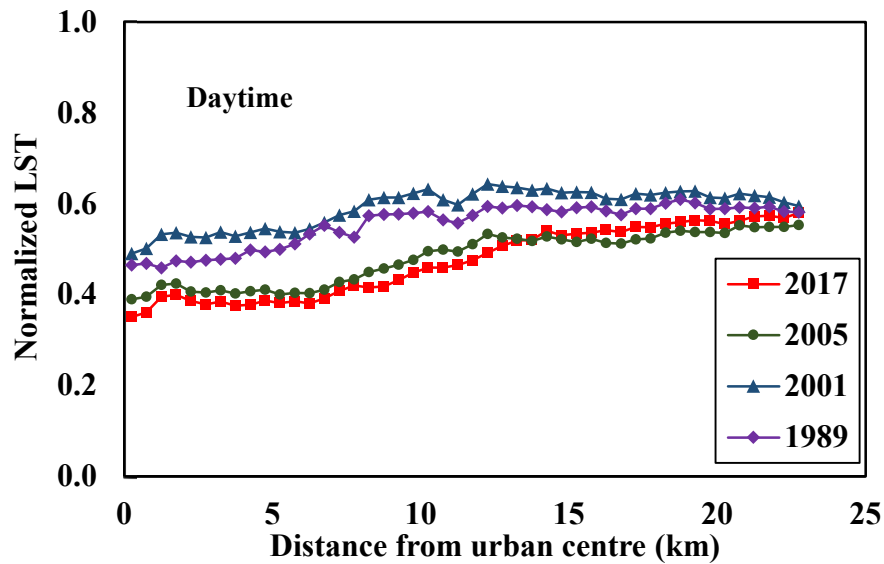
	1989	2001	2005	2017
$k_s$	0.232	0.178	0.120	0.137

There was a significant leap in the urban area from 1989 to 2001, which continued until 2017. The urban core area has increased, and a rapid urbanization has occurred in the outskirts. In comparison to 1989, there has been a significant increase in UD in the outskirts (beyond 15 km from the city centre) in recent years. For the year 2005, some barren land pixels are misclassified as urban; hence it gives a slightly higher UD value in the urban core. The urban area has grown spatially following a monocentric growth pattern. Over the years, the urban density curve has become less steep, especially in suburban regions, signifying the increase in urban areas. The positive drift in UD after 2000 is due to the numerous construction activities in the area during that period. Numerous information technology parks and public sector industries were established in Bengaluru during that period. This has led to the enormous growth of Bengaluru both in terms of population and urban area.

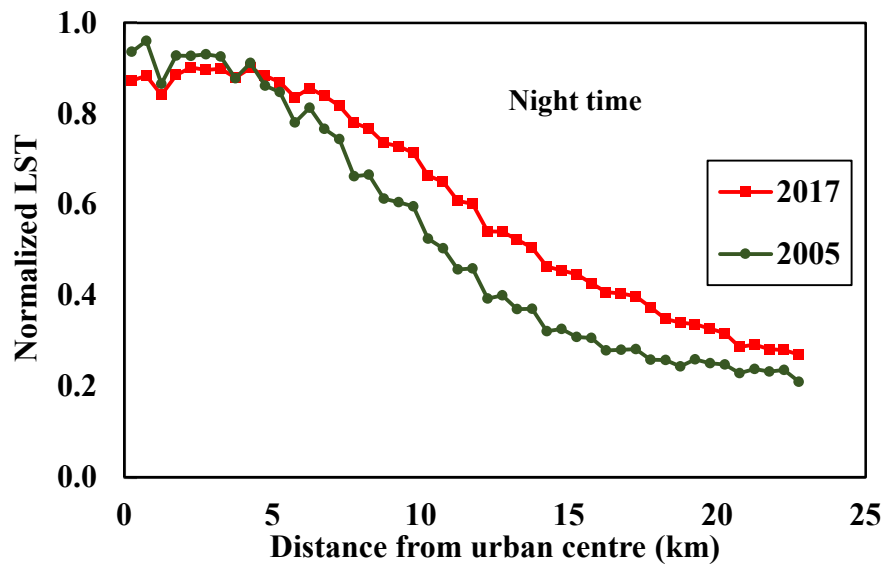
### 6.3.2 Normalized LST modelling

The mean normalized LST with distance from the city centre is assessed based on the concentric ring approach for day and night-time. The variation of mean normalized LST with distance for different years during day and night-time is illustrated in Figure 6.7.

During the daytime, the mean  $LST_n$  values increase from the urban centre to outwards, while at night it is reversed. The urban centre is cooler than the outskirts during the daytime and hotter at night. Even though the trend of mean  $LST_n$  is different during day and night-time, the shape of the curve is similar.



(a)



(b)

**Figure 6.7. Mean normalized LST with distance from the city centre (a) Daytime for the years 1989, 2001, 2005, 2017 (b) Night-time for the years 2005 and 2017**

During the daytime, the range of  $LST_n$  values is from 0.35 to 0.65. During the study period from 1989 to 2017,  $LST_n$  curve has become steeper, and the minimum  $LST_n$  value observed in the urban centre has decreased over the years. Daytime  $LST_n$  observed in the inner and suburban areas shows a significant decreasing trend over the years. The lower  $LST_n$  values are concentrated at a distance of less than 6km from the urban centre during the daytime, signifying the presence of an urban cool island or urban sinks. It is a condition in which the urban area is cooler than the surrounding peri-urban or rural area. Over the years, an urban cooling expansion beyond the urban core is observed during the daytime. The distance beyond which higher  $LST_n$  values are observed is increasing over the time period and is about 15 km in recent years.

The LST patterns can be explained with respect to the land cover surface ratios in the study area (Tables provided in Appendix). The dip in LST is observed in rings where the land area constitutes more vegetation and water bodies than urban land. The study area comprises many urban parks and water tanks which help in lowering LST in the city core. Ring 1 & 2 exhibits a drop in LST due to the presence of Cubbon Park, one of the largest urban vegetation in the study area. Two main urban features spotted in rings 3 and 4 are Race Course and M Chinnaswamy stadium. Another major urban park in the region called Lalbagh Botanical Garden and lake which are positioned in ring 5 and 6. Several lakes and tanks such as Ulsoor lake, Madiwala lake, and Bellandur lake are situated within the 10 km radius of the city centre. Beyond urban core, undulations in LST pattern for the years 1989 and 2001 are smoothened in the later years due to the conversion of a large extent of barren land to urban.

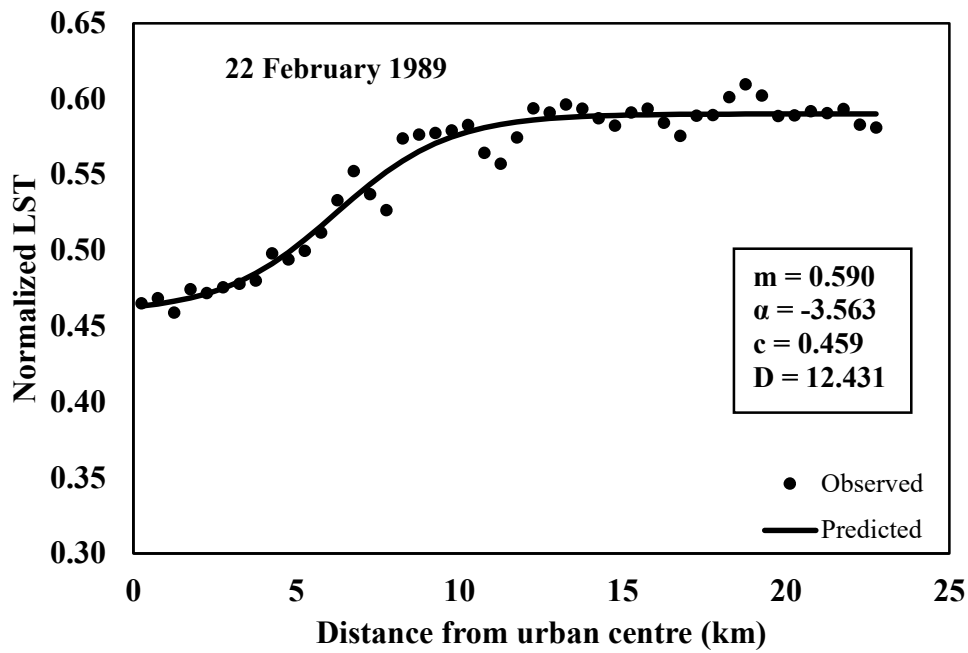
Alternately, night-time LST exhibits different behavior, and the  $LST_n$  value ranges from 0.2 to 1. The mean  $LST_n$  curve of 2005 is steeper than that of 2017, suggesting that urban heat expansion has occurred over the years. Night-time  $LST_n$  values in the urban core do not change significantly, while in the suburban area and urban fringes the value has increased.

**Table 6.4 Model evaluation metrics for normalized LST**

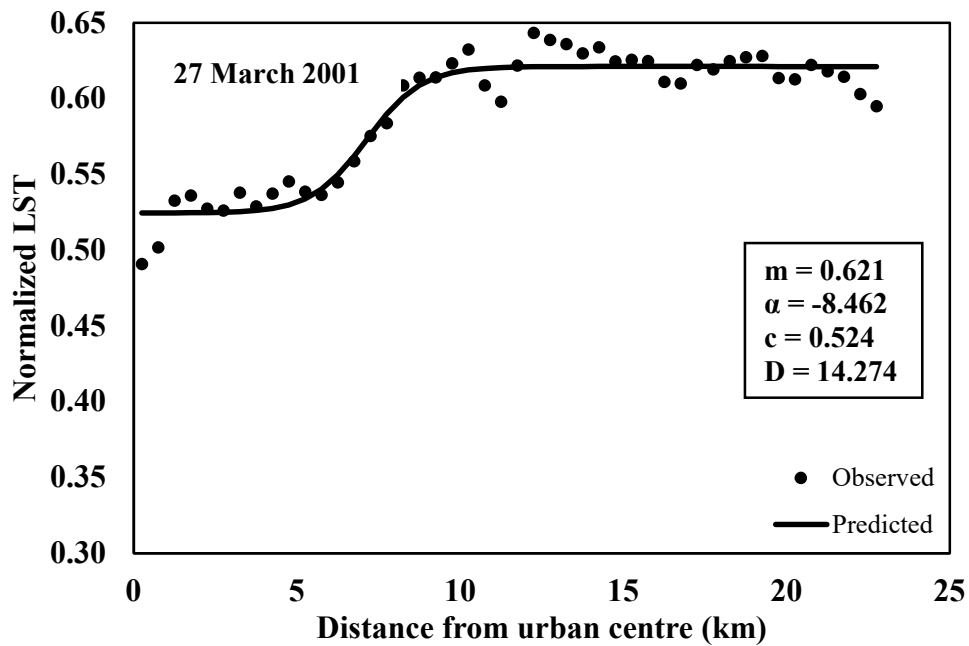
	Daytime				Night-time	
	1989	2001	2005	2017	2005	2017
<b>R<sup>2</sup></b>	0.972	0.907	0.913	0.952	0.97	0.971
<b>CC</b>	0.9798	0.9613	0.9828	0.9931	0.9974	0.9968
<b>RMSE</b>	0.0013	0.0017	0.0015	0.0013	0.0028	0.0026
<b>MAE</b>	0.0071	0.0089	0.0083	0.0068	0.0135	0.0142

The higher  $LST_n$  values are concentrated in the urban centre at a radius of less than 6 km, confirming the presence of an urban heat island effect during night-time. During the night-time, the urban area is hotter than the surrounding peri-urban or rural area. In the years 2005 and 2015, the lower night-time  $LST_n$  values are observed beyond 15 km.

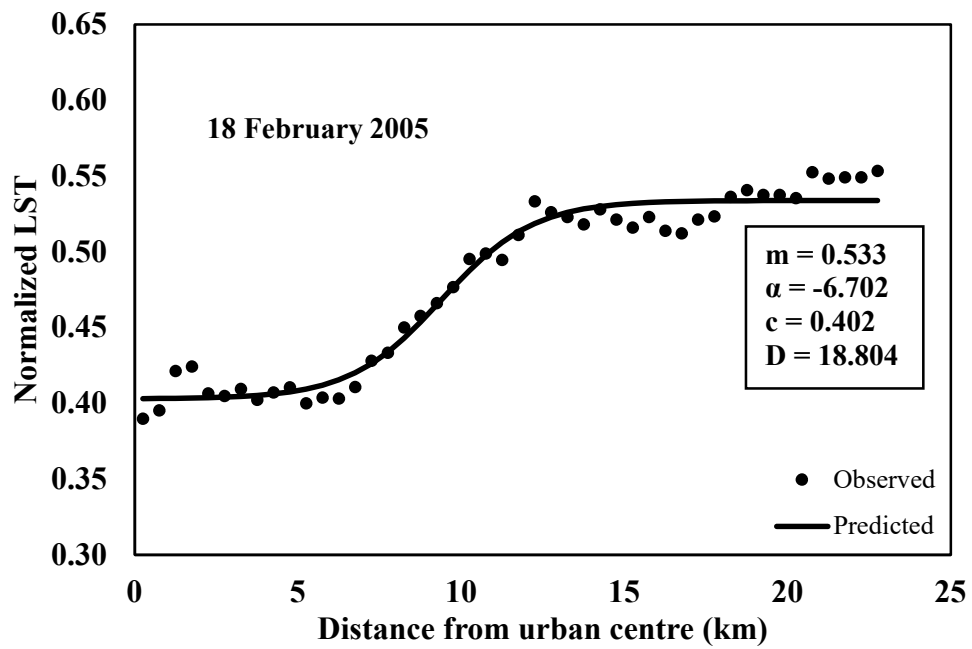
The normalized LST values show that the variation of normalized LST with distance from the urban centre follows an inverse S-shape function. Figure 6.8 and 6.9 illustrate the fitting of the inverse S-shape function to the normalized LST during daytime and night-time respectively. The model parameters  $m$ ,  $c$ ,  $\alpha$ ,  $D$  and the coefficient of determination  $R^2$  are estimated for the corresponding  $LST_n$  values. The  $R^2$ ,  $CC$ ,  $RMSE$  and  $MAE$  values estimated for the corresponding images are described in Table 6.4. The reliability of the model function can be ascertained by high  $R^2$  and  $CC$  values.



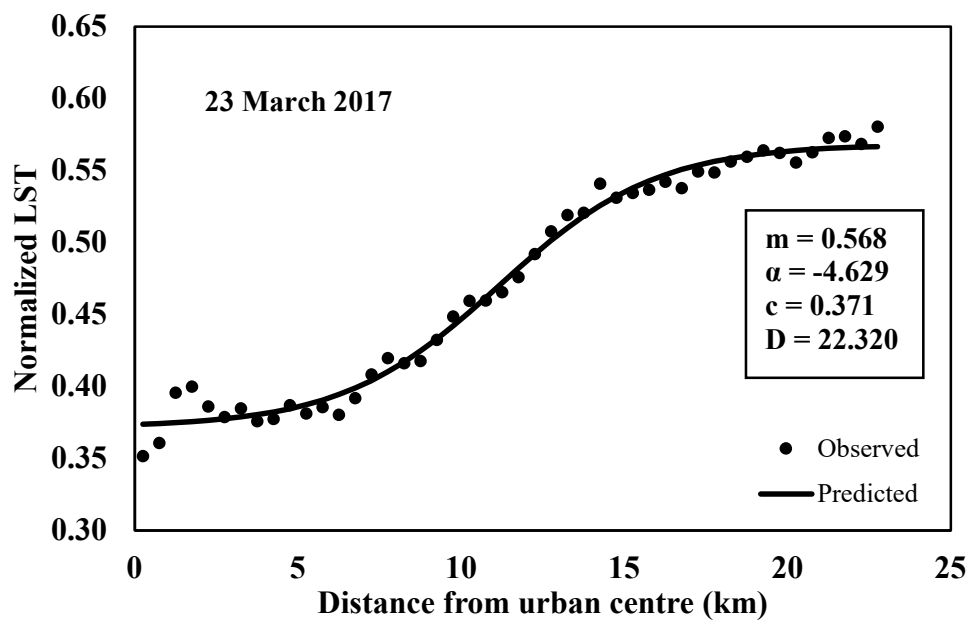
(a)



(b)

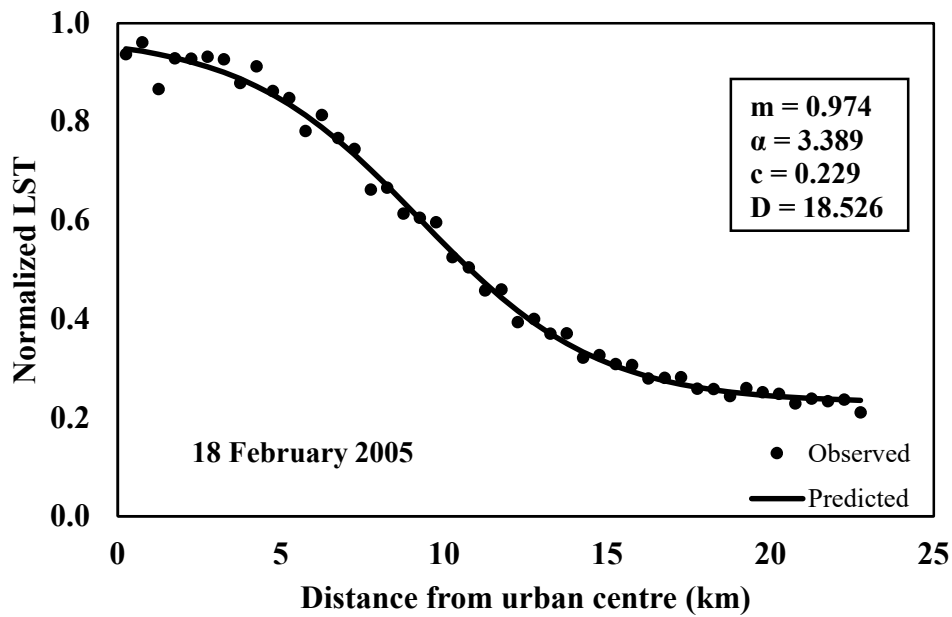


(c)

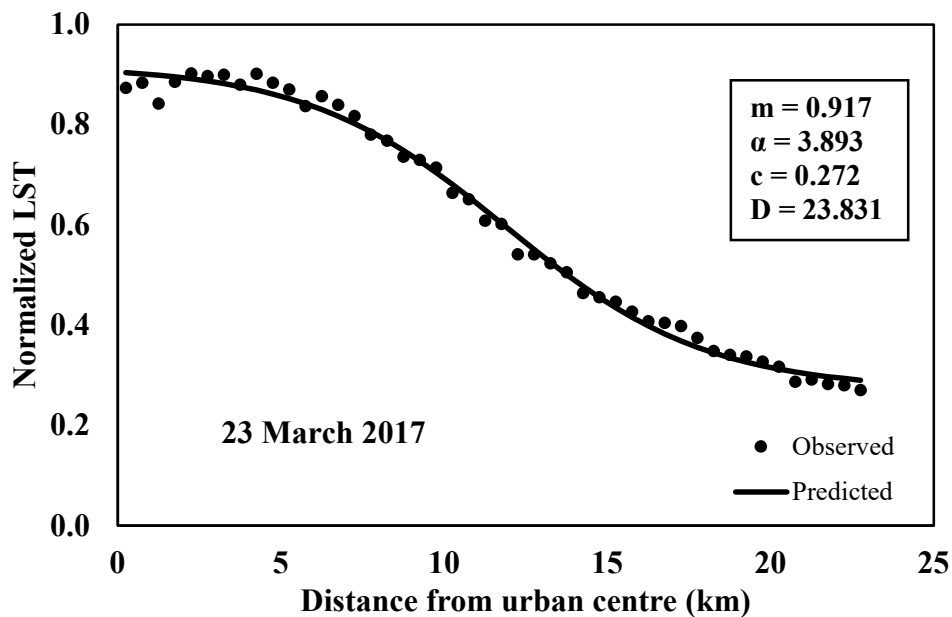


(d)

**Figure 6.8. Fitting of the function for the mean  $LST_n$  values of day time from urban centre: (a) 22 February 1989 (b) 27 March 2001 (c) 18 February 2005 (d) 23 March 2017**



(a)



(b)

**Figure 6.9. Fitting of the function for the mean  $LST_n$  values of the night-time from urban centre: (a) 18 February 2005 (b) 23 March 2017**

Considering the daytime data, the decrease in the value of  $c$  indicates that the LST has fallen in the outskirts during the study period. The main urban cool effect span has

increased over the study period, which is indicated by the increase in the value of  $D$  over the years. The constant  $\alpha$  reports the slope of the function,  $\alpha$  is negative since there is an increasing trend of LST from centre to outwards. The rise in the value of  $\alpha$  indicates an expansive growth of the urban cool effect during the study period. The night-time LST also exhibits similar behaviour with the reverse trend in LST. The night-time LST of suburban and urban fringes has increased as proved by a rise in the value of  $c$  over the years.

**Table 6.5 Slope of the modified sigmoid function for normalized LST**

	1989	2001	2005	2017
$k_s$	0.068	0.124	0.093	0.057

The  $k_s$  parameter values in Table 6.5 indicate that the heat sink effect during the daytime has expanded over the years, which is proved by a less steep curve in 2017. The sprawling of the cooling trend coincides inversely with the suburban growth trend shown in Table 6.3.

The mean  $LST_n$  for day and night-time was successfully modelled using inverse S-shape function. As urban expansion occurs, the study area experiences an expansive cooling effect or urban heat sinks during daytime. While at night-time, an expansive heating effect is experienced in accordance with the growth in UD in the suburban area and outskirts. Therefore, during the daytime, the study area experiences an urban cool island, and during night-time it exhibits an urban heat island. The presence of statistically significant cold spots in the city centre and hot spots in the periphery during daytime was reported in the previous chapter.

The daytime urban heat sinks or cool effect can be attributed to different factors. The Bengaluru urban district comprises several recreational and ecological parks, out of which Lalbagh Botanical Garden and Cubbon Park are the two main spots. The presence of these urban parks and water tanks helps in reducing the LST of the city core. During summer, the city's outskirts will be mostly dry, absorbing more heat than urban areas. Since it is primarily barren, evaporation and transpiration will be less



leading to lower LST in the urban area compared to the surrounding during daytime (Rasul et al., 2015).

The night-time heating can be attributed to the anthropogenic heat released from the impervious surfaces such as concrete road pavements, building glass, concrete roofs etc. In the suburban regions, night-time LST of 2017 is higher compared to 2005, coinciding with the growth of UD in the region during recent years.

### 6.3.3 Relationship between urban density and normalized LST

A scatterplot is prepared with urban land density and mean normalized LST for the different years during daytime and night time as shown in Figure 6.10 and 6.11 respectively. Third-degree polynomial function is fitted to the dataset and the coefficient of determination is computed.

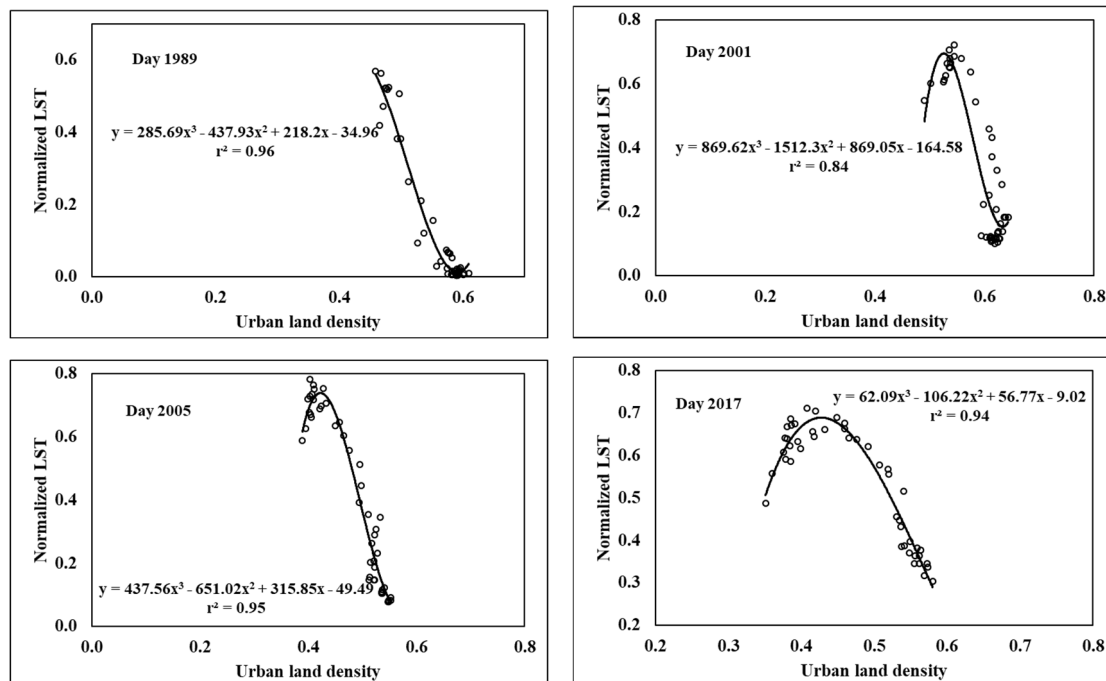


**Figure 6.10. The plot of urban land density with normalized daytime LST computed for each concentric ring: 1989, 2001, 2005, 2017**

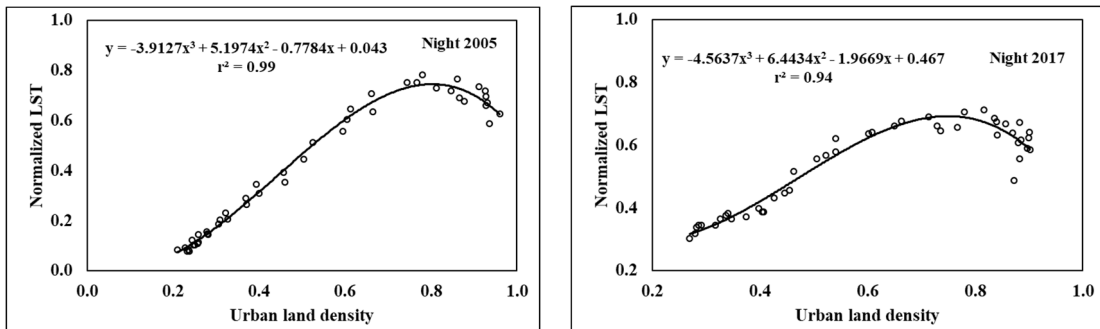


**Figure 6.11 Plot of urban land density with normalized night-time LST computed for each concentric ring: 2005 and 2017**

The  $r^2$  values and the polynomial functions are given in figures 6.10 and 6.11. The urban land density and mean normalized LST computed in each concentric ring exhibit an accurate relationship which is proved by the high  $r^2$  values. The relation between the urban density and the heat waves established can be used as scientific support for the formulation of urban planning policies

Concisely, in Bengaluru, the daytime LST during the summer season and urban density have a negative correlation implying that the urban area is cooler than the surrounding peri-urban area. The night-time LST and urban density have a positive correlation suggesting the presence of an urban heat island at night in the summer season. Therefore, it can be concluded that urban density is not the only factor determining the LST of the study area. The daytime LST pattern of the area is due to the intense heat waves produced in the non-urban area during the summer season. In the summer season, the evapotranspiration in the city's outskirts will be much less due to low vegetation. At the same time, the evapotranspiration in the urban areas will be high due to human population and the planted trees and gardens leading to a cooling effect in the urban area compared to the surrounding (Shastri et al.,2017).

#### **6.3.4 Relationship between LST and surface area ratio**

The relationship between LST, VD, WD and UD was obtained using multiple linear regression. The multiple regression equations developed for the study area for different years is presented in equation 6.4 – 6.7, as follows:

(a) Daytime

$$\text{For the years 2017: } LST_n = 0.94 - 0.51UD - 1.04VD - 0.48WD \quad (6.4)$$

$$2005: \quad LST_n = 0.73 - 0.33UD - 0.33VD - 0.06WD \quad (6.5)$$

$$2001: \quad LST_n = 0.79 - 0.23UD - 0.42VD - 0.05WD \quad (6.6)$$

$$1989: \quad LST_n = 0.61 - 0.24UD - 0.03VD - 0.36WD \quad (6.7)$$

(b) Night-Time

$$\text{For the years 2017: } LST_n = 1.57UD + 2.79VD + 1.13WD - 0.75 \quad (6.8)$$

$$2005: \quad LST_n = 1.43UD + 1.20VD + 0.003WD - 0.46 \quad (6.9)$$

The regression models explaining the relationship between UD, VD, WD and LST during day and night are shown in equations 6.4 to 6.7 and 6.8 to 6.9, respectively. Coefficient of determination ( $R^2$ ) value of approximately 0.94 was obtained for all the regression models. The scatterplot of predicted and observed  $LST_n$  indicates the accuracy of the models (Figure 6.12 & 6.13). The regression models obtained explain the best relationship between LST and land cover types.

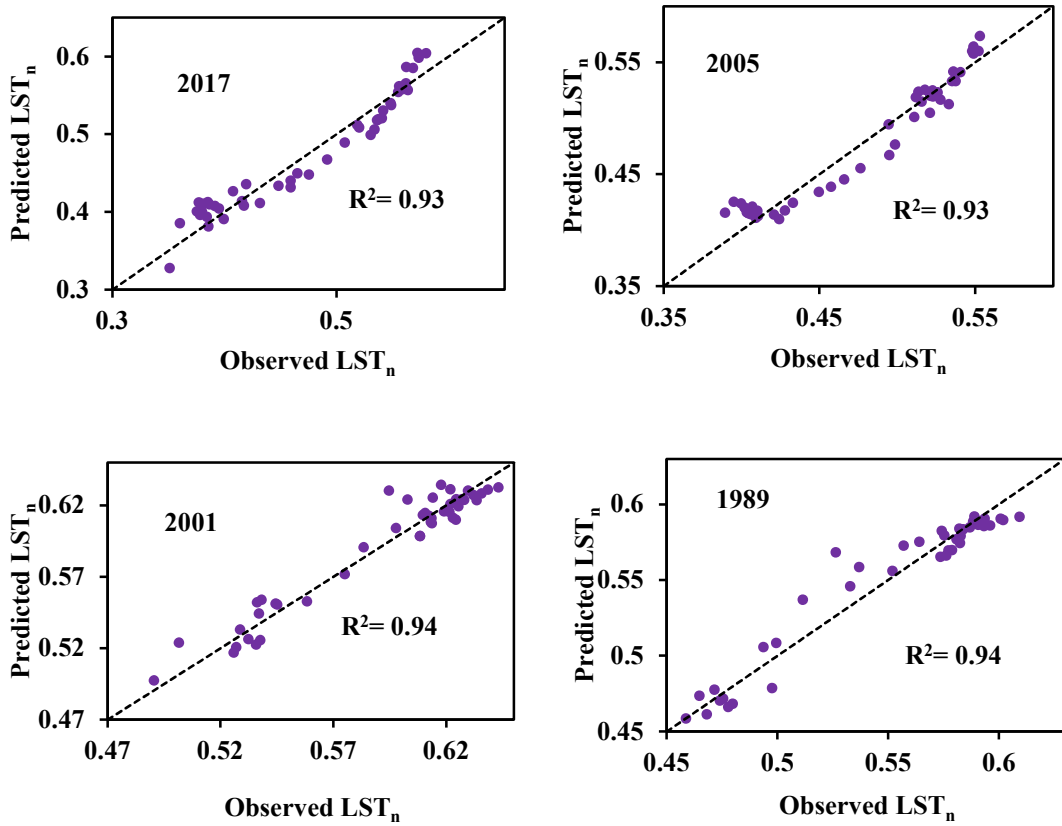


Figure 6.12. Comparison of observed and predicted normalized LST for the daytime

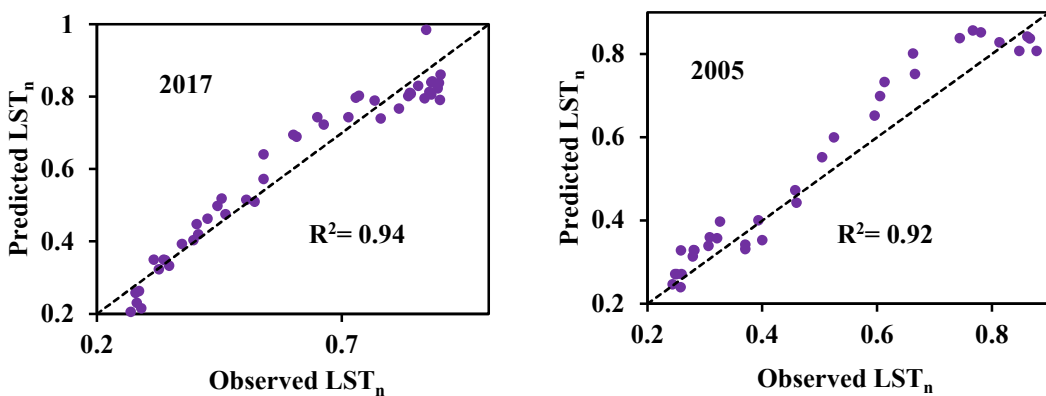


Figure 6.13. Comparison of observed and predicted normalized LST for the night-time

All the parameters of the model exhibit a statistically significant relationship with LST. For the years 2017, 2005 and 2001, the parameters UD and VD exhibit high statistical

significance with a  $p$ -value  $< 0.001$  while for the year 1989, UD and WD have a  $p$ -value  $< 0.001$ . The model suggests a negative correlation exists between LST and VD, WD and UD during the daytime. In the study area, urban land, vegetation and water bodies cause a reduction in LST during the daytime. Many previous studies have reported the negative correlation of LST with vegetation and water bodies (Ramachandra & Kumar, 2010; Bharath et al., 2018). The negative correlation between LST and UD is relatively distinct observation in comparison to the findings in the urban heat island studies of the study area (Ramachandra et al., 2013). However, the urban land, water and vegetation enhance LST pattern during night-time.

Several studies have been conducted on UHI effect in different urban centres of India. In Chennai, LST exhibits a negative correlation with vegetation and a positive correlation with densely built-up (Faris and Sudhakar Reddy, 2010) and air temperature increases in a radial direction from suburbs to city centre (Devadas and Ross 2009). Badarinath et al. (2005) observed the day and night-time UHI in Hyderabad and reported that core urban areas experience a night-time urban heat island. Thomas et al. (2014) noted that the UHI intensity is stronger in winter than in summer and the early night UHI is less intense when compared to the pre-drawn UHI in Kochi. A study carried out in Delhi from 2007 to 2010 suggests that a UCI is experienced during day time in May, June, November and December (Pandey et al., 2012).

### **6.3.5 Hybrid PSO-SVR Model**

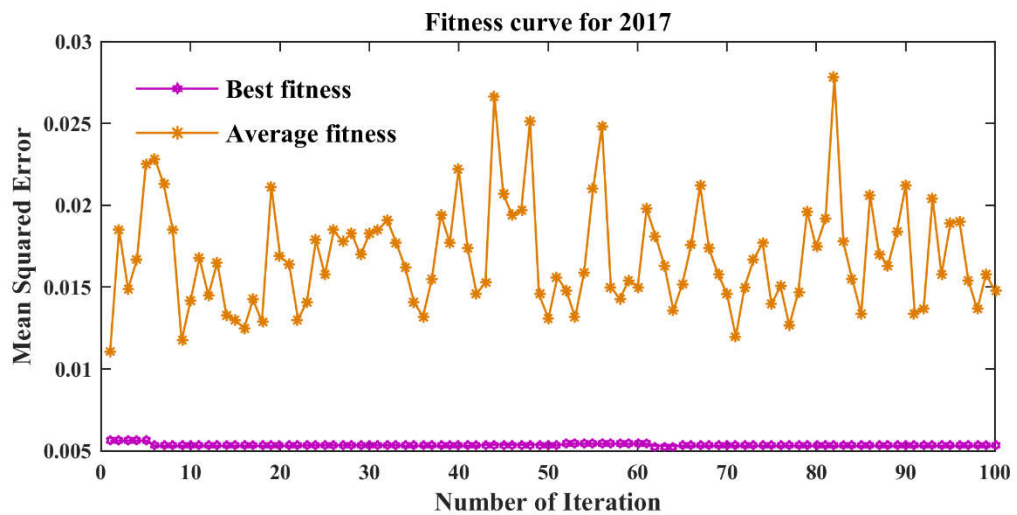
The non-linear relationship between surface area ratios and LST was established using a hybrid PSO-SVR model for the years 1989, 2001, 2005 and 2017. LST for the four time steps was predicted using different combinations of predictive variables. PSO algorithm was used to tune the hyperparameters of SVR model. The proposed model was implemented in MATLAB environment. The model was validated using evaluation indices,  $RMSE$  and Coefficient of Determination ( $R^2$ ). Optimal values of regularization parameter  $C$  and radial bias kernel function  $\gamma$  with the lowest  $MSE$  was estimated from the range specified, (Table 6.1) by employing the PSO algorithm. The SVR model was trained using these optimal hyperparameters. The performance of Hybrid PSO-SVR

model for four different combinations of predictive variables in the testing and training phase at four time steps is presented in Table 6.6.

Model result diagrams of base combination where LST is modelled with respect to UD, VD, WD and BD for the years 2017, 2005, 2001 and 1989 are presented in the following sections.

### 6.3.6 Results of Hyperparameter tuning

The fitness values were recorded during the hyperparameter tuning process by applying PSO, to draw the fitness curves. Figure 6.14 shows the best fitness (minimum MSE) and average fitness (maximum MSE) for the years 2017, 2005, 2001 and 1989.



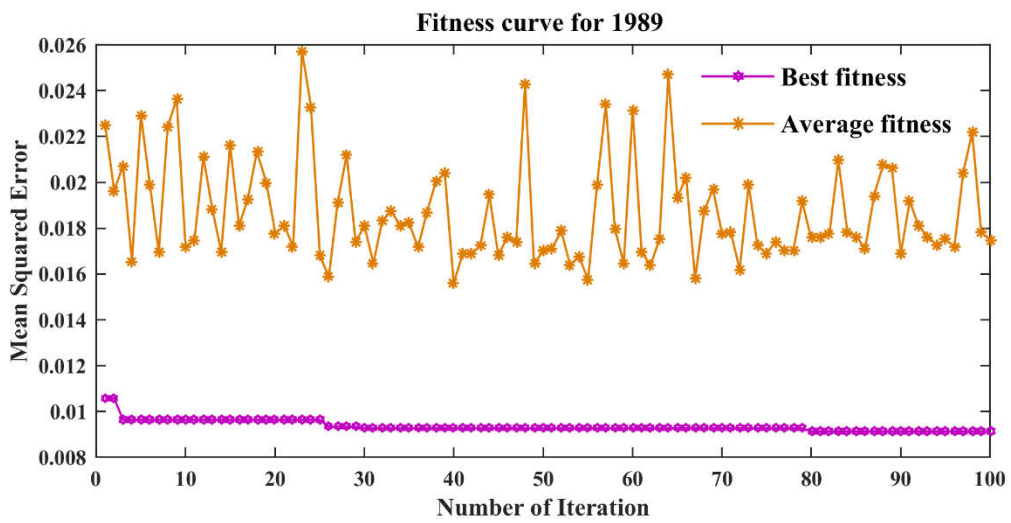
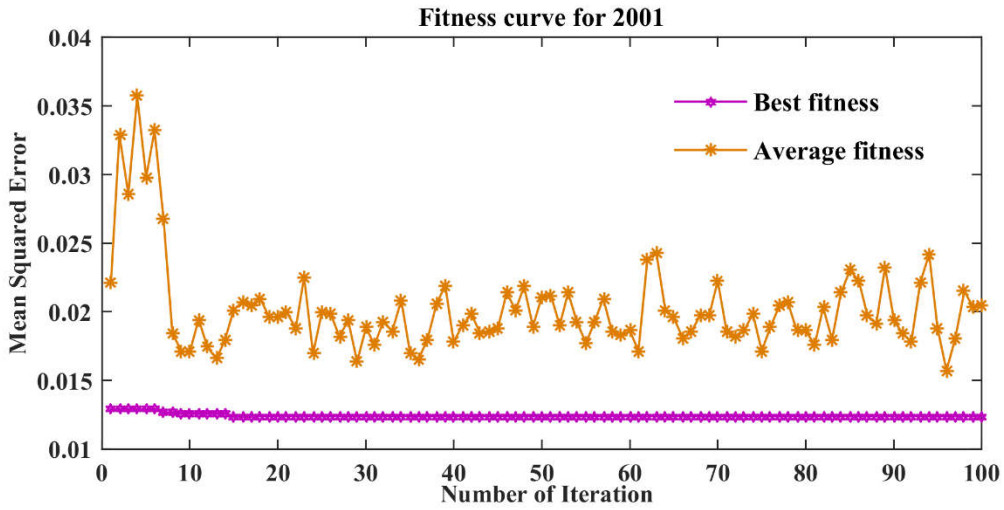
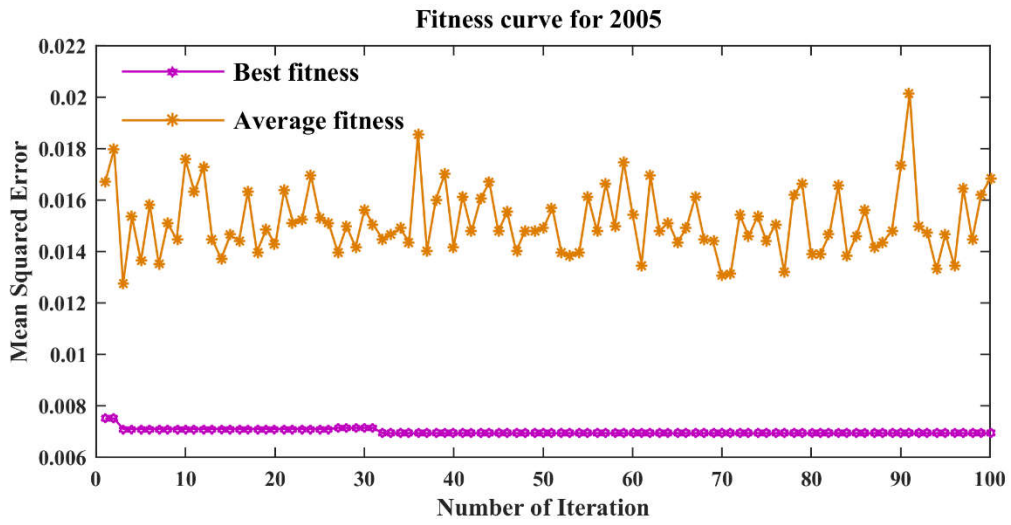


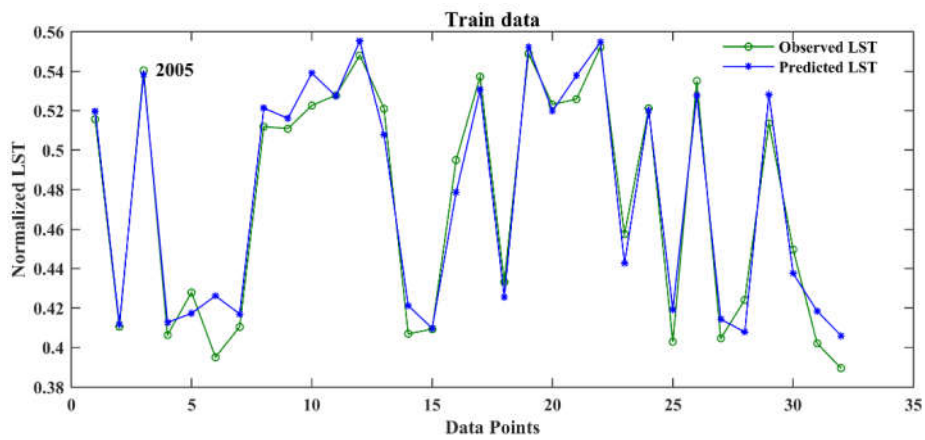
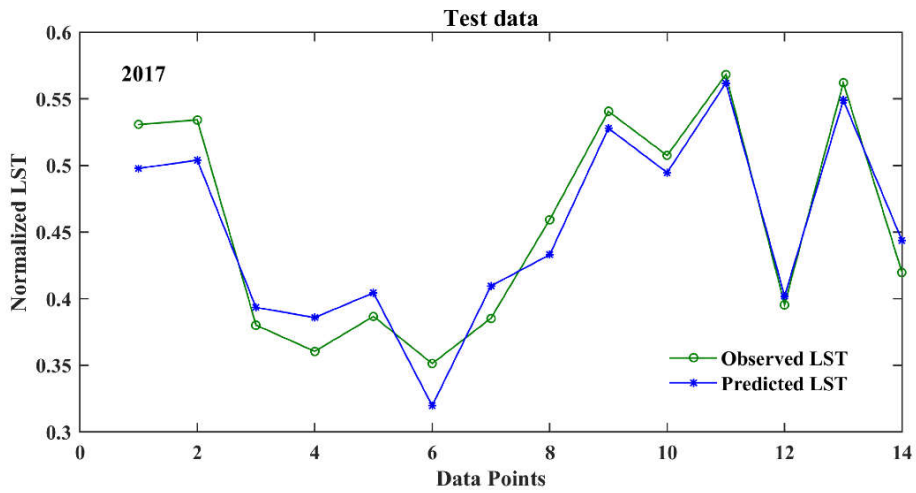
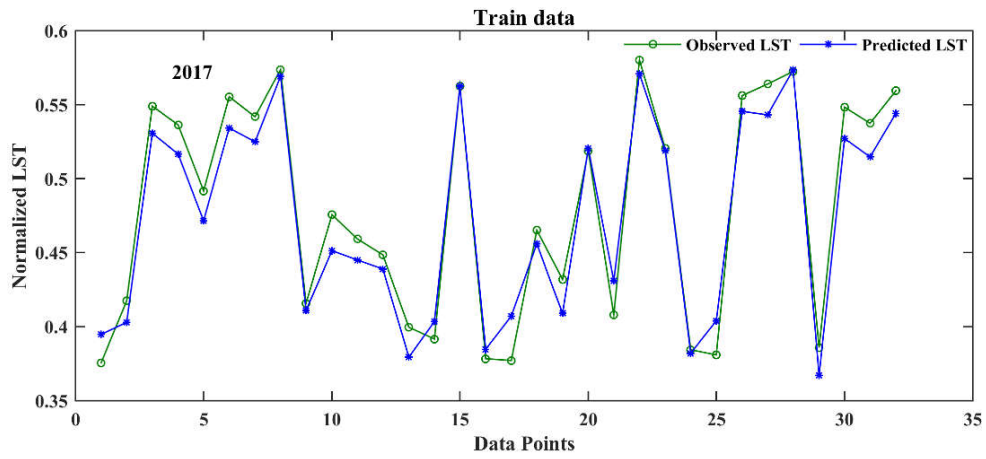
**Figure 6.14** Fitness curves for optimizing hyperparameters using PSO for the years 2017, 2005, 2001, 1989

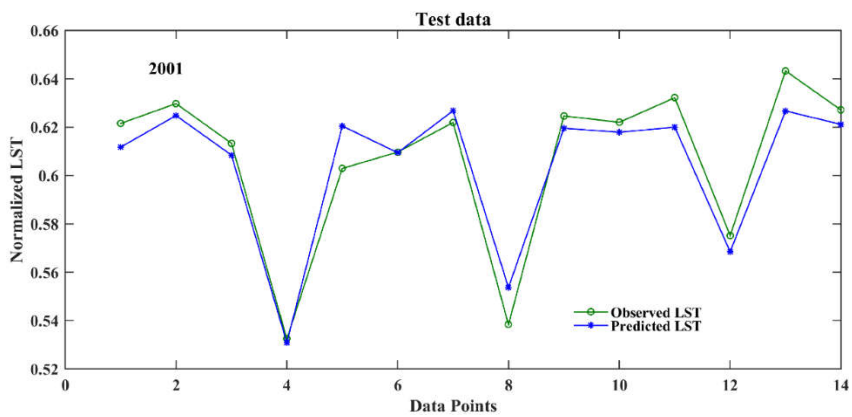
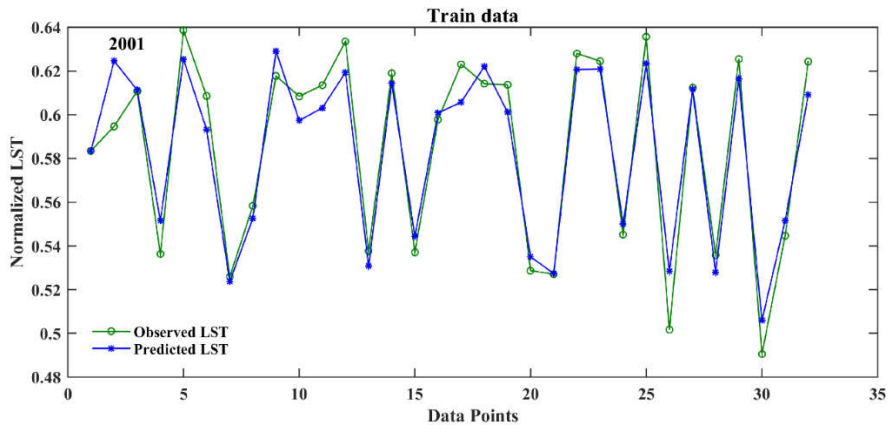
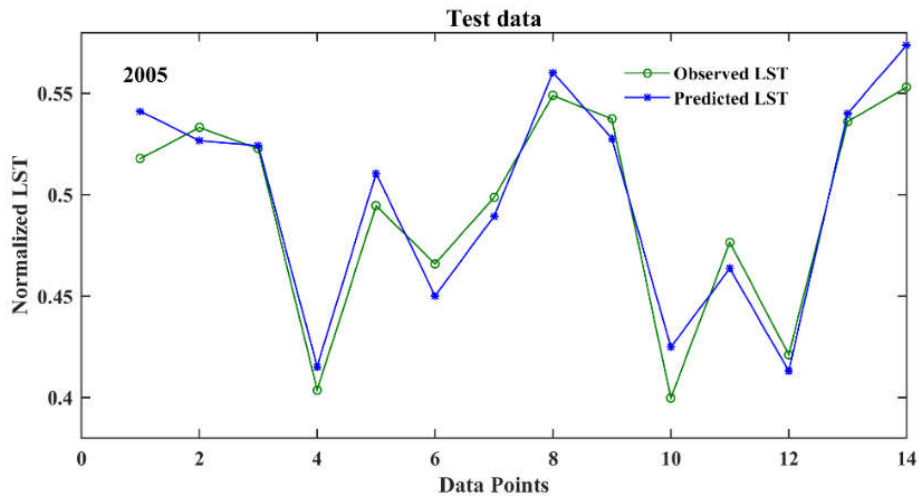
For the year 2017 the average fitness value ranges from 0.0111 to 0.0278 in first 100 iterations. The minimum fitness decreased from 0.00564 to 0.00532 at sixth iteration and decreased further to 0.00529 at sixty second iteration and beyond remain constant. The lowest value of minimum MSE (0.00529) was attained after 62 iterations. In the case of 2005, minimum fitness decreased from 0.00751 to 0.00711 at the third iteration and decreased further to 0.00694 at thirty second iteration and kept constant. The average fitness value ranges from 0.01276 to 0.02015. The lowest value of minimum MSE (0.00694) was attained after 32 iterations. For 2001, the average fitness value ranges from 0.01574 to 0.0357. The minimum fitness decreased from 0.0129 to 0.01266 at the seventh iteration, decreased further to 0.01234 at the fifteenth iteration, and remained constant. In the case of 1989, minimum fitness decreased from 0.01057 to 0.00964 at the third iteration, decreased further to 0.00912 at eightieth iteration and beyond remains constant. The average fitness value ranges from 0.0156 to 0.02573. For 2001 and 1989 the lowest value of minimum MSE (0.01234 and 0.00912) was attained after 15 and 80 iterations respectively. These results prove the feasibility and efficacy of PSO algorithm in tuning the hyperparameters of SVR. The Hybrid PSO-SVR model was built on the tuned hyperparameters for modelling LST with different surface area ratios at different time frames.

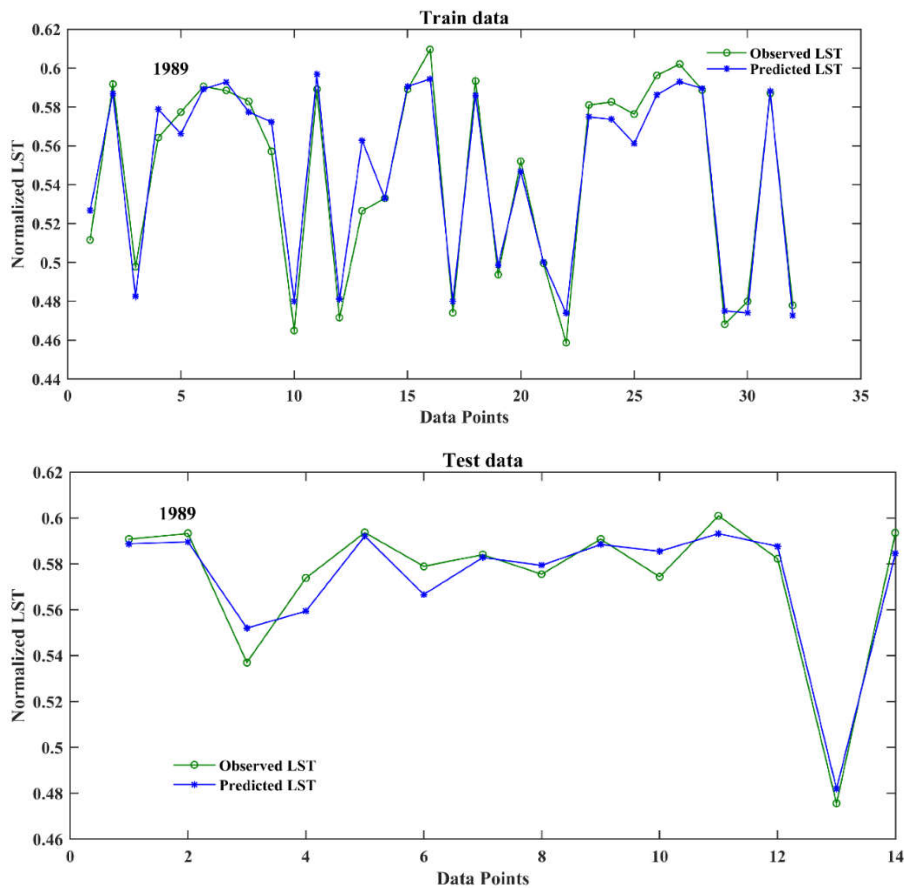
### **6.3.7 Capability of Hybrid PSO-SVR model**

Figure 6.15 demonstrates the capability of the hybrid PSO-SVR model on the training and testing dataset. It can be observed that LST can be effectively modelled by employing the proposed model.  $R^2$  values of the training set was close to the  $R^2$  values testing set suggesting that the proposed model was well trained.









**Figure 6.15 Performance of Hybrid PSO-SVR model at training and testing stages for the four time steps**

The values of optimized SVR hyperparameters ( $C$ ,  $\gamma$ ,  $\epsilon$ ) of the model are given in Table 6.6. These hyperparameters are applied to the test data to predict LST accurately. The value of  $\epsilon$  is kept constant at 0.1 while the values of  $C$  and  $\gamma$  are optimized using PSO method.

The impact of UD, VD, WD and BD on LST can be observed from Table 6.6. The base combination where all the parameters are included has a higher value for  $R^2$  for all the four years. LST of the region is better predicted by using all the four surface area ratios. It can be observed that a single parameter or a combination of two parameters cannot accurately determine the LST of the region. The model results indicate that LST is the combined effect of all the land cover classes of the region. This combined effect is very

effectively modelled using the proposed Hybrid PSO-SVR model and it is consistent for all the four years.

There is a commendable variation in values of UD and VD over the years as Bengaluru witnessed extensive urbanization from 1989 to 2017, however, the proposed method could accurately model the interrelationship of the LST with the predictive variable. This demonstrates the model's superiority in establishing and predicting non-linear relationships between parameters.

**Table 6.6 Optimal SVR hyperparameters and evaluation indices for train and test dataset**

Year	Predictive variables	Train		Test		Optimal SVR Hyper-parameters		
		R <sup>2</sup>	RMSE	R <sup>2</sup>	RMSE	C	$\gamma$	$\epsilon$
1989	UD	0.971	0.076	0.957	0.081	5.971	0.745	0.1
	UD,VD	0.981	0.064	0.970	0.079	7.641	0.520	0.1
	UD,VD,WD	0.972	0.078	0.968	0.094	11.741	0.115	0.1
	UD,VD,WD,BD	0.976	0.074	0.967	0.055	15.819	0.143	0.1
2001	UD	0.917	0.106	0.890	0.159	2.071	2.904	0.1
	UD,VD	0.976	0.067	0.952	0.094	19.236	0.054	0.1
	UD,VD,WD	0.975	0.065	0.958	0.086	13.769	0.071	0.1
	UD,VD,WD,BD	0.968	0.077	0.964	0.062	11.253	0.036	0.1
2005	UD	0.958	0.105	0.953	0.122	8.470	0.447	0.1
	UD,VD	0.973	0.079	0.963	0.097	14.020	0.253	0.1
	UD,VD,WD	0.972	0.078	0.965	0.108	10.070	0.273	0.1
	UD,VD,WD,BD	0.981	0.071	0.965	0.087	20.000	0.184	0.1
2017	UD	0.836	0.188	0.808	0.232	7.114	0.069	0.1
	UD,VD	0.981	0.071	0.969	0.086	2.173	0.981	0.1
	UD,VD,WD	0.981	0.064	0.975	0.090	12.047	0.660	0.1
	UD,VD,WD,BD	0.981	0.072	0.966	0.095	11.525	0.273	0.1

## 6.4 CONCLUSION

The urban land density and mean  $LST_n$  were modelled and parameterized using urban land density function for the years 1989, 2001, 2005 and 2017. The concentric ring-based approach to determine the urban land density and LST with distance from the city centre is useful in characterizing the variation. The change in LST pattern over the years during day and night-time was established using this method relatively accurately. The spatial variation of LST and different land cover types and their interrelationship was explored by the correlation method.

Bengaluru has experienced a significant sprawling urban growth during recent years. Over the years, the suburban areas and the urban fringes have developed. During the summer season, the behavior of LST during daytime and night-time contradict each other. During daytime, urban area experiences a cooling effect, and at night-time an urban heat effect is experienced. Apart from urban density, other land cover types also contribute to the LST pattern of the area.

Regression models so developed could predict LST of the region effectively with  $R^2$  value of about 0.94 for both day and night-time. The positive and negative effects of urban, vegetation and water bodies on LST have been quantified, and the coefficients of the equation indicate the association between LST and the land cover types. LST and land cover interaction was effectively modelled using linear and non-linear regression algorithms. For surface area ratio,  $R^2$  value in the range of 0.94 and 0.97 was obtained for MLR and Hybrid PSO-SVR model respectively.

# MODELLING AND PREDICTION OF LST BASED ON URBAN SURFACE CHARACTERISTICS

---

### 7.1 INTRODUCTION

The relation between LST and urban surface characteristics can be studied by using remote sensing indices like Normalized Difference Vegetation Index (NDVI), Normalized Difference Water Index (NDWI) and Normalized Difference Built-up Index (NDBI). The variation influences the spatio-temporal patterns of LST in the urban surface characteristics such as the spatial arrangement of the urban land uses, the spatial composition, extent of built-up and vegetation. Therefore, the interaction between urban surface characteristics and LST requires further investigation. In this chapter, the relation between LST and NDVI, NDWI, NDBI is modelled by employing linear and non-linear regression techniques and further LST is predicted based on these surface characteristics.

### 7.2 METHODS

Remote sensing indices such as NDVI, NDWI and NDBI were determined from Landsat images for the years 1989, 2001, 2005 and 2017. The relationship between LST and remote sensing indices was analyzed based on linear and non-linear regression methods. The linear relationship between LST and remote sensing indices was studied by using MLR technique. Further, the proposed Hybrid PSO-SVR model was applied to the datasets to predict LST values based on these indices. Hypothetical scenarios were introduced in the prediction to assess the impact of change in vegetation and water bodies on LST. Temporal variation of urban heat anomaly of the region over the period of study was also investigated. The overall methodology is presented in figure 7.1.

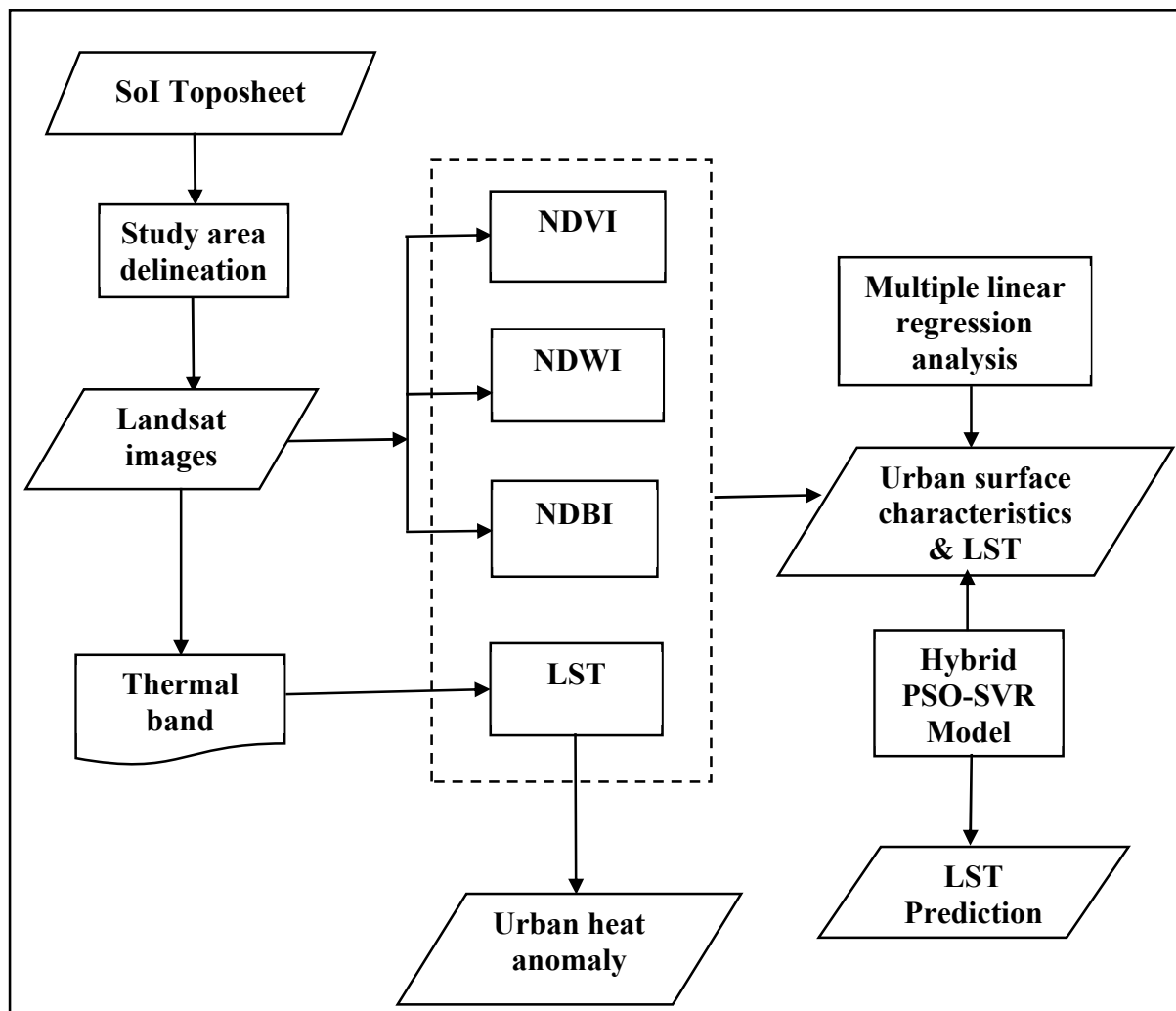


**Figure 7.1 Flowchart of methodology**

### 7.2.1 Urban Surface Characteristics

Three remote sensing indices, NDVI, NDWI and NDBI were used to characterize the urban surface in the study area. NDVI, NDWI and NDBI were estimated from the Landsat images for the years 1989, 2001, 2005 and 2017.

#### 7.2.1.1 NDVI

Researchers have formulated the NDVI index to evaluate the above-ground biomass. Features with lower red reflectance and higher Near-Infrared (NIR) reflectance will be

enhanced and those with low NIR and red reflectance will be eliminated (Chen et al., 2006). NDVI is calculated using eq. (7.1)

$$\text{NDVI} = \frac{\text{NIR} - \text{Red}}{\text{NIR} + \text{Red}} \quad (7.1)$$

The value ranges from -1 to +1. Negative values indicate open water features, zero refers to bare soil and positive values indicate vegetated surfaces

#### 7.2.1.2 NDWI

NDWI was formulated by (McFeeters, 1996) to delineate open water features from satellite images and is based on the same assumption as NDVI. Green and NIR bands are used for the computation of this index. It is calculated using eq. (7.2)

$$\text{NDWI} = \frac{\text{Green} - \text{NIR}}{\text{Green} + \text{NIR}} \quad (7.2)$$

The empirical equation was framed by taking advantage of the condition that open water features have maximum reflectance for the green band and low reflectance for NIR wavelength. Soil and terrestrial vegetation possess negative or zero value for NDWI while open water features have higher positive values.

#### 7.2.1.3 NDBI

NDBI was introduced by Zha et al. (2003b) to delineate built-up area based on the spectral response and other land covers using the eq.(7.3). A drastic increase in the reflectance of Mid-Infrared (MIR) and NIR is exhibited for built-up areas and barren land. The index will have a negative value for water bodies while the vegetated surface will have zero or close to zero values

$$\text{NDBI} = \frac{\text{MIR} - \text{NIR}}{\text{MIR} + \text{NIR}} \quad (7.3)$$

### 7.2.2 Multiple linear regression analysis

The main objective of regression is to fit a model to a training dataset to understand the relationship between input and output variables. MLR was applied to datasets of the four-time steps in this study. Linear regression analysis was performed to model LST combining the three remote sensing indices. LST, NDVI, NDWI and NDBI were



employed to develop linear regression models of the study area for the years 1989, 2001, 2005 and 2017. MLR was applied using two window sizes of 3x3 and 5x5. The correlation between LST and the indices is reported by developing linear equations for daytime for the study period.

### 7.2.3 Establishment of proposed Hybrid PSO-SVR model

The parameters of the SVR model  $C$ ,  $\varepsilon$  and  $\gamma$  are tuned using PSO algorithm. The methodology explained in Chapter 6 section 6.2.6 is employed for developing the Hybrid PSO-SVR model.

**Table 7.1 PSO and SVR parameter values**

<b>Method</b>	<b>Parameters</b>	<b>Assigned values</b>
	Cognitive Parameter	1.5
	Social Parameter	1.7
<b>PSO</b>	Number of Iterations	100
	Inertia weight( $w$ )	0.6
	Swarm size	20
	Regularization parameter ( $C$ )	0.01 - 100
<b>SVR</b>	Parameter of kernel function( $\gamma$ )	0.01 - 100
	Insensitivity( $\varepsilon$ )	0.1

The SVR model intends to develop a relationship of the form:

$$Q = f(p)$$

Where  $p$  is the input vector comprising variables  $p_1$ ,  $p_2$ ,  $p_3$  and  $p_4$  and  $Q$  is the output vector. In this case, the input variables are NDVI, NDWI and NDBI, while the output variable is LST. The proposed model was developed for the years 1989, 2001, 2005 and 2017 to evaluate the interaction between LST and urban surface characteristics.

The dataset for each year is divided into two sets: 70% for training the model and 30% for testing. Thereafter, the LST for the year 2020 was predicted by employing the datasets of the years 2001, 2005 and 2017. The input datasets used were resampled to 300m resolution for better generalization of the results.

#### **7.2.4 Formulation of hypothetical scenarios**

Four different scenarios were formulated to explore the impact of change in remote sensing indices on LST for the year 2020. Polygons generated for the scenario formulation were randomly distributed in the suburban regions and urban fringes of the study area.

- Scenario 1 and 2 constitutes a change in area of 225 km<sup>2</sup> (10% of total area)
- Scenario 3 and 4 has a change in area of 445 km<sup>2</sup> (20% of total area)

The values of remote sensing indices corresponding to the maximum value of NDVI for the scene was identified and in scenario 1, these values were assigned to the generated polygons. In scenario 2, the remote sensing indices values corresponding to the maximum value of NDWI was assigned to the generated polygons. The same methodology was used for the input data preparation of scenario 3 and 4 with 20% increase in vegetation and water body respectively. The Hybrid PSO-SVR model developed for the year 2020 was applied to the input data to predict the LST for all the four scenarios.

#### **7.2.5 Urban Heat Anomaly**

Urban heat anomaly is a relative concept and is defined by the temperature difference between urban and surrounding rural areas. The quantification of urban heat anomaly is one of the main aspects of UHI studies. Urban heat anomaly of a region can be quantified by employing the Urban Heat Island Intensity (UHII) equation. The rural baseline for the different periods was defined based on the surface area ratios formulated by the concentric ring approach.

UHII (eq. 7.4) for each year was calculated with respect to the rural baseline.

$$UHII = T_u - T_r \quad (7.4)$$

Where  $T_u$  is the mean LST of urban area and  $T_r$  is the mean LST of the rural area demarcated by the concentric ring approach.

Urban Heat Island Intensity Index (UHIII) introduced by (Cheng & Zhang, 2017) is a relative intensity to demonstrate the UHII. It is given by the eq. (7.5)

$$UHIII = (T_u - T_r) / T_r \quad (7.5)$$

The effect of land cover change on UHII can be identified from the values of UHIII. UHI intensity and UHI intensity index for the years 1989, 1994, 2001, 2005, 2014 and 2017 was estimated for the daytime and nighttime heat intensities were calculated for the years 2005 and 2017.

## **7.3 RESULTS AND DISCUSSION**

### **7.3.1 Characteristics of LST, NDBI, NDVI & NDWI**

The remote sensing indices (NDVI, NDWI and NDBI) for Bengaluru urban district for the years 1989, 2001, 2005 and 2017 were extracted based on the equations (7.1 to 7.3). Higher LST values are distributed in the outskirts of the city while lower LST is concentrated in the city centre. Areas with relatively higher temperatures are mostly barren land, while the lower temperature in the city centre can be attributed to the urban parks and water bodies in the region. Each remote sensing index is a good reflection of the characteristics of the study area, the spatial variation of LST, NDVI, NDWI and NDBI has a notable difference in the year 2017 (Figure 7.5). Figures 7.2 to 7.5 show that higher values of NDBI are scattered in the outskirts, which is in correlation with higher LST values while higher NDVI and NDWI values are distributed in the urban centre. The spatial distribution of LST and NDBI is in line with each other.

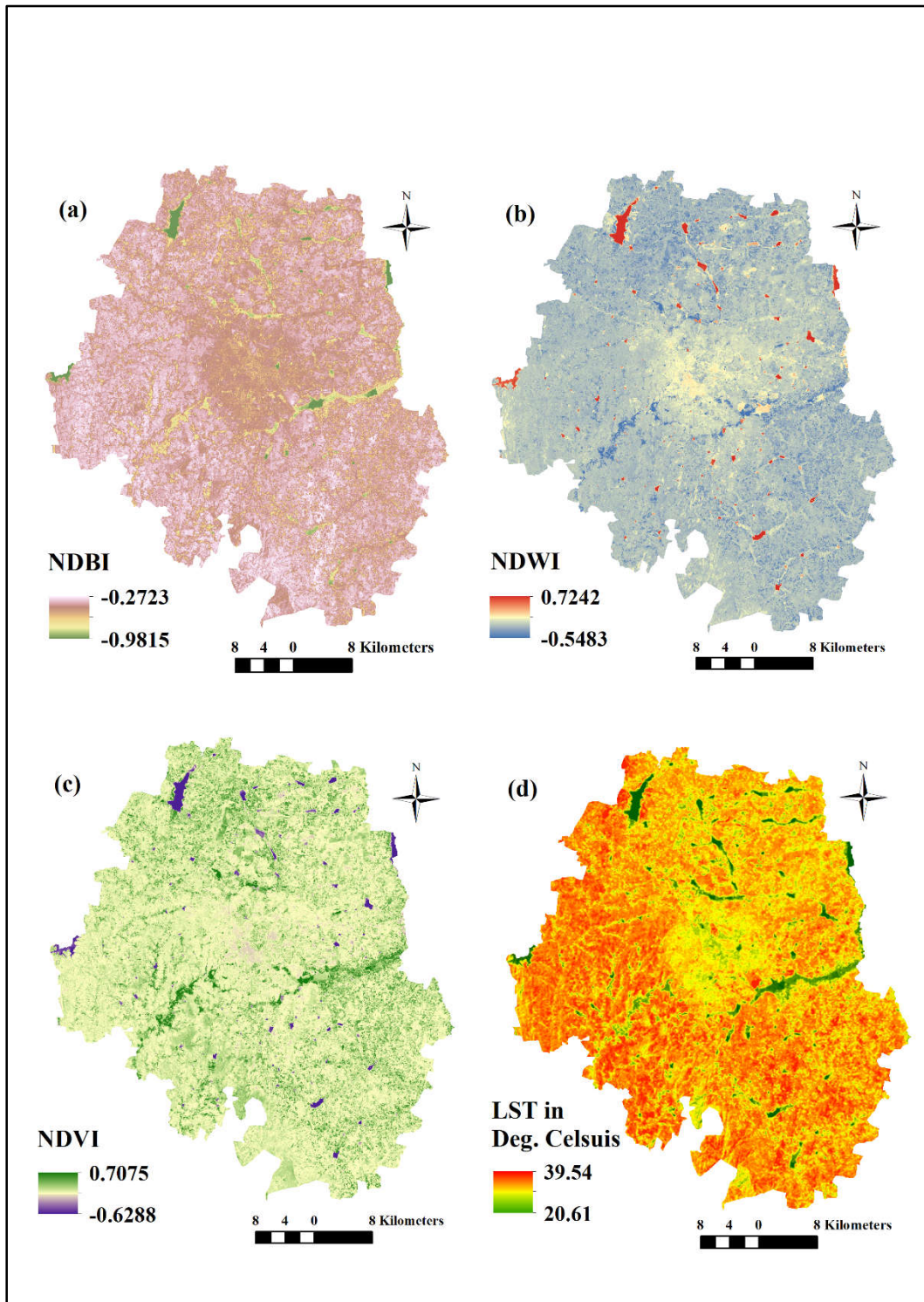


**Figure 7.2 Spatial Distribution of NDBI, NDWI, NDVI and LST for the year 1989**

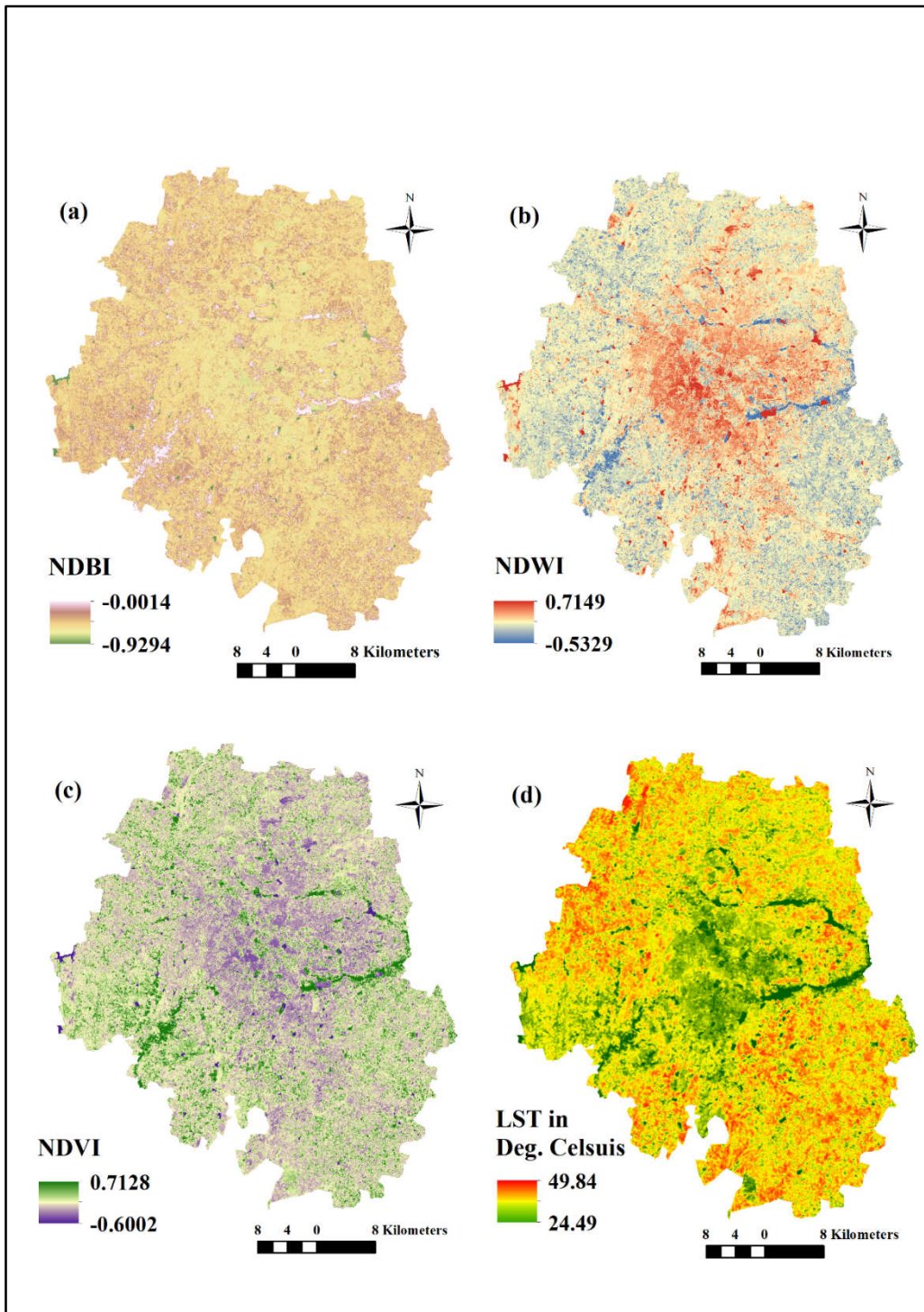


**Figure 7.3 Spatial Distribution of NDBI, NDWI, NDVI and LST for the year 2001**



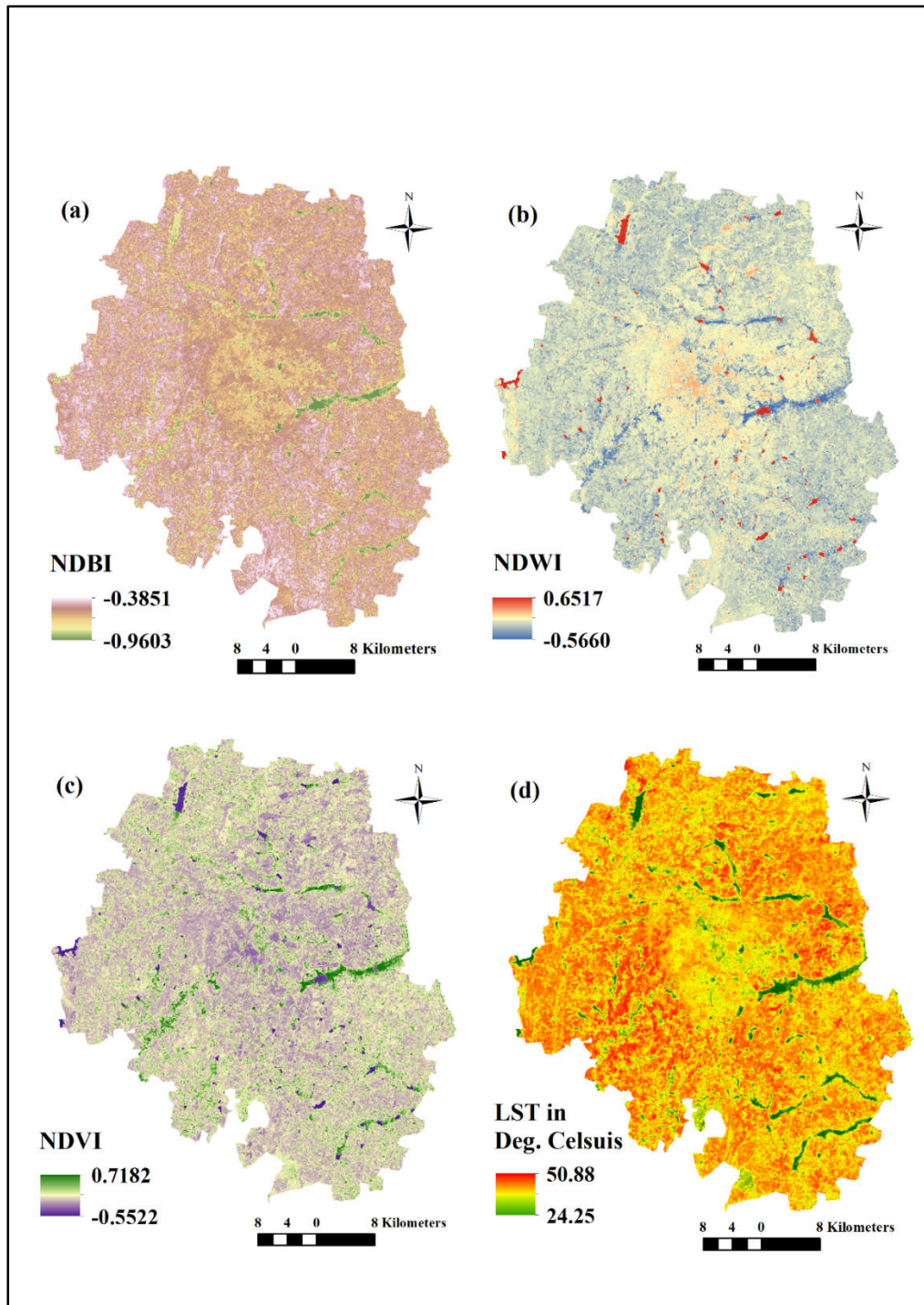


**Figure 7.4 Spatial Distribution of NDBI, NDWI, NDVI and LST for the year 2005**

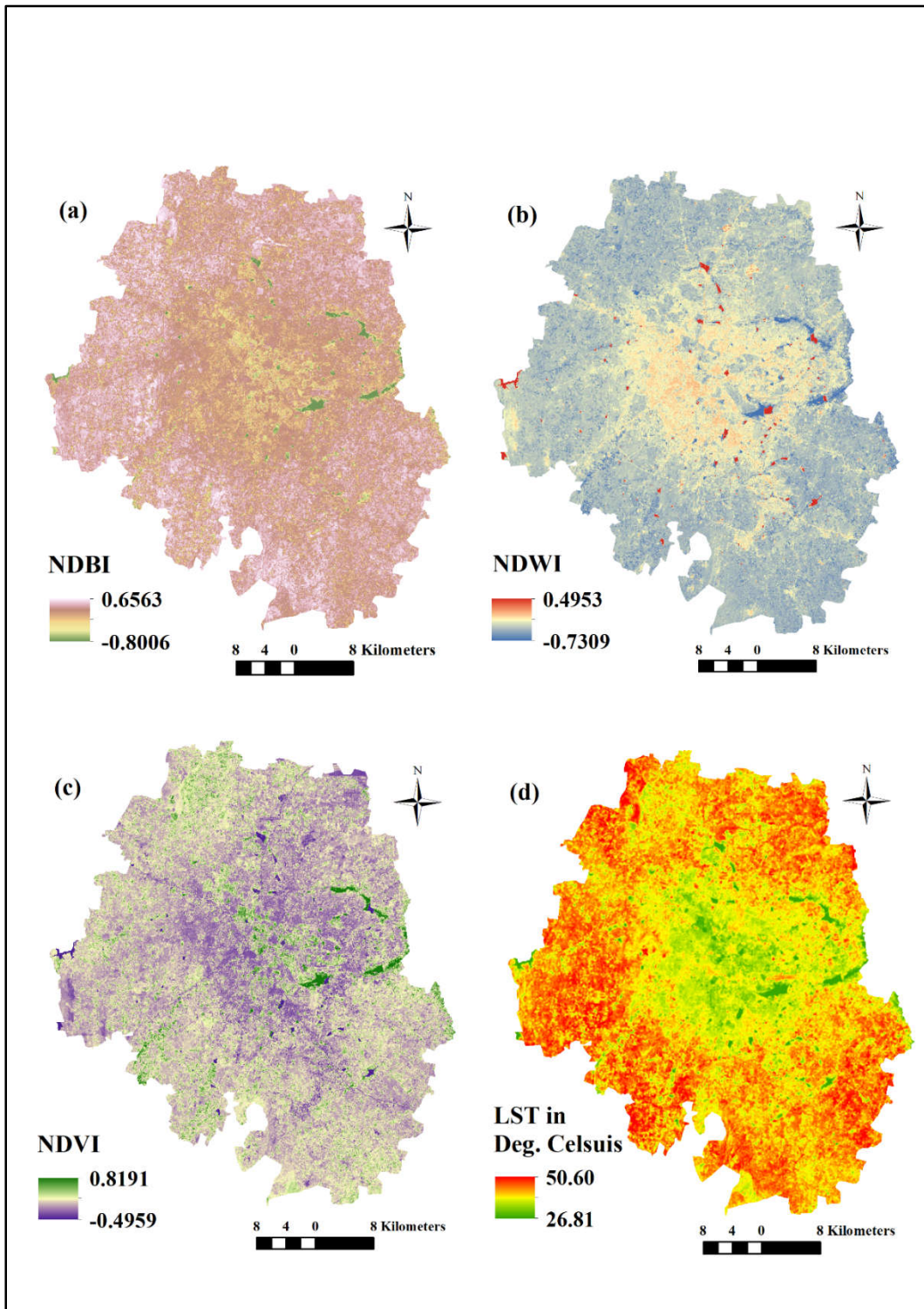


**Figure 7.5 Spatial Distribution of NDBI, NDWI, NDVI and LST for the year 2017**

Researchers have documented that land cover changes especially due to urbanization causes significant of surface thermal anomalies. Hence, it is necessary to establish a quantifiable relationship between LST and these indices. NDBI has drastically increased in the year caused by the increase in barren land and urban areas while NDVI and NDWI have decreased over the years (Table 7.2). For the year 2017, there is a significant variation in the values of NDVI, NDWI and NDBI.

**Table 7.2 Descriptive statistics of LST, NDVI, NDBI and NDWI**

<b>Year</b>	<b>Parameter</b>	<b>Minimum</b>	<b>Maximum</b>	<b>Mean</b>	<b>Standard deviation</b>	<b>Correlation with LST</b>
<b>1989</b>	<b>LST (°C)</b>	20.61	39.54	31.67	2.24	1
	<b>NDBI</b>	-0.9815	-0.2723	-0.6031	0.0719	0.80
	<b>NDVI</b>	-0.6287	0.7075	0.0217	0.1053	-0.19
	<b>NDWI</b>	-0.5483	0.7242	-0.0248	0.0908	-0.15
<b>2001</b>	<b>LST(°C)</b>	24.25	50.89	40.46	3.27	1
	<b>NDBI</b>	-0.9602	-0.3851	-0.6350	0.0676	0.79
	<b>NDVI</b>	-0.5521	0.7182	0.0662	0.1219	-0.48
	<b>NDWI</b>	-0.5660	0.6517	-0.0450	0.0971	0.19
<b>2005</b>	<b>LST(°C)</b>	24.50	49.84	37.81	2.88	1
	<b>NDBI</b>	-0.9294	-0.0014	-0.6794	0.0699	0.41
	<b>NDVI</b>	-0.6002	0.7127	0.0697	0.1136	-0.38
	<b>NDWI</b>	-0.5329	0.7150	-0.0395	0.0936	0.09
<b>2017</b>	<b>LST(°C)</b>	26.81	50.60	39.55	2.81	1
	<b>NDBI</b>	-0.8006	0.6563	0.0330	0.1163	0.76
	<b>NDVI</b>	-0.4959	0.8191	0.2791	0.1094	-0.31
	<b>NDWI</b>	-0.7309	0.4953	-0.3162	0.1009	-0.20



Pearson’s correlation coefficient was employed to determine the correlation between LST and remote sensing indices. In comparison with other indices, LST has more correlation with NDBI. The correlation coefficient of NDBI and LST was fairly high in all the time periods. In order to determine the combined effect of the remote sensing indices on LST, a multiple linear regression model is required. A statistically significant correlation ( $P<0.01$ ) was obtained between LST and remote sensing indices for all the years.

### 7.3.2 Multiple Linear Regression Analysis

Linear regression models were fitted to LST and remote sensing indices of the four time periods.

**Table 7.3 MLR results for different window size**

<b>Year</b>	<b>Window size</b>	<b>RMSE</b>	<b>Adjusted R-squared</b>
<b>1989</b>	1x1	1.268	0.6785
	3x3	1.077	0.7615
	5x5	0.951	0.8057
<b>2001</b>	1x1	1.930	0.6520
	3x3	1.617	0.7469
	5x5	1.416	0.7949
<b>2005</b>	1x1	2.097	0.4681
	3x3	1.840	0.5767
	5x5	1.689	0.6249
<b>2017</b>	1x1	1.729	0.6207
	3x3	1.451	0.7263
	5x5	1.296	0.7739

LST is chosen as the dependent variable and NDVI, NDWI and NDBI are the independent variables. Regression analysis was performed with two window sizes of (3x3) and (5x5) and original data. Table 7.3 shows the performance of the regression models for different window sizes.

A modified version of  $R^2$  which depends on the number of predictor variables termed as adjusted  $R^2$  is adopted to assess the performance of MLR models. For all the years, (5x5) window gives better results (higher Adjusted  $R^2$  and lower RMSE) compared to the other two datasets.

Multiple linear regression equations developed for LST and remotes sensing indices using (5x5) window are given in equations (7.6 to 7.9).

For the years

$$2017: \quad LST = 37.33 + 20.11NDBI - 7.63NDVI - 11.65NDWI \quad (7.6)$$

$$2005: \quad LST = 14.96 + 33.82NDBI - 30.22NDVI - 50.13NDWI \quad (7.7)$$

$$2001: \quad LST = 64.08 + 36.68NDBI - 19.35NDVI - 21.03NDWI \quad (7.8)$$

$$1989: \quad LST = 46.44 + 24.62NDBI - 11.35NDVI - 13.12NDWI \quad (7.9)$$

### 7.3.3 Hybrid PSO-SVR Model

The non-linear relationship between remote sensing indices and LST was established using a hybrid PSO-SVR model for the years 1989, 2001, 2005 and 2017. NDVI, NDWI and NDBI were chosen as predictive variables while LST is the dependent variable. PSO algorithm was used to tune the hyperparameters of SVR model. The proposed model was implemented in MATLAB environment. The model was validated using evaluation indices, RMSE and Coefficient of Determination ( $R^2$ ). Optimal values of regularization parameter  $C$  and radial bias kernel function  $\gamma$  with the lowest MSE was estimated from the range specified, (table 6.1) by employing the PSO algorithm. The SVR model was trained using these optimal hyperparameters. The performance of Hybrid PSO-SVR model for the predictive variables in the testing and training phase at four-time steps is demonstrated in Table 7.4.

The fitness values (MSE) were recorded during the hyperparameter tuning process by applying PSO algorithm. For the year 2017, the average fitness value ranges from 0.00298 to 0.00736 in the first 100 iterations. The lowest value of minimum MSE of 0.00265 was attained in the first 100 iterations. In the case of 2005, the lowest value of minimum MSE attained was 0.00419 while the average fitness value ranges from 0.00425 to 0.00665. The average fitness value ranges from 0.00227 to 0.00384 and 0.00233 to 0.00454 for the years 2001 and 1989 respectively. The lowest value of minimum MSE obtained for the years 2001 and 1989 was 0.00219 and 0.00228 respectively. These results prove the feasibility of PSO algorithm in tuning the hyperparameters of SVR. The Hybrid PSO-SVR model was built on the tuned hyperparameters for modelling LST with remote sensing indices at different time frames.

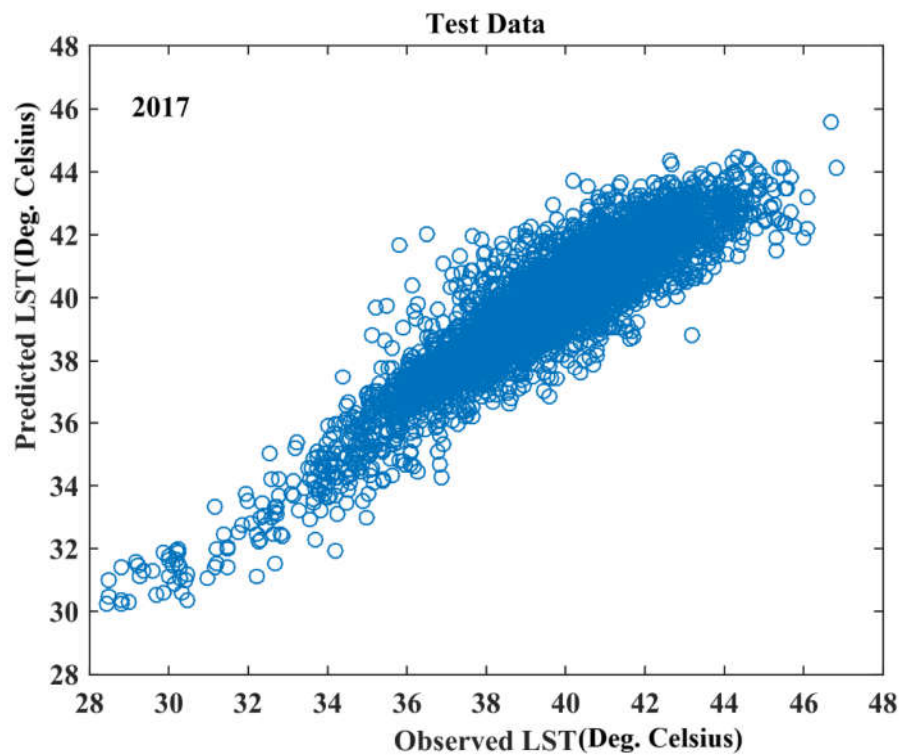
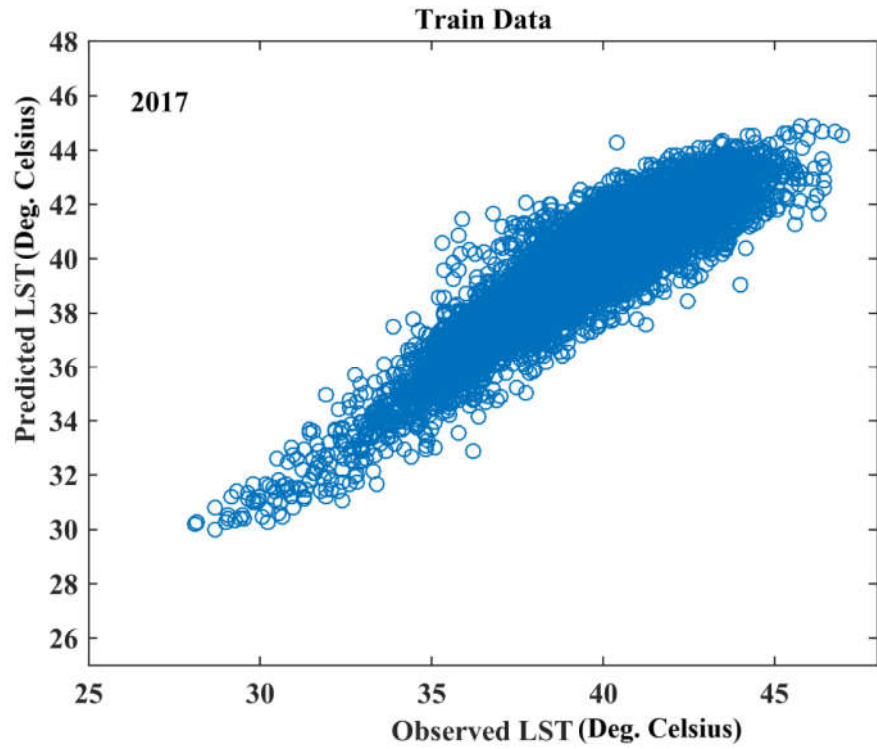
**Table 7.4 Optimal SVR hyper-parameters and evaluation indices for train and test dataset**

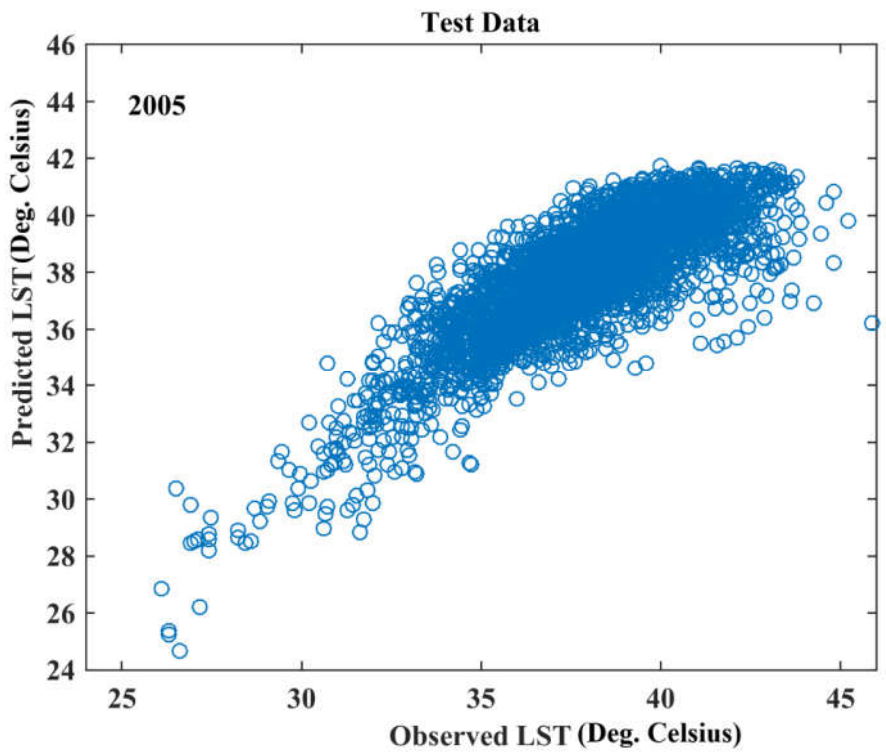
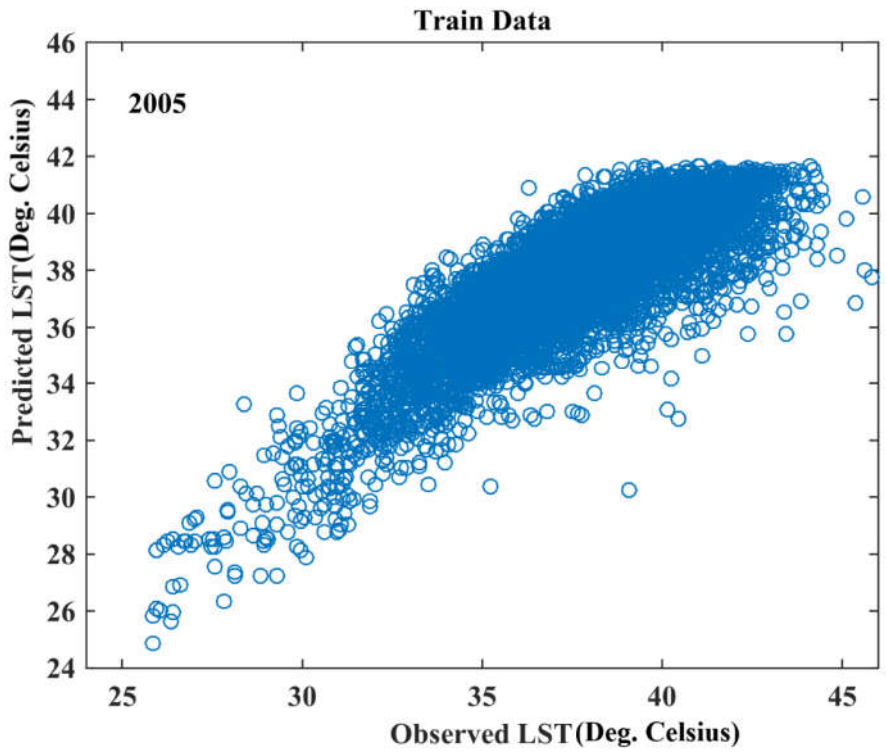
Year	Predictive variables	Train		Test		Optimal SVR Hyper-parameters		
		$R^2$	$RMSE$	$R^2$	$RMSE$	$C$	$\gamma$	$\epsilon$
1989	NDBI, NDVI, NDWI	0.850	0.047	0.850	0.048	4.167	14.452	0.1
2001	NDBI, NDVI, NDWI	0.849	0.046	0.838	0.048	7.815	40.000	0.1
2005	NDBI, NDVI, NDWI	0.698	0.064	0.680	0.066	7.377	22.821	0.1
2017	NDBI, NDVI, NDWI	0.836	0.051	0.832	0.052	1.779	5.514	0.1

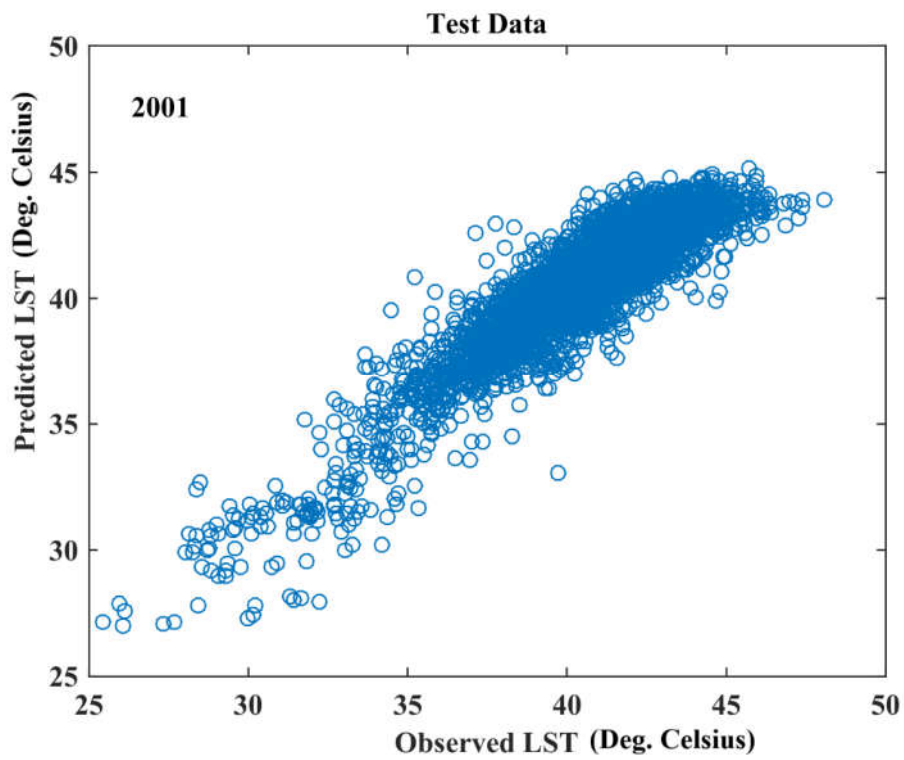
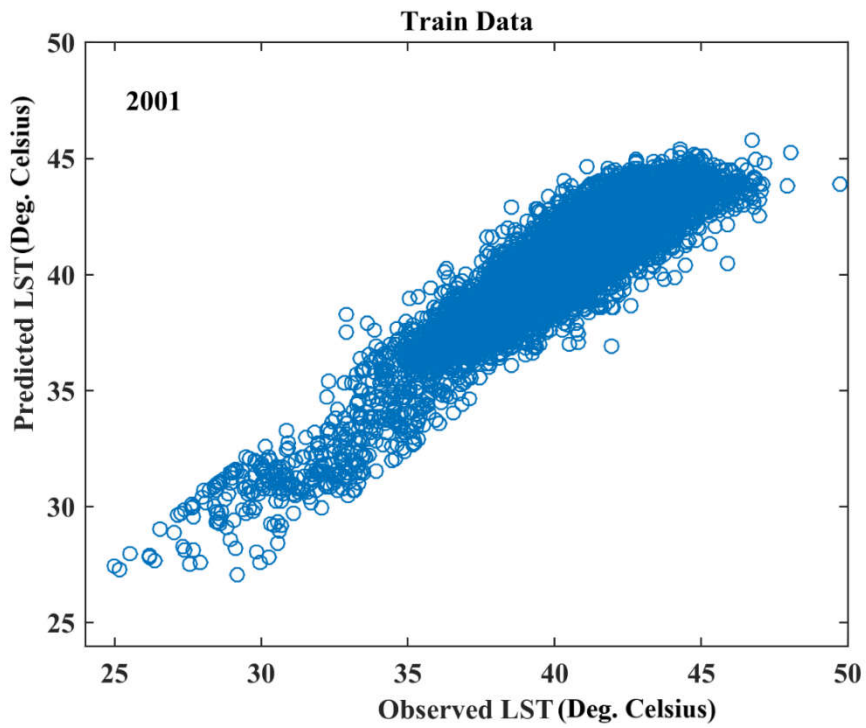
### 7.3.4 Capability of Hybrid PSO-SVR Model

Figure 7.6 demonstrates the capability of the hybrid PSO-SVR model on the training and testing dataset. It can be observed that LST can be effectively modelled from remote sensing indices by employing the proposed model.  $R^2$  values of the training set

were close to the  $R^2$  values testing set indicating that the proposed model was well trained.







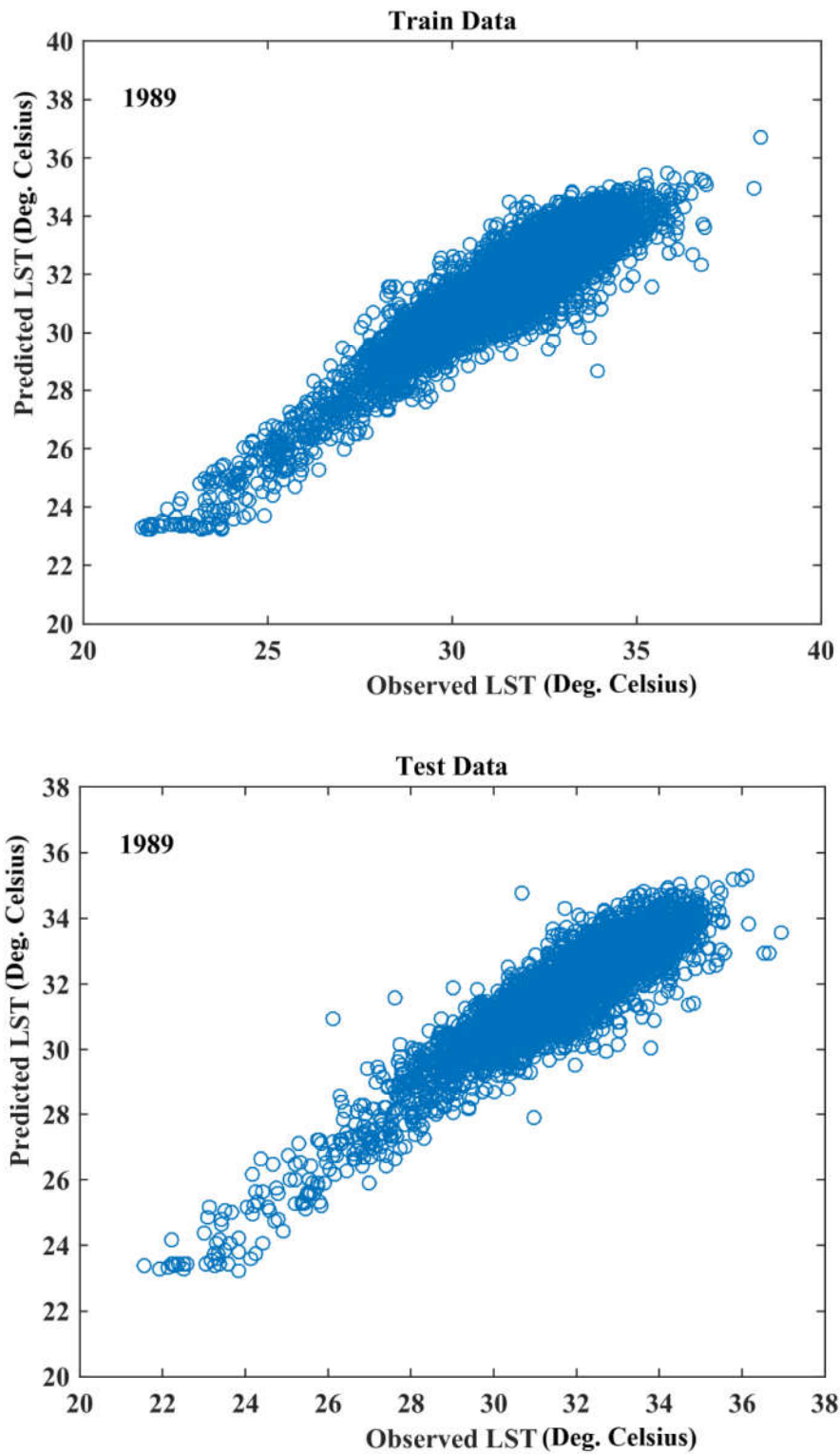


**Figure 7.6 Performance of Hybrid PSO-SVR model at training and testing stages for the four-time steps.**

The values of optimized SVR hyperparameters ( $C$ ,  $\gamma$ ,  $\epsilon$ ) of the model are given in Table 7.4. These hyperparameters are applied to the test data to predict LST accurately. The value of  $\epsilon$  is kept constant at 0.1 while the values of  $C$  and  $\gamma$  are optimized using PSO method.

The model results indicate that LST is the combined effect of all the urban surface characteristics of the region. This combined effect is very effectively modelled using the proposed Hybrid PSO-SVR model. The proposed method could accurately model the interrelationship of the LST with the predictive variable. This demonstrates the superiority of the model in establishing and predicting non-linear relationships between parameters.

### **7.3.5 Comparison of MLR and Hybrid PSO-SVR results**

The MLR was executed using a 10 x10 window and the performance was compared with Hybrid PSO-SVR model. In MLR analysis, RMSE values obtained for the years 2017, 2005, 2001 and 1989 are 1.1241, 1.4699, 1.2160 and 0.8114 respectively.  $R^2$  value obtained for the year 2017, 2005, 2001 and 1989 are 0.8089, 0.6641, 0.8174 and 0.8355 respectively. RMSE values obtained using Hybrid PSO-SVR model are significantly less than MLR method and  $R^2$  values are higher, confirming the superiority of the proposed model. Therefore, it can ascertain that Hybrid PSO-SVR model is performing better than MLR analysis for modelling the LST based on remote sensing indices.

### **7.3.6 Prediction of LST**

LST for the year 2020 was predicted using remote sensing indices by employing Hybrid PSO-SVR model. Datasets for the years 2001, 2005 and 2017 were used as the training set. Optimal hyperparameters obtained from the training data were applied to testing data (remote sensing indices of 2020) to predict the LST of the region in the year 2020. RBF kernel was selected for the prediction and the values obtained for the optimal hyperparameters  $C$  and  $\gamma$  are 0.0677 and 78.28 respectively. RMSE and  $R^2$  for train data are 0.04338 and 0.7768 respectively (Figure 7.7). An  $R^2$  value of 0.6432 was obtained



for predicted LST (Figure 7.8). The results obtained demonstrate the efficiency of the Hybrid PSO-SVR model in the prediction of LST from NDVI, NDWI and NDBI. The performance of the proposed model for LST prediction can be improved by incorporating more input variables.

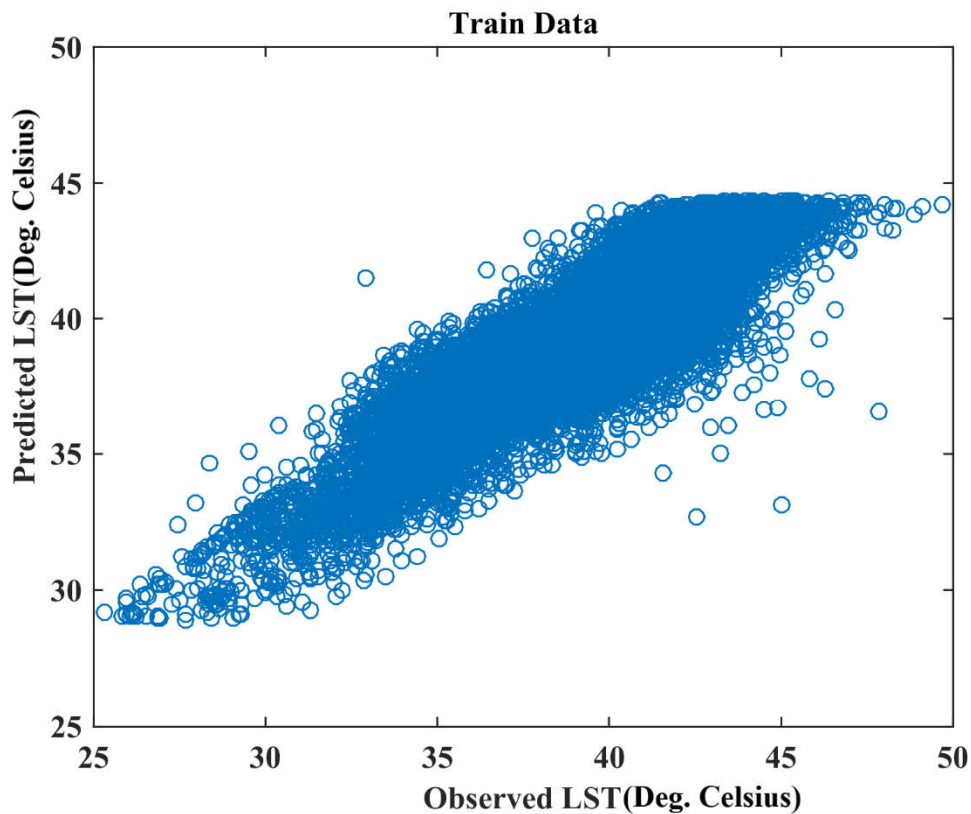


**Figure 7.7. Performance of Hybrid PSO-SVR model for LST prediction at the training stage**

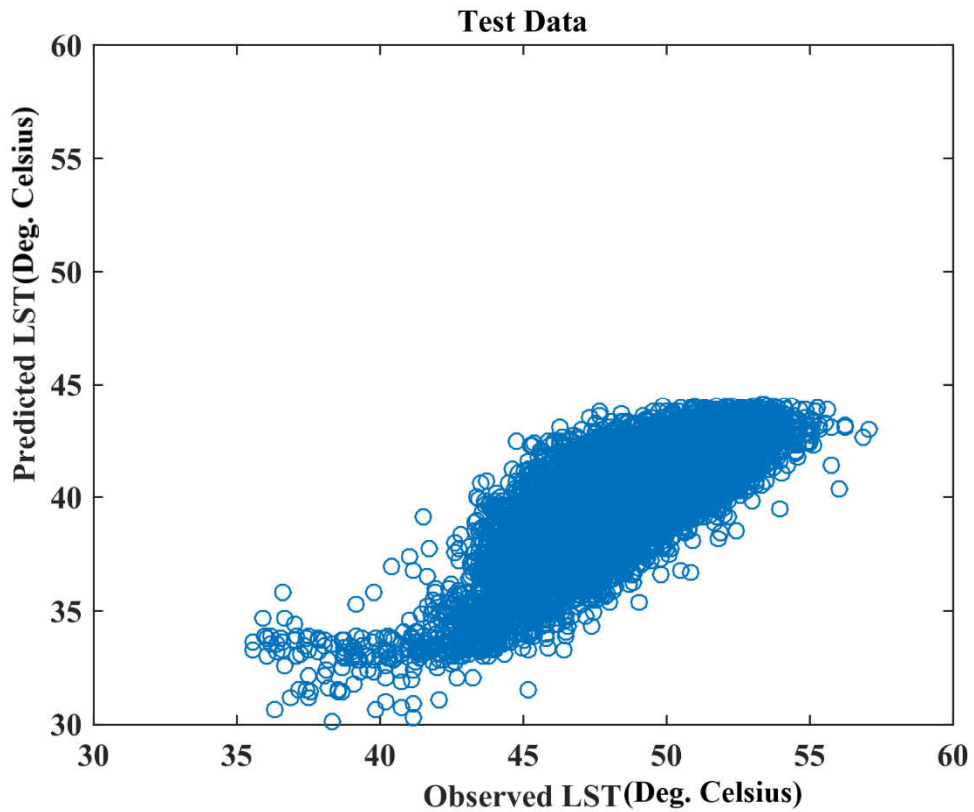


**Figure 7.8 Performance of Hybrid PSO-SVR model for LST prediction at the testing stage**

### **7.3.7 Hypothetical Scenario Analysis**

Hypothetical scenarios were formulated to represent green corridors and artificial lakes. Four different scenarios were developed to predict LST in the year 2020. Scenario 1 and 2 includes 10% increase in vegetation and water bodies and scenario 3 and 4 includes 20% increase in vegetation and water bodies respectively. The results indicate a notable change in the distribution of LST across the study area.

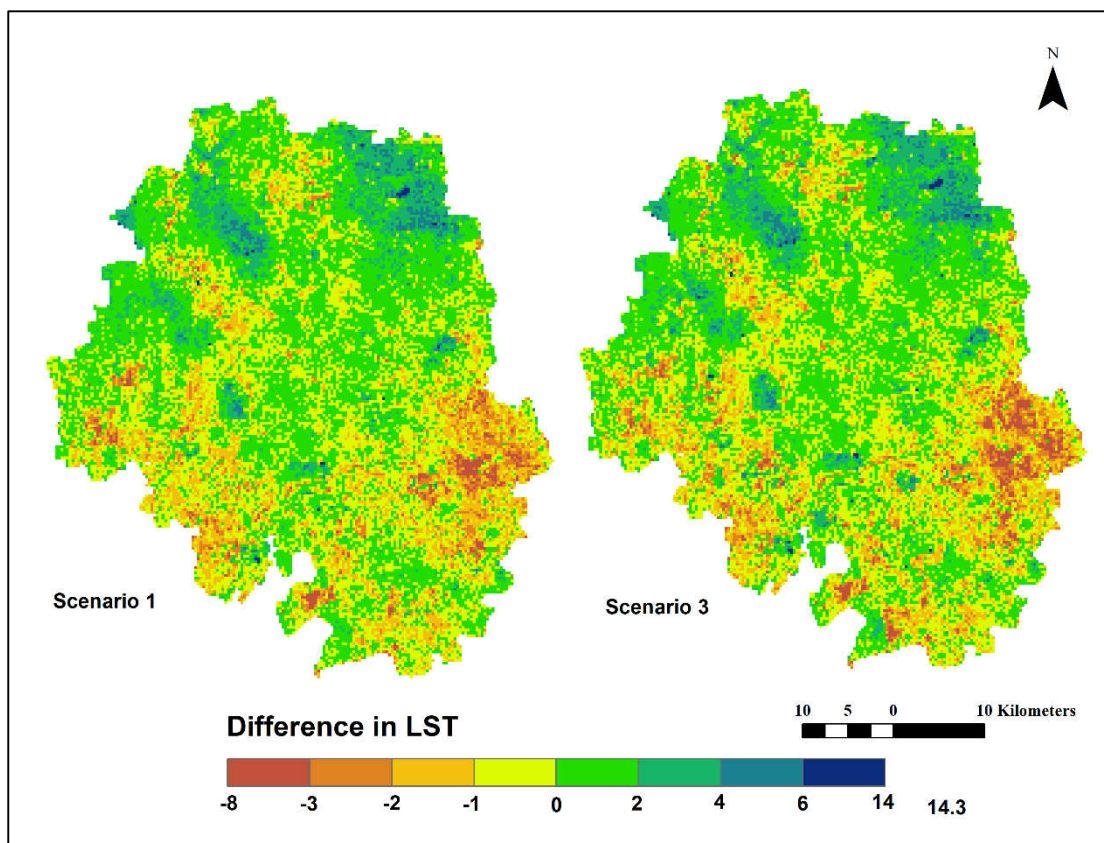


**Figure 7.9 Spatial variation of difference in LST for scenario1 and 3 compared to the estimated LST of the year 2020**

Figure 7.9 illustrates the spatial distribution of change in predicted LST for scenario 1 and 3. Positive values refer to the increase in the LST predicted using hypothetical scenarios while a negative value indicates a decrease in LST compared to the estimated LST for the year 2020. For all the scenarios, the predicted LST has decreased in the eastern and southern regions, but increased on the northern side. The change in LST for scenario 1 and 2 are almost similar. In scenario 3, there is a slight increase in the areas experiencing lower LST and it is concentrated on the eastern side of the study area. It can be observed that a major portion of the study area experiences a change in predicted LST of about -1 to +1°C. The regions experiencing higher LST (52°C - 56°C) has reduced by approximately 104 km<sup>2</sup> in scenario 1 and 2 and 112 km<sup>2</sup> in scenario 3 and 4 respectively. There is no significant change in LST distribution when vegetation is replaced by water.

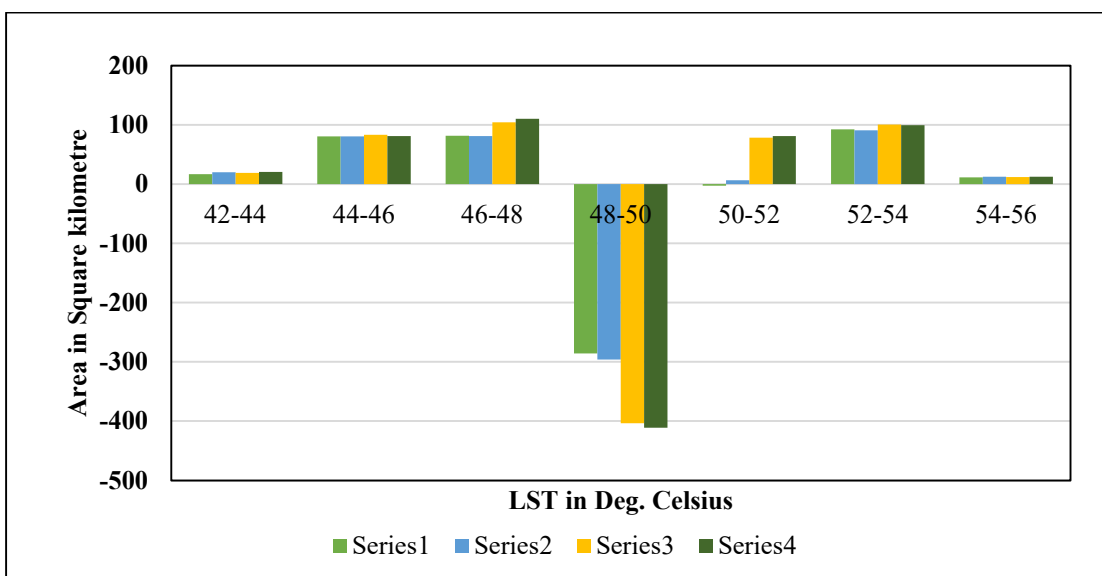


**Figure 7.10 Change in area experiencing a different range of predicted LST for the four scenarios.**

Figure 7.10 highlights the change in area corresponding to different ranges of LST predicted. A positive value indicates a decrease in area corresponding to a particular range of predicted LST and a negative value refers to the increase in area. It can be clearly observed that the area experiencing the predicted LST range of 48 to 50°C has increased in all four scenarios. It can be inferred that introduction of hypothetical scenarios in the prediction of LST has increased in regions experiencing mean LST (48 to 50°C). In all the four scenarios, the maximum predicted LST has been reduced from 57 to 55°C. From the analysis, it can be ascertained that an increase in vegetation or water bodies will reduce the maximum LST of the study area.

### 7.3.8 Analysis of Urban Heat Anomaly

The study area exhibits an anomalous behaviour compared to the urban heat island effect experienced by most cities. During the day, a surface urban cool island is observed while an urban heat island is experienced in the study region at night. The negative value of UHII for daytime and positive values during night-time confirms this phenomenon (Table 7.5). The surface urban cool island effect has been consistent over

the years and shows an increasing trend from 1989 to 2017. The increasing values of UHII over the years indicate a significant difference in the mean LST of rural and urban areas. For night-time, the UHII of 2005 and 2017 (based on MODIS LST data) was analysed and shows a decreasing trend. The UHI intensity index also shows an increasing trend from 1989 to 2017.

**Table 7.5. Temporal variation of UHI intensity in the study area**

	Year	Mean LST (Deg. Celsius)		UHII	UHIII
		Urban	Rural		
		area	area		
<b>Day time</b>	<b>1989</b>	29.78	31.75	-1.97	-0.0620
	<b>1994</b>	23.86	24.85	-0.99	-0.0398
	<b>2001</b>	38.86	40.61	-1.75	-0.0431
	<b>2005</b>	35.16	38.13	-2.97	-0.0779
	<b>2014</b>	35.04	37.91	-2.87	-0.0757
	<b>2017</b>	36.88	40.21	-3.33	-0.0828
<b>Night time</b>	<b>2005</b>	21.01	16.56	4.45	0.2687
	<b>2017</b>	23.24	20.46	2.78	0.1359

The major land cover type in the rural area is barren land and since the study is conducted during the summer season, there is very less vegetative cover and hence the LST is higher. Urban region comprises built-up area, urban parks and lakes which causes a cooling effect leading to the lower values of LST compared to the rural area. Analysis of urban characteristics indicates a significant shift in the NDBI value over the years. In 1989, NDBI values were negative, while in 2017 positive. NDBI values were observed in 45% of the urban area and 75% of rural area. The positive NDVI values were observed in 80% of the urban area and 23% of the rural area in the year 1989, which has considerably reduced for both urban and rural area in the year 2017. The areas with positive NDVI values increased in urban and rural regions from 1989 to

2017. The investigations on urban surface characteristics demonstrate a significant urbanizing trend in the study area consistent with land cover change analysis. Even though the study area has experienced remarkable urbanization over the years, the surface temperature is lower in the urban area compared to the rural surroundings causing a surface urban cool island during the daytime. In the night-time, the process is reversed.

#### **7.4 CONCLUSION**

The variation of urban surface characteristics and LST and its correlation was analysed for the years 1989, 2001, 2005 and 2017. The spatio-temporal variation of urban surface characteristics indicates an urbanizing trend in the study area from 1989 to 2017. NDBI has drastically increased in the year 2017, which is caused by the increase in barren land and urban areas while NDVI and NDWI have decreased over the years. Higher values of NDBI are scattered in the outskirts while higher NDVI and NDWI values are distributed in the urban centre. NDBI has a high positive correlation with LST during the period of study.

The relationship between urban surface characteristics and LST was efficiently modelled using linear and non-linear regression algorithms.  $R^2$  value in the range of 0.80 and 0.85 was obtained for MLR and Hybrid PSO-SVR model respectively. Hybrid PSO-SVR model proved to be effective in establishing the relationship between LST and urban surface characteristics, NDVI, NDBI and NDWI and in predicting the future LST.

Hypothetical scenarios were developed in the prediction of LST to quantify the impact of urban surface characteristics. The results of future prediction scenarios indicate that the regions experiencing higher LST (52°C - 56°C) has reduced by approximately 104 km<sup>2</sup> in scenario 1 and 2 and 112 km<sup>2</sup> in scenario 3 and 4 respectively. An increase in either vegetation or water bodies will reduce the maximum LST of the study area. It can be concluded that the introduction of vegetation and water bodies in the suburban and urban fringes will reduce the difference in LST between urban and rural areas. An urban heat anomaly was observed in the area wherein an urban cool island is

experienced during daytime and an urban heat island during night-time. The intensity of heat anomaly has increased from 1989 to 2017. The magnitude of urban heat anomaly can be curtailed by developing green corridors and artificial lakes in the suburban and urban fringes of Bengaluru.

### SUMMARY AND CONCLUSIONS

---

---

#### 8.1 SUMMARY

The study presents a comprehensive approach for analysing the spatio-temporal variation of LC and LST and the impacts of LC change on the environment. The study area was delineated from satellite images based on SoI toposheets. The land cover map for Bengaluru Urban district was prepared for the years 1989, 1994, 2001, 2005, 2014 and 2017. Four broad land cover classes were identified: urban, barren, vegetation and water body. Over the years from 1989 to 2017, the study area has experienced a drastic increase in the urban area.

The primary objective of the study was to explore the spatio-temporal patterns of land cover and LST from 1989 to 2017. The extent and rate of LC change for the time period in the entire area and in each category are examined using Intensity Analysis. The intensity analysis can be divided into three levels: interval, category, and transition. At interval level analysis, the LC change experienced during both the periods is analysed and the period in which the land transition is faster is identified. At the category level, the four categories, viz., vegetation, water, urban and barren, were examined. The active and dormant categories were also determined. The LC class which is intensively avoided or targeted is identified in the transition level analysis. LST of the study area was retrieved from the thermal infrared band of Landsat images using a simple single-channel algorithm. The spatial correlation of LST in the study area was investigated by employing an optimized hot spot analysis tool (Getis-Ord  $G_i^*$ ) in the ArcGIS software. The LST pattern was linked with the change in LC to assess the impact of LC change on LST. The hot spot maps were created for three years 1989, 2001 and 2017.



The second objective of the study comprehends a detailed analysis of the urban growth pattern, modelling of surface cover and LST. The urban growth and LST pattern were modelled based on the concentric ring approach. The urban land density and LST for the years 1989, 2001, 2005 and 2017 were modelled as a function of distance from the urban centre. The spatial variation of urban land density and LST with distance from the urban centre was quantified by a modified sigmoid function providing an inverse S-shape curve. The relationship between land cover types and LST was established using multiple linear regression algorithms. Further, the non-linear relationship between LST and surface cover types were quantified by developing a Hybrid PSO-SVR model.

The third objective was to investigate the spatio-temporal patterns of urban surface characteristics and their interaction with LST. The urban surface characteristics were assessed based on remote sensing based indices such as NDVI, NDWI and NDBI. The MLR models and Hybrid PSO-SVR model were developed to establish the inter relationship between LST and urban surface characteristics for the years 1989, 2001, 2005 and 2017. The LST for the year 2020 was predicted using Hybrid PSO-SVR model and three hypothetical scenarios were developed to quantify the impact of vegetation and water bodies on LST. The urban heat anomaly of the study area was analysed from 1989 to 2017 and shows an increasing trend.

## **8.2 CONCLUSIONS**

The methodology proposed in this study provided a detailed understanding of the spatial and temporal patterns of LC and LST and their interrelationships. The Bengaluru Urban district has witnessed a tremendous increase in an urban area (4 to 43%) from 1989 to 2017 and experiences a surface urban cool island effect. The magnitude of urban heat anomaly could be reduced by developing green corridors and artificial lakes in the suburban and urban fringes of the Bengaluru Urban district.

Hybrid PSO-SVR model proved to be effective in modelling LST based on surface area ratio and urban surface characteristics compared to MLR. Radial Basis Function (RBF)

was used as the kernel function for achieving the best performing SVR model as observed in previous literature. Gamma parameter governs the smoothing of the shape of the regression curve, thereby providing RBF function results with better flexibility in dealing with non-linear data. Determining the kernel function and tuning the hyperparameters is crucial in establishing a robust predictive model. The PSO algorithm accurately optimized the hyperparameters of the SVR model. Machine learning algorithms are based on statistical learning theory, which explains their performance better when compared to MLR. Assumptions of probability and distribution of data account for the poor performance of MLR. The present study emphasizes the application of remote sensing data with a machine learning approach to minimize the cost of ground inventory.

The methodology proposed in this study can be implemented in other urban areas, as it provides a scientific reference for the management of the surface temperature of the area. This approach could be applied to other geophysical parameters to understand its variation over the urban area. The study aids urban planners in designing comfortable environments for new urban areas by optimizing the benefits of the urban thermal environment at the city scale. In future land use planning, a sufficient proportion of public space, green area, and water bodies should be provided in metropolitan cities to cater to the effect of climate change due to urbanization. This study provides a scientific basis for the land use planners and policymakers to manage cities confronting rapid urban growth.

The objective specific conclusions are highlighted below:

The LC change from 1989 to 2001 is faster than the period from 2001 to 2017. The mean LST of the study area has increased overall by 6°C during the period from 1989 to 2017. It was found that examining LST patterns at different time frames can be effectively performed using hot spot analysis by Getis-Ord  $G_i^*$  statistics. Seven categories were identified from the statistical results: very cold spot, cold spot, cool spot, not statistically significant, warm spot, hot spot, and very hot spot. Approximately 24% of the study area is warmer, while 14% is cooler throughout the time period. As

the urban expansion occurs, the cold spots have increased, and it is mainly clustered in the urban area. It confirms the presence of an urban cool island in the Bengaluru urban district.

Bengaluru has experienced significant urban sprawling during recent years. Over the years, the suburban areas and the urban fringes have developed. During the summer season, the behaviour of LST during daytime and night-time contradict each other. For surface area ratio,  $R^2$  value in the range of 0.94 and 0.97 was obtained for MLR and Hybrid PSO-SVR model respectively.

Higher values of NDBI are scattered in the outskirts, which correlates with higher LST values, while higher NDVI and NDWI values are distributed in the urban centre. The  $R^2$  value in the range of 0.80 and 0.85 were obtained for MLR and Hybrid PSO-SVR model respectively. The results of future prediction scenarios indicate that the regions experiencing higher LST (52°C - 56°C) has reduced by approximately 104 km<sup>2</sup> in scenario 1 and 2 and 112 km<sup>2</sup> in scenario 3 and 4 respectively. The intensity of urban heat anomaly has also increased from 1989 to 2017, indicating the disparity in the surface heating capacity of rural and urban areas.

### **8.3 LIMITATIONS**

1. The limitations of the study was that the usage of single satellite image for a particular year with relatively large spatial resolution and the vertical growth has not been fully considered. Also, anthropogenic activities such as industrial emissions, vehicular exhaust, etc., are not integrated.
2. The inclusion of more images with a high spatial resolution for assessing the mean LST for the particular years will provide more generalized relationship between the various parameters used in the study.

#### **8.4 FUTURE PERSPECTIVES**

- The impact of urban morphology and vehicular emissions on LST can be explored.
- Application of other machine learning algorithms for the prediction of LST and comparing it with the proposed Hybrid PSO-SVR model.
- The future scope of the study could explore the correlation of LST of Bengaluru with other megacities in India.
- A detailed investigation of the latent heat transfer occurring in the study area can be conducted.



## REFERENCES

---

- Abu Awad, Y., Koutrakis, P., Coull, B. A., and Schwartz, J. (2017). “A spatio-temporal prediction model based on support vector machine regression: Ambient Black Carbon in three New England States.” *Environ. Res.*, 159(July 2016), 427–434.
- Ahmed, Z., Ali, S., Saud, S., and Shahzad, S. J. H. (2020). “Transport CO<sub>2</sub> emissions, drivers, and mitigation: an empirical investigation in India.” *Air Qual. Atmos. Heal.*, 13(11), 1367–1374.
- Aithal, B. H., Vinay, S., Durgappa, S., and Ramachandra, T. V. (2013). “Modeling and Simulation of Urbanisation in Greater Bangalore, India.” *Natl. Spat. Data Infrastruct. Conf.*, 1=7.
- Aithal, B. H., Vinay, S., and Ramachandra, T. V. (2018). “Simulating urban growth by two state modelling and connected network.” *Model. Earth Syst. Environ.*, 4(4), 1297–1308.
- Akande, K. O., Owolabi, T. O., Olatunji, S. O., and AbdulRaheem, A. A. (2017). “A hybrid particle swarm optimization and support vector regression model for modelling permeability prediction of hydrocarbon reservoir.” *J. Pet. Sci. Eng.*, 150(October 2016), 43–53.
- Akbari, H., Cartalis, C., Kolokotsa, D., Muscio, A., Pisello, A. L., Rossi, F., Santamouris, M., Synnefa, A., Wong, N. H., and Zinzi, M. (2016). “Local climate change and urban heat island mitigation techniques - The state of the art.” *J. Civ. Eng. Manag.*, 22(1), 1–16.
- Ambinakudige, S. (2011). “Remote sensing of land cover’s effect on surface temperatures: A case study of the urban heat island in Bangalore, India.” *Appl. GIS*, 7(1), 1–12.
- Aryal, K., Thapa, P. S., and Lamichhane, D. (2019). “Revisiting agroforestry for

- building climate resilient communities: A case of package-based integrated agroforestry practices in Nepal.” *Emerg. Sci. J.*, 3(5), 303–311.
- Asgarian, A., Amiri, B. J., and Sakieh, Y. (2015). “Assessing the effect of green cover spatial patterns on urban land surface temperature using landscape metrics approach.” *Urban Ecosyst.*, 18(1), 209–222.
- Badarinath, K. V. S., Kiran Chand, T. R., Madhavi Latha, K., and Raghavaswamy, V. (2005). “Studies on urban heat islands using ENVISAT AATSR data.” *J. Indian Soc. Remote Sens.*, 33(4), 495–501.
- Bendib, A., Dridi, H., and Kalla, M. I. (2017). “Contribution of Landsat 8 data for the estimation of land surface temperature in Batna city, Eastern Algeria.” *Geocarto Int.*, 32(5), 503–513.
- Benmecheta, A., Abdellaoui, A., and Hamou, A. (2013). “A comparative study of land surface temperature retrieval methods from remote sensing data.” *Can. J. Remote Sens.*, 39(1), 59–73.
- Bharath, H. A., Chandan, M. C., Vinay, S., and Ramachandra, T. V. (2018). “Modelling urban dynamics in rapidly urbanising Indian cities.” *Egypt. J. Remote Sens. Sp. Sci.*, 21(3), 201–210.
- Bhat, P. A., Shafiq, M. ul, Mir, A. A., and Ahmed, P. (2017). “Urban sprawl and its impact on landuse/land cover dynamics of Dehradun City, India.” *Int. J. Sustain. Built Environ.*, 6(2), 513–521.
- Bhatti, N. B., Siyal, A. A., Qureshi, A. L., and Bhatti, I. A. (2019). “Land Covers Change Assessment After Small Dam’s Construction Based on the Satellite Data.” *Civ. Eng. J.*, 5(4), 810–818.
- Blanzieri, E., and Melgani, F. (2008). “Nearest neighbor classification of remote sensing images with the maximal margin principle.” *IEEE Trans. Geosci. Remote Sens.*, 46(6), 1804–1811.
- Bocquier, P. (2005). *World urbanization prospects: An alternative to the UN model*

*of projection compatible with the mobility transition theory. Demogr. Res.*

- Bokaie, M., Kheirkhah, M., Daneshkar, P., and Hosseini, A. (2016). "Assessment of Urban Heat Island based on the relationship between land surface temperature and Land Use / Land Cover in Tehran." *Sustain. Cities Soc.*, 23, 94–104.
- Bolstad, P. V., and Lillesand, T. M. (1991). "Rapid maximum likelihood classification." *Photogramm. Eng. Remote Sens.*, 57(1), 67–74.
- Bonafoni, S., and Keeratikasikorn, C. (2018). "Land surface temperature and urban density: Multiyear modeling and relationship analysis using modis and landsat data." *Remote Sens.*, 10(9).
- Bovolo, F., Bruzzone, L., and Marconcini, M. (2008). "A novel approach to unsupervised change detection based on a semisupervised SVM and a similarity measure." *IEEE Trans. Geosci. Remote Sens.*, 46(7), 2070–2082.
- Bozorgi, M., Nejadkoorki, F., and Mousavi, M. B. (2018). "Land surface temperature estimating in urbanized landscapes using artificial neural networks." *Environ. Monit. Assess.*, 190(4).
- Cai, Z., Han, G., and Chen, M. (2018). "Do water bodies play an important role in the relationship between urban form and land surface temperature?" *Sustain. Cities Soc.*, 39, 487–498.
- Campana, E. F., Diez, M., Fasano, G., and Peri, D. (2013). "Initial particles position for PSO, in bound constrained optimization." *Lect. Notes Comput. Sci. (including Subser. Lect. Notes Artif. Intell. Lect. Notes Bioinformatics)*, 7928 LNCS(PART 1), 112–119.
- Camps-valls, G., Member, S., Mooij, J., and Schölkopf, B. (2010). "Kernel Dependence Measures." *Ieee Geosci. Remote Sens. Lett.*, 7(3), 587–591.
- Chang, C.-C., & Lin, C.-J. (2011). LIBSVM: A library for support vector machines. *ACM Transactions on Intelligent Systems and Technology (TIST)*, 2(3), 1–27.



- Chaudhuri, G., and Mishra, N. B. (2016). "Spatio-temporal dynamics of land cover and land surface temperature in Ganges-Brahmaputra delta: A comparative analysis between India and Bangladesh." *Appl. Geogr.*, 68, 68–83.
- Chen, X. L., Zhao, H. M., Li, P. X., and Yin, Z. Y. (2006). "Remote sensing image-based analysis of the relationship between urban heat island and land use/cover changes." *Remote Sens. Environ.*, 104(2), 133–146.
- Chen, X., and Zhang, Y. (2017). "Impacts of urban surface characteristics on spatiotemporal pattern of land surface temperature in Kunming of China." *Sustain. Cities Soc.*, 32, 87–99.
- Chun, B., and Guldmann, J. M. (2014). "Spatial statistical analysis and simulation of the urban heat island in high-density central cities." *Landsc. Urban Plan.*, 125, 76–88.
- Dai, X., Guo, Z., and Chen, C. (2016). "Improvement of mono-window algorithm for land surface temperature retrieval integrated with subpixel mapping for Landsat imagery." *4th Int. Work. Earth Obs. Remote Sens. Appl. EORSA 2016 - Proc.*, 24–27.
- Deng, Y., Wang, S., Bai, X., Tian, Y., Wu, L., Xiao, J., Chen, F., and Qian, Q. (2018). "Relationship among land surface temperature and LUCC, NDVI in typical karst area." *Sci. Rep.*, 8(1), 1–12.
- Denis, E., and Zerah, M.-H. eds. (2017). *Subaltern Urbanisation in India: An Introduction to the Dynamics of Ordinary Towns. Explor. Urban Chang. South Asia Ser. New York Springer Nature, Springer.*
- Devadas, M. D., and A. L. Ross (2009). "Urban Factors and the Intensity of Heat Island in the City of Chennai." *seventh Int. Conf. Urban Clim. 29 June - 3 July 2009, Yokohama, Japan, (July)*, 3–6.
- Directorate of Census operations, K. (2011). "Census of India 2011 KARNATAKA SERIES-30 PART XII-A DISTRICT CENSUS HANDBOOK BANGALORE VILLAGE AND TOWN DIRECTORY DIRECTORATE OF CENSUS

OPERATIONS KARNATAKA.” 1–476.

- Dixon, B., and Candade, N. (2008). “Multispectral landuse classification using neural networks and support vector machines: One or the other, or both?” *Int. J. Remote Sens.*, 29(4), 1185–1206.
- Durbha, S. S., King, R. L., and Younan, N. H. (2007). “Support vector machines regression for retrieval of leaf area index from multiangle imaging spectroradiometer.” *Remote Sens. Environ.*, 107(1–2), 348–361.
- Estoque, R. C., and Murayama, Y. (2017). “Monitoring surface urban heat island formation in a tropical mountain city using Landsat data (1987–2015).” *ISPRS J. Photogramm. Remote Sens.*, 133, 18–29.
- ESRI, 2017. How Hot Spot Analysis (Getis-Ord  $G_i^*$ ) works?  
<http://pro.arcgis.com/en/pro-app/tool-reference/spatial-statistics/h-how-hot-spot-analysis-getis-ord-gi-spatial-stati.htm>. Accessed on 8<sup>th</sup> February 2017
- Eswar, R., Sekhar, M., and Bhattacharya, B. K. (2016). “Disaggregation of LST over India: comparative analysis of different vegetation indices.” *Int. J. Remote Sens.*, 37(5), 1035–1054.
- Fadhillah, M. F., Lee, S., Lee, C. W., and Park, Y. C. (2021). “Application of support vector regression and metaheuristic optimization algorithms for groundwater potential mapping in gangneung-si, South Korea.” *Remote Sens.*, 13(6).
- Fan, C., Myint, S. W., Kaplan, S., Middel, A., Zheng, B., Rahman, A., Huang, H. P., Brazel, A., and Blumberg, D. G. (2017). “Understanding the impact of urbanization on surface urban heat Islands-A longitudinal analysis of the oasis effect in subtropical desert cities.” *Remote Sens.*, 9(7).
- Faris, A. A., and Sudhakar Reddy, Y. (2010). “Estimation of urban heat Island using Landsat ETM+ imagery at Chennai city-A case study.” *Int. J. Earth Sci. Eng.*, 3(3), 332–340.

- Franco, S., Mandla, V. R., and Ram Mohan Rao, K. (2017). “Urbanization, energy consumption and emissions in the Indian context A review.” *Renew. Sustain. Energy Rev.*, 71(December), 898–907.
- Gaur, A., Eichenbaum, M. K., and Simonovic, S. P. (2018). “Analysis and modelling of surface Urban Heat Island in 20 Canadian cities under climate and land-cover change.” *J. Environ. Manage.*, 206, 145–157.
- Ghazvinian, H., Mousavi, S. F., Karami, H., Farzin, S., Ehteram, M., Hossain, M. S., Fai, C. M., Hashim, H. Bin, Singh, V. P., Ros, F. C., Ahmed, A. N., Afan, H. A., Lai, S. H., and El-Shafie, A. (2019). “Integrated support vector regression and an improved particle swarm optimization-based model for solar radiation prediction.” *PLoS One*, 14(5).
- Ghoggali, N., and Melgani, F. (2008). “Genetic SVM approach to semisupervised multitemporal classification.” *IEEE Geosci. Remote Sens. Lett.*, 5(2), 212–216.
- Ghosh, A., and Joshi, P. K. (2014). “Hyperspectral imagery for disaggregation of land surface temperature with selected regression algorithms over different land use land cover scenes.” *ISPRS J. Photogramm. Remote Sens.*, 96, 76–93.
- Gleason, C. J., and Im, J. (2012). “Forest biomass estimation from airborne LiDAR data using machine learning approaches.” *Remote Sens. Environ.*, 125, 80–91.
- Guo, G., Wu, Z., Xiao, R., Chen, Y., Liu, X., and Zhang, X. (2015). “Impacts of urban biophysical composition on land surface temperature in urban heat island clusters.” *Landsc. Urban Plan.*, 135, 1–10.
- He, B. J. (2018). “Potentials of meteorological characteristics and synoptic conditions to mitigate urban heat island effects.” *Urban Clim.*, 24(December 2017), 26–33.
- He, B. J., Zhao, Z. Q., Shen, L. Du, Wang, H. B., and Li, L. G. (2019). “An approach to examining performances of cool/hot sources in mitigating/enhancing land surface temperature under different temperature backgrounds based on landsat 8 image.” *Sustain. Cities Soc.*, 44(October 2018),

416–427.

Ibrahim, G. R. F. (2017). “Urban land use land cover changes and their effect on land surface temperature: Case study using Dohuk City in the Kurdistan Region of Iraq.” *Climate*, 5(1), 13.

Imam, A. U. K., and Banerjee, U. K. (2016). “Urbanisation and greening of Indian cities: Problems, practices, and policies.” *Ambio*, 45(4), 442–457.

Jain, M., and Jehling, M. (2020). “Urban cycle models revisited: Insights for regional planning in India.” *Cities*, 107(August), 102923.

Jain, M., and Korzhenevych, A. (2020). “Urbanisation as the rise of census towns in India: An outcome of traditional master planning?” *Cities*, 99(December 2019), 102627.

Javed Mallick, Y. K., and B.D.Bharath. (2008). “Estimation of land surface temperature over Delhi using Landsat-7 ETM+.” *J. Ind. Geophys. Union*, 12(3), 131–140.

Jiao, L. (2015). “Urban land density function: A new method to characterize urban expansion.” *Landsc. Urban Plan.*, 139(41771429), 26–39.

Kaheil, Y. H., Rosero, E., Gill, M. K., McKee, M., and Bastidas, L. A. (2008). “Downscaling and forecasting of evapotranspiration using a synthetic model of wavelets and support vector machines.” *IEEE Trans. Geosci. Remote Sens.*, 46(9), 2692–2707.

Kennedy, J., and Eberhart, R. (1995). “Particle Swarm Optimization.” 1942–1948.

Khosla, R., and Bhardwaj, A. (2019). “Urbanization in the time of climate change: Examining the response of Indian cities.” *Wiley Interdiscip. Rev. Clim. Chang.*, 10(1), 1–13.

Kolokotroni, M., Giannitsaris, I., and Watkins, R. (2006). “The effect of the London urban heat island on building summer cooling demand and night ventilation strategies.” *Sol. Energy*, 80(4), 383–392.

- Kotharkar, R., and Bagade, A. (2018). “Evaluating urban heat island in the critical local climate zones of an Indian city.” *Landsc. Urban Plan.*, 169(August 2017), 92–104.
- Kotharkar, R., Ramesh, A., and Bagade, A. (2018). “Urban Heat Island studies in South Asia: A critical review.” *Urban Clim.*, 24(October 2017), 1011–1026.
- Lai, J., Zhan, W., Quan, J., Bechtel, B., Wang, K., Zhou, J., Huang, F., Chakraborty, T., Liu, Z., and Lee, X. (2021). “Statistical estimation of next-day nighttime surface urban heat islands.” *ISPRS J. Photogramm. Remote Sens.*, 176(163), 182–195.
- Landsat, N.A.S.A. (7). Science Data Users Handbook. 2011-03-11.  
[http://landsathandbook.gsfc.nasa.gov/inst\\_cal/prog\\_sect8\\_2.html](http://landsathandbook.gsfc.nasa.gov/inst_cal/prog_sect8_2.html). Accessed on 12th December 2017.
- Landsat, N.A.S.A. (8). Science Data Users Handbook. 2015-June. <http://landsat.usgs.gov/18handbook.php>. Accessed on 12th December 2017.
- Levermore, G., Parkinson, J., Lee, K., Laycock, P., and Lindley, S. (2018). “The increasing trend of the urban heat island intensity.” *Urban Clim.*, 24, 360–368.
- Li, H., Zhou, Y., Li, X., Meng, L., Wang, X., Wu, S., and Sodoudi, S. (2018). “A new method to quantify surface urban heat island intensity.” *Sci. Total Environ.*, 624, 262–272.
- Li, H., Zhou, Y., Wang, X., Zhou, X., Zhang, H., and Sodoudi, S. (2019). “Quantifying urban heat island intensity and its physical mechanism using WRF/UCM.” *Sci. Total Environ.*, 650, 3110–3119.
- Li, W., Cao, Q., Lang, K., and Wu, J. (2017). “Linking potential heat source and sink to urban heat island: Heterogeneous effects of landscape pattern on land surface temperature.” *Sci. Total Environ.*, 586, 457–465.
- Liu, G., Zhang, Q., Li, G., and Doronzo, D. M. (2016). “Response of land cover types to land surface temperature derived from Landsat-5 TM in Nanjing

- Metropolitan Region, China.” *Environ. Earth Sci.*, 75(20), 1–12.
- Marconcini, M., Camps-Valls, G., and Bruzzone, L. (2009). “A composite semisupervised SVM for classification of hyperspectral images.” *IEEE Geosci. Remote Sens. Lett.*, 6(2), 234–238.
- Mathew, A., Khandelwal, S., and Kaul, N. (2016). “Spatial and temporal variations of urban heat island effect and the effect of percentage impervious surface area and elevation on land surface temperature: Study of Chandigarh city, India.” *Sustain. Cities Soc.*, 26, 264–277.
- Mathew, A., Khandelwal, S., and Kaul, N. (2018). “Analysis of diurnal surface temperature variations for the assessment of surface urban heat island effect over Indian cities.” *Energy Build.*, 159, 271–295.
- Mathew, A., Sreekumar, S., Khandelwal, S., and Kumar, R. (2019). “Prediction of land surface temperatures for surface urban heat island assessment over Chandigarh city using support vector regression model.” *Sol. Energy*, 186(March), 404–415.
- MATLAB. (2015). version 8.5.0 (R2015a). Natick, Massachusetts: The MathWorks Inc.
- McFeeters, S. K. (1996). “The use of the Normalized Difference Water Index (NDWI) in the delineation of open water features.” *Int. J. Remote Sens.*, 17(7), 1425–1432.
- Moosavi, V., Talebi, A., Mokhtari, M. H., and Hadian, M. R. (2016). “Estimation of spatially enhanced soil moisture combining remote sensing and artificial intelligence approaches.” *Int. J. Remote Sens.*, 37(23), 5605–5631.
- Morabito, M., Crisci, A., Messeri, A., Orlandini, S., Raschi, A., Maracchi, G., and Munafò, M. (2016). “The impact of built-up surfaces on land surface temperatures in Italian urban areas.” *Sci. Total Environ.*, 551–552, 317–326.
- Moser, G., and Serpico, S. B. (2009). “Land and Sea Surface Temperature

- Estimation by Support Vector Regression.” *Kernel Methods Remote Sens. Data Anal.*, 47(3), 301–325.
- Mountrakis, G., Im, J., and Ogole, C. (2011). “Support vector machines in remote sensing: A review.” *ISPRS J. Photogramm. Remote Sens.*, 66(3), 247–259.
- Myint, S. W., Wentz, E. A., Brazel, A. J., and Quattrochi, D. A. (2013). “The impact of distinct anthropogenic and vegetation features on urban warming.” *Landsc. Ecol.*, 28(5), 959–978.
- Nichol, J. E., and To, P. H. (2012). “Temporal characteristics of thermal satellite images for urban heat stress and heat island mapping.” *ISPRS J. Photogramm. Remote Sens.*, 74, 153–162.
- Okujeni, A., Linden, S. van der, Tits, L., Somers, B., and Hostert, P. (2013). “Support vector regression and synthetically mixed training data for quantifying urban land cover.” *Remote Sens. Environ.*, 137, 184–197.
- Panahi, M., Dodangeh, E., Rezaie, F., Khosravi, K., Le, H. Van, Lee, M. J., Lee, S., and Thai Pham, B. (2021). “Flood spatial prediction modeling using a hybrid of meta-optimization and support vector regression modeling.” *Catena*, 199(January 2020), 105114.
- Pandey, P., Kumar, D., Prakash, A., Kumar, K., and Jain, V. K. (2009). “A study of the summertime urban heat island over Delhi.” *Int. J. Sustain. Sci. Stud.*, 1(1), 27–34.
- Pandey, P., Kumar, D., Prakash, A., Masih, J., Singh, M., Kumar, S., Jain, V. K., and Kumar, K. (2012). “A study of urban heat island and its association with particulate matter during winter months over Delhi.” *Sci. Total Environ.*
- Phelan, P. E., Kaloush, K., Miner, M., Golden, J., Phelan, B., Silva, H., and Taylor, R. A. (2015). “Urban Heat Island: Mechanisms, Implications, and Possible Remedies.” *Annu. Rev. Environ. Resour.*, 40, 285–307.
- Pillonetto, G., Dinuzzo, F., Chen, T., Nicolao, G. De, and Ljung, L. (2014). “Kernel

- methods in system identification, machine learning and function estimation: A survey.” *Automatica*, 50(3), 657–682.
- Piri, J., Shamshirband, S., Petković, D., Tong, C. W., and Rehman, M. H. U. (2015). “Prediction of the solar radiation on the Earth using support vector regression technique.” *Infrared Phys. Technol.*, 68, 179–185.
- Pradhan, K. C. (2017). “Unacknowledged urbanisation: The new census towns in India.” *Explor. Urban Chang. South Asia*, 39–66.
- Qin, Z., Karnieli, A., and Berliner, P. (2001). “A mono-window algorithm for retrieving land surface temperature from Landsat TM data and its application to the Israel-Egypt border region.” *Int. J. Remote Sens.*, 22(18), 3719–3746.
- R Core Team (2021). R: A language and environment for statistical computing. R Foundation for Statistical Computing, Vienna, Austria. URL <https://www.R-project.org/>.
- Rajabi-Kiasari, S., and Hasanlou, M. (2020). “An efficient model for the prediction of SMAP sea surface salinity using machine learning approaches in the Persian Gulf.” *Int. J. Remote Sens.*, 41(8), 3221–3242.
- Rajasekar, U., and Weng, Q. (2009). “Urban heat island monitoring and analysis using a non-parametric model: A case study of Indianapolis.” *ISPRS J. Photogramm. Remote Sens.*, 64(1), 86–96.
- Ramachandra, T. ., and Uttam, K. (2009). “Geoinformatic for Urbanisation and Urban Sprawl Pattern Analysis.” *Geoinformatic Nat. Resour. Manag.*
- Ramachandra, T., and Kumar, U. (2010). “Greater Bangalore: Emerging urban heat island.” *GIS Dev.*, 14(1), 1–16.
- Ramachandra, T. V., and Kumar, U. (2009). “Land surface temperature with land cover dynamics: Multi-resolution, spatio-temporal data analysis of greater bangalore, india.” *Int. J. Geoinformatics*, 5(3), 43–53.
- Ramachandra, T. V, Bharath Aithal, H., Vinay, S., Joshi, N. V, Kumar, U., and Rao,



- K. V. (2013). “Modelling Urban Revolution in Greater Bangalore, India.” *30th Annu. In-House Symp. Sp. Sci. Technol.*, (November), 7–8.
- Rasul, A., Balzter, H., and Smith, C. (2015). “Urban Climate Spatial variation of the daytime Surface Urban Cool Island during the dry season in Erbil , Iraqi Kurdistan , from Landsat 8.” *Urban Clim.*, 14, 176–186.
- Rasul, A., Balzter, H., and Smith, C. (2017). “Applying a normalized ratio scale technique to assess influences of urban expansion on land surface temperature of the semi-arid city of Erbil.” *Int. J. Remote Sens.*, 38(13), 3960–3980.
- Rinner, C., and Hussain, M. (2011). “Toronto’s urban heat island-exploring the relationship between land use and surface temperature.” *Remote Sens.*, 3(6), 1251–1265.
- Sabet Sarvestani, M., Ibrahim, A. L., and Kanaroglou, P. (2011). “Three decades of urban growth in the city of Shiraz, Iran: A remote sensing and geographic information systems application.” *Cities*, 28(4), 320–329.
- Sankhe, S., Vittal, I., Dobbs, R., Mohan, A., Gulati, A., Ablett, J., Gupta, S., Kim, A., Paul, S., Sanghvi, A., Sethy, G., and McKinsey. (2010). “India ’ s urban awakening : Building inclusive cities , sustaining economic growth.” *McKinsey Q.*, (April), 1–33.
- Santamouris, M., Haddad, S., Fiorito, F., Osmond, P., Ding, L., Prasad, D., Zhai, X., and Wang, R. (2017). “Urban heat island and overheating characteristics in Sydney, Australia. An analysis of multiyear measurements.” *Sustain.*, 9(5).
- Seto, K. C., Güneralp, B., and Hutyrá, L. R. (2012). “Global forecasts of urban expansion to 2030 and direct impacts on biodiversity and carbon pools.” *Proc. Natl. Acad. Sci. U. S. A.*, 109(40), 16083–16088.
- Shastri, H., Barik, B., Ghosh, S., Venkataraman, C., and Sadavarte, P. (2017). “Flip flop of Day-night and Summer-Winter Surface Urban Heat Island Intensity in India.” *Sci. Rep.*, 7(January), 1–8.

- Sheng, X., Xi, M., Sun, J., and Xu, W. (2015). “Quantum-behaved particle swarm optimization with novel adaptive strategies.” *J. Algorithms Comput. Technol.*, 9(2), 143–161.
- Shi, H., Xian, G., Auch, R., Gallo, K., and Zhou, Q. (2021). “Urban heat island and its regional impacts using remotely sensed thermal data—a review of recent developments and methodology.” *Land*, 10(8).
- Shi, Y., and Zhang, Y. (2018). “Remote sensing retrieval of urban land surface temperature in hot-humid region.” *Urban Clim.*, 24, 299–310.
- Smola, A. J., and Schölkopf, B. (2004). “A tutorial on support vector regression.” *Stat. Comput.*, 14(3), 199–222.
- Sobrino, J. A., Jiménez-Muñoz, J. C., and Paolini, L. (2004). “Land surface temperature retrieval from LANDSAT TM 5.” *Remote Sens. Environ.*, 90(4), 434–440.
- Solangi, G. S., Siyal, A. A., and Siyal, P. (2019). “Spatiotemporal Dynamics of Land Surface Temperature and Its Impact on the Vegetation.” *Civ. Eng. J.*, 5(8), 1753–1763.
- Song, J., Du, S., Feng, X., and Guo, L. (2014a). “The relationships between landscape compositions and land surface temperature: Quantifying their resolution sensitivity with spatial regression models.” *Landsc. Urban Plan.*, 123, 145–157.
- Song, L., Zhao, Z., Xu, J., Liu, S., and Peng, K. (2014b). “Improvements in land surface temperature retrieval based on atmospheric water vapour content and atmospheric temperature.” *Int. J. Remote Sens.*, 35(13), 4881–4904.
- Stewart, I. D., and Oke, T. R. (2012). “Local climate zones for urban temperature studies.” *Bull. Am. Meteorol. Soc.*, 93(12), 1879–1900.
- Streutker, D. R. (2002). “A remote sensing study of the urban heat island of Houston, Texas.” *Int. J. Remote Sens.*, 23(13), 2595–2608.

- Sudhira, H. S., Ramachandra, T. V., and Subrahmanya, M. H. B. (2007). "Bangalore." *Cities*, 24(5), 379–390.
- Sun, Q., Wu, Z., and Tan, J. (2012). "The relationship between land surface temperature and land use/land cover in Guangzhou, China." *Environ. Earth Sci.*, 65(6), 1687–1694.
- Szymanowski, M., and Kryza, M. (2011). "Application of remotely sensed data for spatial approximation of urban heat island in the city of Wrocław, Poland." *2011 Jt. Urban Remote Sens. Event, JURSE 2011 - Proc.*, 353–356.
- Tan, J., Zheng, Y., Tang, X., Guo, C., Li, L., Song, G., Zhen, X., Yuan, D., Kalkstein, A. J., Li, F., and Chen, H. (2010). "The urban heat island and its impact on heat waves and human health in Shanghai." *Int. J. Biometeorol.*, 54(1), 75–84.
- Theeuwes, N. E., Steeneveld, G. J., Ronda, R. J., Rotach, M. W., and Holtslag, A. A. M. (2015). "Cool city mornings by urban heat." *Environ. Res. Lett.*, 10(11), 1994–1998.
- Thomas, G., Sherin, A. P., Ansar, S., and Zachariah, E. J. (2014). "Analysis of Urban Heat Island in Kochi, India, Using a Modified Local Climate Zone Classification." *Procedia Environ. Sci.*, 21, 3–13.
- Touchaei, A. G., and Wang, Y. (2015). "Characterizing urban heat island in Montreal (Canada) - Effect of urban morphology." *Sustain. Cities Soc.*, 19, 395–402.
- Tran, D. X., Pla, F., Latorre-Carmona, P., Myint, S. W., Caetano, M., and Kieu, H. V. (2017). "Characterizing the relationship between land use land cover change and land surface temperature." *ISPRS J. Photogramm. Remote Sens.*, 124, 119–132.
- Tuia, D., and Camps-Valls, G. (2009). "Semisupervised remote sensing image classification with cluster kernels." *IEEE Geosci. Remote Sens. Lett.*, 6(2), 224–228.

UN-DESA. 2012. World Urbanisation Prospects, The 2011 Revision. New York:  
UN

United Nations, Department of Economic and Social Affairs, Population Division  
(2015). World Urbanization Prospects: The 2014 Revision,  
(ST/ESA/SER.A/366)

Valor, E., and Caselles, V. (1996). "Mapping Land Surface Emissivity from NDVI :  
Application to European , African , and South American Areas." 184(December  
1995), 167–184.

Vapnik, V. N. (1995). "The Nature of Statistical Learning." *Theory*.

Verrelst, J., Muñoz, J., Alonso, L., Delegido, J., Rivera, J. P., Camps-Valls, G., and  
Moreno, J. (2012). "Machine learning regression algorithms for biophysical  
parameter retrieval: Opportunities for Sentinel-2 and -3." *Remote Sens.  
Environ.*, 118, 127–139.

Vogt, W., and Johnson, R. (2015). "Correlation and Regression Analysis." *Correl.  
Regres. Anal.*

Voogt, J. A., and Oke, T. R. (2003). "Thermal remote sensing of urban climates." *Remote Sens. Environ.*, 86(3), 370–384.

Wiesner, S., Bechtel, B., Fischereit, J., Gruetzun, V., Hoffmann, P., Leitl, B.,  
Rechid, D., Schlünzen, K., and Thomsen, S. (2018). "Is It Possible to  
Distinguish Global and Regional Climate Change from Urban Land Cover  
Induced Signals? A Mid-Latitude City Example." *Urban Sci.*, 2(1), 12.

Yang, X., Li, Y., Luo, Z., and Chan, P. W. (2017). "The urban cool island  
phenomenon in a high-rise high-density city and its mechanisms." *Int. J.  
Climatol.*, 37(2), 890–904.

Zha, Y., Gao, J., and Ni, S. (2003a). "Use of normalized difference built-up index in  
automatically mapping urban areas from TM imagery." *Int. J. Remote Sens.*,  
24(3), 583–594.

- Zha, Y., Gao, J., and NI, S. (2003b). "Use of normalized difference built-up index in automatically mapping urban areas from TM imagery." *Int. J. Remote Sens.*, 24, 583–594.
- Zhang, H., Qi, Z. fang, Ye, X. yue, Cai, Y. bin, Ma, W. chun, and Chen, M. nan. (2013). "Analysis of land use/land cover change, population shift, and their effects on spatiotemporal patterns of urban heat islands in metropolitan Shanghai, China." *Appl. Geogr.*, 44, 121–133.
- Zhang, R., and Ma, J. (2008). "An improved SVM method P-SVM for classification of remotely sensed data." *Int. J. Remote Sens.*, 29(20), 6029–6036.
- Zhao, Z. Q., He, B. J., Li, L. G., Wang, H. B., and Darko, A. (2017). "Profile and concentric zonal analysis of relationships between land use/land cover and land surface temperature: Case study of Shenyang, China." *Energy Build.*, 155, 282–295.
- Zhou, J., Zhou, J., Chen, Y., Wang, J., Zhan, W., and Wang, J. (2011). "Maximum Nighttime Urban Heat Island (UHI) Intensity Simulation by Integrating Remotely Sensed Data and Meteorological Observations." *IEEE J. Sel. Top. Appl. Earth Obs. Remote Sens.*, 4(1), 138–146.
- Zullo, F., Fazio, G., Romano, B., Marucci, A., and Fiorini, L. (2019). "Effects of urban growth spatial pattern (UGSP) on the land surface temperature (LST): A study in the Po Valley (Italy)." *Sci. Total Environ.*, 650, 1740–1751.

## Appendix

**Table A.1.** Spatial distribution of surface area of land cover for each concentric ring for 2017

Concentric ring 2017	Distance from centre point(km)	Area of the concentric ring(km <sup>2</sup> )	Surface Area ratio			
			Urban	Vegetation	Water	Barren
1	0.25	0.20	0.49	0.35	0.01	0.16
2	0.75	0.59	0.56	0.24	0.05	0.16
3	1.25	0.98	0.63	0.19	0.03	0.14
4	1.75	1.37	0.62	0.22	0.02	0.15
5	2.25	1.77	0.59	0.24	0.02	0.16
6	2.75	2.16	0.59	0.23	0.02	0.17
7	3.25	2.55	0.62	0.22	0.01	0.15
8	3.75	2.94	0.61	0.21	0.03	0.16
9	4.25	3.34	0.64	0.19	0.02	0.16
10	4.75	3.73	0.67	0.18	0.00	0.15
11	5.25	4.12	0.64	0.19	0.01	0.16
12	5.75	4.51	0.69	0.17	0.01	0.14
13	6.25	4.91	0.67	0.19	0.01	0.13
14	6.75	5.30	0.67	0.18	0.01	0.14
15	7.25	5.69	0.71	0.14	0.02	0.13
16	7.75	6.08	0.70	0.13	0.03	0.14
17	8.25	6.48	0.66	0.18	0.02	0.15
18	8.75	6.87	0.64	0.19	0.02	0.15
19	9.25	7.26	0.66	0.17	0.02	0.14
20	9.75	7.65	0.69	0.14	0.03	0.15
21	10.25	8.05	0.68	0.14	0.02	0.16
22	10.75	8.44	0.66	0.16	0.02	0.16
23	11.25	8.83	0.64	0.14	0.03	0.19
24	11.75	9.22	0.64	0.15	0.02	0.19
25	12.25	9.62	0.62	0.15	0.01	0.23
26	12.75	10.01	0.58	0.15	0.01	0.27
27	13.25	10.40	0.57	0.13	0.01	0.29
28	13.75	10.79	0.56	0.13	0.02	0.29
29	14.25	11.19	0.52	0.14	0.02	0.33
30	14.75	11.58	0.46	0.19	0.01	0.34
31	15.25	11.97	0.45	0.19	0.01	0.35
32	15.75	12.36	0.43	0.19	0.02	0.37
33	16.25	12.76	0.39	0.19	0.02	0.40
34	16.75	13.15	0.39	0.20	0.03	0.38
35	17.25	13.54	0.40	0.19	0.01	0.40
36	17.75	13.93	0.37	0.20	0.01	0.42
37	18.25	14.33	0.36	0.18	0.01	0.45
38	18.75	14.72	0.38	0.18	0.01	0.43
39	19.25	15.11	0.38	0.18	0.01	0.44
40	19.75	15.50	0.36	0.18	0.01	0.45
41	20.25	15.90	0.35	0.20	0.00	0.45
42	20.75	16.29	0.34	0.17	0.01	0.48
43	21.25	16.68	0.34	0.15	0.00	0.50
44	21.75	17.07	0.34	0.16	0.01	0.50
45	22.25	17.47	0.32	0.18	0.02	0.49
46	22.75	17.86	0.30	0.17	0.01	0.52

**Table A.2.** Spatial distribution of surface area of land cover for each concentric ring for 2005

Concentric ring 2005	Distance from centre point(km)	Area of the concentric ring(km <sup>2</sup> )	Surface Area ratio			
			Urban	Vegetation	Water	Barren
1	0.25	0.20	0.59	0.35	0.05	0.01
2	0.75	0.59	0.62	0.29	0.02	0.07
3	1.25	0.98	0.69	0.26	0.01	0.04
4	1.75	1.37	0.70	0.27	0.01	0.03
5	2.25	1.77	0.66	0.29	0.01	0.04
6	2.75	2.16	0.67	0.28	0.01	0.05
7	3.25	2.55	0.72	0.24	0.01	0.03
8	3.75	2.94	0.68	0.25	0.03	0.04
9	4.25	3.34	0.73	0.19	0.02	0.06
10	4.75	3.73	0.76	0.17	0.01	0.06
11	5.25	4.12	0.72	0.20	0.01	0.07
12	5.75	4.51	0.78	0.16	0.01	0.05
13	6.25	4.91	0.73	0.21	0.01	0.06
14	6.75	5.30	0.75	0.20	0.00	0.04
15	7.25	5.69	0.75	0.19	0.01	0.05
16	7.75	6.08	0.71	0.21	0.02	0.07
17	8.25	6.48	0.64	0.25	0.01	0.10
18	8.75	6.87	0.64	0.23	0.03	0.10
19	9.25	7.26	0.60	0.25	0.03	0.12
20	9.75	7.65	0.56	0.26	0.03	0.15
21	10.25	8.05	0.51	0.28	0.02	0.19
22	10.75	8.44	0.45	0.31	0.01	0.23
23	11.25	8.83	0.39	0.31	0.03	0.27
24	11.75	9.22	0.35	0.33	0.01	0.30
25	12.25	9.62	0.35	0.31	0.01	0.34
26	12.75	10.01	0.31	0.31	0.01	0.37
27	13.25	10.40	0.29	0.33	0.01	0.38
28	13.75	10.79	0.26	0.35	0.02	0.37
29	14.25	11.19	0.23	0.41	0.02	0.35
30	14.75	11.58	0.21	0.47	0.01	0.32
31	15.25	11.97	0.20	0.44	0.01	0.35
32	15.75	12.36	0.19	0.45	0.01	0.36
33	16.25	12.76	0.15	0.46	0.02	0.36
34	16.75	13.15	0.15	0.48	0.02	0.35
35	17.25	13.54	0.15	0.48	0.01	0.36
36	17.75	13.93	0.15	0.48	0.01	0.36
37	18.25	14.33	0.11	0.46	0.01	0.43
38	18.75	14.72	0.12	0.44	0.00	0.43
39	19.25	15.11	0.11	0.47	0.00	0.41
40	19.75	15.50	0.11	0.49	0.00	0.41
41	20.25	15.90	0.11	0.49	0.00	0.41
42	20.75	16.29	0.10	0.41	0.00	0.49
43	21.25	16.68	0.09	0.42	0.00	0.49
44	21.75	17.07	0.09	0.43	0.00	0.48
45	22.25	17.47	0.10	0.40	0.00	0.50
46	22.75	17.86	0.11	0.36	0.01	0.52

**Table A.3.** Spatial distribution of surface area of land cover for each concentric ring for 2001

Concentric ring 2001	Distance from centre point(km)	Area of the concentric ring(km <sup>2</sup> )	Surface Area ratio			
			Urban	Vegetation	Water	Barren
1	0.25	0.20	0.55	0.39	0.04	0.02
2	0.75	0.59	0.60	0.30	0.02	0.08
3	1.25	0.98	0.66	0.26	0.01	0.07
4	1.75	1.37	0.65	0.28	0.01	0.06
5	2.25	1.77	0.61	0.30	0.01	0.08
6	2.75	2.16	0.61	0.31	0.01	0.07
7	3.25	2.55	0.65	0.27	0.01	0.07
8	3.75	2.94	0.63	0.26	0.03	0.08
9	4.25	3.34	0.68	0.21	0.02	0.09
10	4.75	3.73	0.72	0.17	0.01	0.10
11	5.25	4.12	0.67	0.19	0.01	0.13
12	5.75	4.51	0.71	0.18	0.01	0.11
13	6.25	4.91	0.69	0.19	0.00	0.12
14	6.75	5.30	0.68	0.19	0.01	0.13
15	7.25	5.69	0.64	0.17	0.02	0.18
16	7.75	6.08	0.54	0.17	0.05	0.24
17	8.25	6.48	0.46	0.20	0.03	0.32
18	8.75	6.87	0.43	0.18	0.04	0.35
19	9.25	7.26	0.37	0.22	0.04	0.37
20	9.75	7.65	0.33	0.23	0.03	0.41
21	10.25	8.05	0.29	0.22	0.02	0.47
22	10.75	8.44	0.25	0.31	0.02	0.42
23	11.25	8.83	0.22	0.31	0.03	0.44
24	11.75	9.22	0.21	0.29	0.02	0.48
25	12.25	9.62	0.18	0.27	0.01	0.54
26	12.75	10.01	0.18	0.27	0.01	0.54
27	13.25	10.40	0.18	0.28	0.01	0.53
28	13.75	10.79	0.16	0.28	0.01	0.54
29	14.25	11.19	0.14	0.31	0.02	0.54
30	14.75	11.58	0.13	0.34	0.01	0.51
31	15.25	11.97	0.14	0.32	0.01	0.53
32	15.75	12.36	0.13	0.31	0.01	0.54
33	16.25	12.76	0.12	0.34	0.03	0.51
34	16.75	13.15	0.12	0.34	0.03	0.51
35	17.25	13.54	0.11	0.33	0.01	0.55
36	17.75	13.93	0.10	0.35	0.00	0.55
37	18.25	14.33	0.11	0.33	0.01	0.56
38	18.75	14.72	0.11	0.32	0.00	0.56
39	19.25	15.11	0.11	0.32	0.00	0.56
40	19.75	15.50	0.11	0.36	0.00	0.52
41	20.25	15.90	0.11	0.35	0.01	0.53
42	20.75	16.29	0.11	0.31	0.00	0.58
43	21.25	16.68	0.12	0.30	0.00	0.58
44	21.75	17.07	0.12	0.32	0.00	0.56
45	22.25	17.47	0.12	0.32	0.01	0.55
46	22.75	17.86	0.13	0.30	0.02	0.55



**Table A.4.** Spatial distribution of surface area of land cover for each concentric ring for 1989

Concentric ring 1989	Distance from centre point(km)	Area of the concentric ring(km <sup>2</sup> )	Surface Area ratio			
			Urban	Vegetation	Water	Barren
1	0.25	0.20	0.42	0.50	0.06	0.02
2	0.75	0.59	0.56	0.36	0.01	0.07
3	1.25	0.98	0.57	0.37	0.01	0.05
4	1.75	1.37	0.52	0.38	0.01	0.09
5	2.25	1.77	0.47	0.41	0.02	0.10
6	2.75	2.16	0.52	0.38	0.01	0.09
7	3.25	2.55	0.52	0.37	0.02	0.09
8	3.75	2.94	0.52	0.31	0.02	0.15
9	4.25	3.34	0.51	0.28	0.00	0.20
10	4.75	3.73	0.38	0.31	0.01	0.30
11	5.25	4.12	0.38	0.27	0.00	0.34
12	5.75	4.51	0.26	0.31	0.00	0.43
13	6.25	4.91	0.21	0.28	0.01	0.49
14	6.75	5.30	0.15	0.33	0.02	0.49
15	7.25	5.69	0.12	0.38	0.03	0.47
16	7.75	6.08	0.09	0.36	0.02	0.52
17	8.25	6.48	0.07	0.35	0.04	0.53
18	8.75	6.87	0.07	0.37	0.04	0.52
19	9.25	7.26	0.07	0.40	0.03	0.51
20	9.75	7.65	0.06	0.40	0.03	0.50
21	10.25	8.05	0.05	0.42	0.03	0.50
22	10.75	8.44	0.04	0.49	0.02	0.44
23	11.25	8.83	0.03	0.45	0.04	0.48
24	11.75	9.22	0.02	0.44	0.02	0.52
25	12.25	9.62	0.02	0.38	0.01	0.59
26	12.75	10.01	0.02	0.38	0.01	0.58
27	13.25	10.40	0.03	0.38	0.01	0.58
28	13.75	10.79	0.02	0.37	0.02	0.59
29	14.25	11.19	0.02	0.43	0.02	0.53
30	14.75	11.58	0.02	0.45	0.02	0.52
31	15.25	11.97	0.01	0.41	0.02	0.56
32	15.75	12.36	0.01	0.36	0.02	0.61
33	16.25	12.76	0.01	0.39	0.03	0.57
34	16.75	13.15	0.01	0.41	0.04	0.54
35	17.25	13.54	0.01	0.40	0.02	0.57
36	17.75	13.93	0.00	0.42	0.01	0.57
37	18.25	14.33	0.00	0.40	0.01	0.58
38	18.75	14.72	0.01	0.39	0.01	0.59
39	19.25	15.11	0.01	0.41	0.01	0.57
40	19.75	15.50	0.01	0.43	0.01	0.55
41	20.25	15.90	0.00	0.40	0.02	0.57
42	20.75	16.29	0.00	0.38	0.03	0.59
43	21.25	16.68	0.00	0.38	0.02	0.59
44	21.75	17.07	0.01	0.38	0.02	0.59
45	22.25	17.47	0.01	0.38	0.05	0.57
46	22.75	17.86	0.01	0.36	0.05	0.58

## PUBLICATIONS

---

---

### International Journals

- **Nithya R Govind**, Ramesh, H. (2020). Exploring the relationship between LST and land cover of Bengaluru by concentric ring approach. *Environmental Monitoring and Assessment*. 192: 650. <https://doi.org/10.1007/s10661-020-08601-x>
- **Nithya R Govind**, Ramesh, H. (2019). The impact of spatiotemporal patterns of land use land cover and land surface temperature on an urban cool island: a case study of Bengaluru. *Environmental Monitoring and Assessment*. 191: 283. doi:10.1007/s10661-019-7440-1

### International Conferences

- **Nithya R Govind & Ramesh, H** (2019). Analyzing the relationship between land surface temperature and urban growth through concentric ring approach in a semi-arid tropical metropolitan city of Bengaluru, India. Abstract: GC51O-1091 presented at 2019 American Geophysical Union Fall Meeting, Moscone Centre, San Francisco, California, USA, 9 - 13 December 2019.
- **Nithya R Govind & Ramesh, H** (2019). Spatio-temporal variation of Land Surface Temperature due to urbanization: A case study of Bengaluru, India, International conference on Hydraulics, Water resources and Coastal Engineering, 18 - 20 December 2019, University College of Engineering, Osmania University, Hyderabad, India.
- **Nithya R Govind**, Rishikeshan, C. A. and Ramesh, H (2019). Comparison of different Pan sharpening techniques using Landsat 8 imagery, 2019 IEEE 5<sup>th</sup> International conference for Convergence in Technology (I2CT), pp. 1-4, doi: 10.1109/I2CT45611.2019.9033659.

## RESUME

Name : Nithya R Govind

Date of Birth : 08.09.1989

Address : Pradeepthy, Kureepuzha,  
Kavanad P.O  
Kollam - 691003  
Kerala

Mobile : +91-9496328784

E-mail : nithyargovind@gmail.com

Qualifications : B.Tech. (Civil Engineering)  
M.Tech. (Geoinformatics)

Publications : International Journals : 2  
International Conferences : 3

Awards : American Geophysical Union Travel  
Grant

